Nonadiabatic dynamics in open quantum systems excited by coherent and incoherent light sources

Leonardo Fabián Calderón Mantilla

A thesis submmited in partial fulfillment of the requirements for the degree of Doctor in Physics

Director

Ilia D. Mikhailov

Ph.D. in Physics

Co-director

Leonardo A. Pachón

Ph.D. in Physics

Universidad Industrial de Santander

Facultad de Ciencias

Escuela de Física

Doctorado en Física

Bucaramanga

2021

Contents

List of figures

List of appendices

pag.

Resumen

Título: Dinámica no adiabática en sistemas cuánticos abiertos excitados por fuentes de luz coherentes e incoherentes [*]

Autor: Leonardo Fabián Calderón Mantilla [**]

Palabras Clave: Sistemas cuánticos abiertos, dinámica no-adiabática, excitación con luz incoherente.

Descripción: Hace más de una década, las oscilaciones coherentes en los espectros no lineales de complejos fotosintéticos captadores de luz suscitaron un intenso debate sobre la existencia de efectos cuánticos no triviales en reacciones biológicas inducidas por luz. Las evidencias experimentales y teóricas señalan el papel crucial de los modos vibracionales intramoleculares resonantes con brechas energéticas de estados excitónicos en la interpretación de las coherencias de larga duración observadas en los espectros bidimensionales de algunos complejos naturales y sintéticos de captación de luz. Para el caso de iluminación por luz (solar) natural incoherente, en esta tesis se analizó la relevancia de estos modos vibracionales intramoleculares en dímeros vibrónicos recolectores de luz. El análisis de la dinámica de la matriz de densidad revela que la inclusión de modos vibracionales intramoleculares refuerza hasta un orden de magnitud la coherencia en la base de excitones, y puede aumentar las poblaciones de estados de excitones individuales de menor energía, así como las poblaciones y coherencias en la base de sitios. En claro contraste con el caso de la preparación del estado inicial por fuentes de luz coherentes (láser), el estado térmico inicial de los modos vibracionales locales y del modo vibracional anticorrelacionado evoluciona sin correlaciones no clásicas. Esto se confirma por la ausencia de valores negativos en su distribución de cuasi-probabilidad en el espacio de fase para todo tiempo. Por lo tanto, el transporte de energía en los complejos recolectores de luz en condiciones de iluminación natural no es impulsado por procesos vibracionales intramoleculares no clásicos.

---

[*] Tesis doctoral.

[**] Facultad de Ciencias. Escuela de Física. Doctorado en Física. Director: Ilia D. Mikhailov (Doctorado en Física). Codirector: Leonardo A. Pachón (Doctorado en Física).

Abstract

Title: Nonadiabatic dynamics in open quantum systems excited by coherent and incoherent light sources [*]

Author: Leonardo Fabián Calderón Mantilla [**]

Keywords: Open quantum systems, nonadiabatic dynamics, incoherent light excitation.

Description: More than a decade ago, the coherent oscillations in nonlinear spectra of photosynthetic light-harvesting complexes ignited an intense debate on the existence of nontrivial quantum effects in light-induced reactions in biology. Experimental and theoretical evidence indicates the crucial role of specific intramolecular vibrational modes in the long-lived coherences observed in two-dimensional spectra of some natural and synthetic light-harvesting complexes. For the case of illumination by natural incoherent (sun)light, the relevance of these intramolecular vibrational modes is analyzed in the present thesis for light-harvesting vibronic prototype dimers. The analysis of the density matrix dynamics reveals that the presence of intramolecular vibrational modes reinforces up to one order of magnitude the coherence in the exciton basis and may increase the populations of lowest energy single exciton states, as well as populations and coherences in the site basis. In sharp contrast to the case of initial-state preparation provided by coherent (laser)light-sources, the initial thermal state of the local vibrational modes and the anticorrelated vibrational mode evolves devoid of non-classical correlations. It is confirmed by the absence of negative values of its phase-space quasi–probability distribution at all times. Therefore, energy transport in light-harvesting complexes under natural illumination conditions is not driven by non-classical intramolecular vibrational processes.

---

[*] Doctoral Thesis

[**] Facultad de Ciencias. Escuela de Física. Doctorado en Física. Director: Ilia D. Mikhailov (Ph.D. in Physics). Co-director: Leonardo A. Pachón (Ph.D. in Physics).

Introduction

One of the biggest challenges in science and engineering is finding clean, renewable, and sustainable energy sources. The prospect of contributing to new technologies or improving existing technologies related to the collection and conversion of sunlight is sufficient motivation to develop new experimental techniques and theoretical models [Romero et al., 2017; Brédas et al., 2017]. Nature shows the possibility of achieving high efficiency, in some cases close to 100% in the energy harvesting and transfer processes carried out in photosynthesis [Chin et al., 2013; Alharbi and Kais, 2015]. A clear understanding of these processes can lead to a better design of photovoltaic devices and, therefore, to the implementation of clean and sustainable energy technologies based on sunlight [Brédas et al., 2017; Mirkovic et al., 2017].

Photosynthesis is the fundamental basis for life on earth. This natural process begins with sunlight capturing by photosynthetic light-harvesting complexes (pigment- protein complexes, see Fig. 1). The light-harvesting apparatus of photosynthetic organisms is composed of a reaction center, where the primary reactions (charge separation) associated with chemical energy production occur. The reaction center is surrounded by a network of light-harvesting

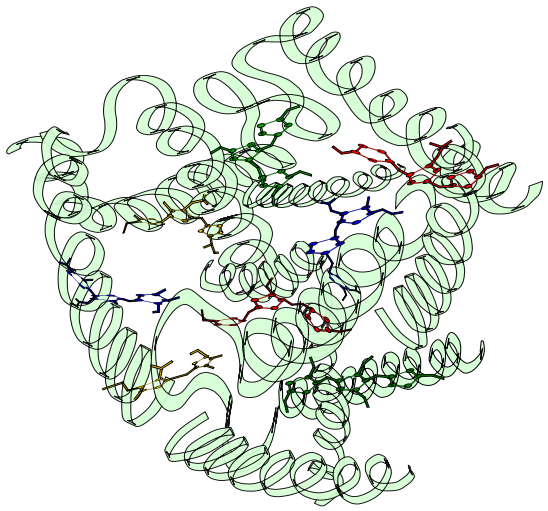

Figure 1. Illustration of a photosynthetic light-harvesting complex. The chromophores are indicated in colors blue, red, yellow, and dark green. The protein structure is represented in a light green color.

antennae consisting of pigments, called chromophores (e.g., chlorophyll). They are responsible for the colors observed in the different photosynthetic complexes. These pigments are fixed and oriented in a protein structure and inside an aqueous medium. Pigments represent organic molecules arranged to capture light from blue to near-infrared wavelengths [Blankenship, 2014].

The light absorption by photosynthetic complexes leads to the excitation of an electron from the highest energy occupied molecular orbital to the lowest energy unoccupied molecular orbital [Scholes and Rumbles, 2006; May and Kühn, 2011]. The excited electron in the lowest energy unoccupied molecular orbital and the hole in the highest energy occupied molecular orbital interact with each other by Coulomb forces, forming an excited state or quasiparticle called a Frenkel exciton. The lifetime of these quasiparticles, related to the electron-hole pair recombination process, can vary from hundreds of femtoseconds to nanoseconds [Mirkovic et al., 2017]. After the exciton is created, it must travel through the pigment-protein antenna complex, transferring between chromophores until it is collected at the reaction center [Mirkovic et al., 2017].

A first approach proposed for describing the electronic excitation energy transfer process was Förster resonant energy transfer theory [May and Kühn, 2011; Förster, 1948, 1965]. This theory relies on the following. When a large distance separates two molecules compared to their size, the electronic coupling between the molecules can be represented by dipole-dipole interaction. The energy transfer efficiency will depend on the overlap of the emission spectrum of the donor molecule and the absorption spectrum of the acceptor molecule.

Förster theory offers accurate predictions when the electronic coupling between molecules is weak compared with the coupling to the surrounding vibrational environment. The vibrational environment is associated with other pigments, the protein structure to which the pigments are fixed, and the aqueous medium. Strong coupling to the environment suppresses any correlation between the donor and acceptor molecular states. The electronic excitation is localized in one molecule and transmitted randomly between one molecule and another. Förster model for electronic excitation energy transfer is known to describe an incoherent energy transfer regime [Chenu and Scholes, 2015; Cheng and Fleming, 2009].

In most photosynthetic complexes, there is a high density of pigments in the light-harvesting antennae. The

spatial separation between pigments varies between 5 to 20 Å [Mirkovic et al., 2017], so the electronic coupling between pigments can become strong due to their proximity. This situation does not agree with the assumption of weak electronic coupling in Förster theory, so its applicability is limited in describing the energy transfer process in various photosynthetic complexes [Chenu and Scholes, 2015; Cheng and Fleming, 2009; Levi et al., 2015]. As a consequence of strong electronic coupling between pigments, collective or delocalized excited electronic states are produced, known as Frenkel excitons, or molecular excitons [Chenu and Scholes, 2015; Scholes and Rumbles, 2006; May and Kühn, 2011]. The excited states are delocalized over two or more pigments. Thus, the excitation corresponds to a quantum superposition of excited electronic states of different molecules [Chenu and Scholes, 2015; Cheng and Fleming, 2009; May and Kühn, 2011]. The relative phases associated with the quantum superposition can evolve coherently during the energy transfer process. Different paths can be realized simultaneously, modifying the transport properties through quantum interference [Chenu and Scholes, 2015; Scholes et al., 2017; Feynman and Hibbs, 1965; Valkunas et al., 2013].

Spectroscopic techniques allow determining critical information from the electronic excitation energy transfer process by using ultrafast laser techniques. Spectroscopic techniques determine the energy spectrum structure and reveal details about the collective excited states, providing insight into the chromophore-system Hamiltonian and its coupling to the environment [Brumer, 2018]. Also, make it possible to detect the collective absorption and redistribution of excitation energy, which are elementary processes characterizing exciton dynamics [Mukamel, 1995]. Thanks to the development of the two-dimensional electron spectroscopy techniques [Jonas, 2003], long-duration oscillations ($\sim$1 ps) attributed to the coherent dynamics of electronic excitations were reported in Fenna-Mathews-Olson (FMO) pigment-protein complex isolated from the green sulfur bacteria [Brixner et al., 2005; Engel et al., 2007; Panitchayangkoon et al., 2010; Collini et al., 2010] (see Fig. 2).

The duration of these oscillations was similar to the expected time scales of energy transfer, which was interpreted as electronic excitations traveling coherently through the photosynthetic FMO complex, contrary to the incoherent transfer regime of Förster theory. Similar observations were reproduced at cryogenic temperatures and even at room temperature, again in FMO complexes [Panitchayangkoon et al., 2010; Hayes et al., 2011], marine algae

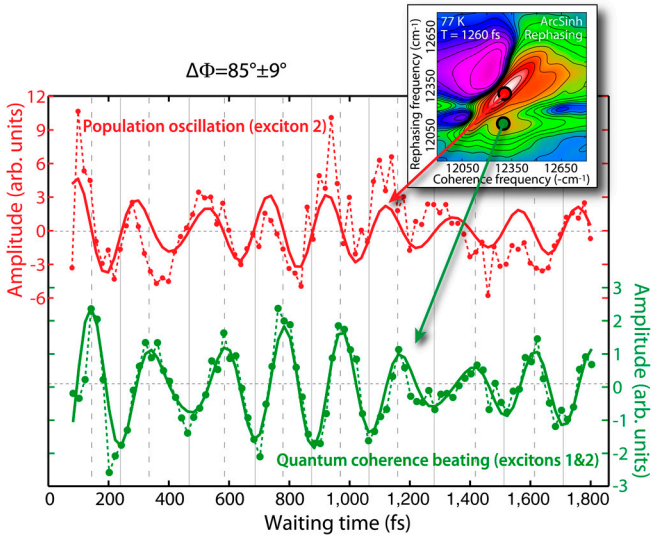

Figure 2. Figure taken from Ref. [Panitchayangkoon et al., 2010]. Quantum coherence beating and population oscillation were reported in experimental signals of two-dimensional electronic spectra in the Fenna-Matthews-Olson (FMO) complex of the green sulfur bacteria, *Chlorobaculum tepidum*.

[Collini et al., 2010], LHCII photosynthetic complexes [Calhoun et al., 2009], vascular plant reaction centers [Fuller et al., 2014; Romero et al., 2014], among others [Romero et al., 2017; Scholes et al., 2017]. The above stimulated the search for theoretical models describing these experimental results and their relation to possible non-trivial quantum effects [Brumer, 2018; Scholak and Brumer, 2017] (interference, entanglement, nonlocality, sub-Poissonian bosonic statistics, etc.), particularly the definition of different types of quantum correlations (electronic, vibrational, vibronic) and their relevance to the high efficiency of the energy transfer process [Ishizaki et al., 2010; Pachón and Brumer, 2011, 2012; Chenu and Scholes, 2015].

Gradually, with the refinement of experimental techniques and more sophisticated theoretical models, a consensus has been reached. The origin and frequency of the long-lived oscillations observed in experiments must be attributed to the intricate interaction between electronic and vibrational degrees of freedom present in photosynthetic complexes [Romero et al., 2017; Chin et al., 2013; Kolli et al., 2012; Christensson et al., 2012; Scholes et al., 2017]. The origin of the long-lived oscillations reported in experiments has been related to couplings between electronic and intramolecular vibrational degrees of freedom (vibronic couplings) of pigments interacting in diverse coupling regimes

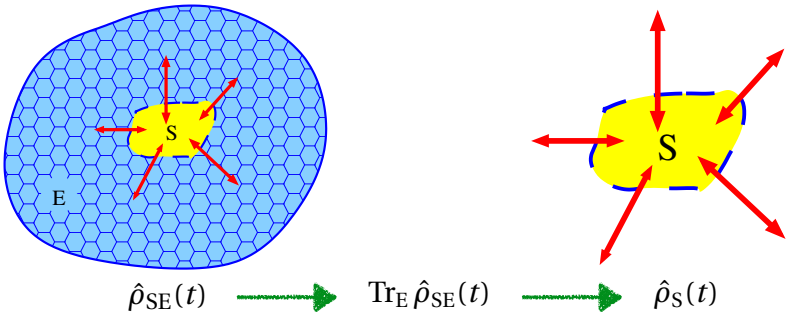

Figure 3. Illustration of a global system (open system + environment). The reduced density operator $\hat{\rho}_S(t)$ of the open system is defined by taking the partial trace over the environment degrees of freedom Tr_E from the global system density operator $\hat{\rho}_{SE}(t)$.

with vibrational environments. In 2013, it was reported that intramolecular vibrations with energies comparable to the energy difference between excitonic states lead to nonadiabatic energy transfer in the Fenna-Matthews-Olson complex [Tiwari et al., 2013]. These results have been tested in different photosynthetic complexes and recognize the fundamental role of vibronic couplings in the energy transfer process in photosynthetic complexes [Chin et al., 2013; Fuller et al., 2014; Romero et al., 2014; Dijkstra et al., 2015; Malý et al., 2016; Dean et al., 2016; Bennett et al., 2018; Wang et al., 2019; Yeh et al., 2019; Wang et al., 2019; Arsenault et al., 2020; Cao et al., 2020; Higgins et al., 2021].

Modeling energy transport in photosynthetic complexes is generally structured in open quantum systems theory [Breuer and Petruccione, 2002; Schlosshauer, 2007; May and Kühn, 2011; Rivas and Huelga, 2012; Weiss, 2012] since the many electronic and vibrational degrees of freedom involved in the energy transfer process [May and Kühn, 2011; Pachón and Brumer, 2012; Chenu and Scholes, 2015]. Then open quantum system represents the set pigments associated with the energy transfer process. The environment in which the pigments are immersed (protein structure, solvent) is modeled as a set of harmonic oscillators (phonon bath), whose influence on the system causes energy dissipation and deterioration of quantum correlations (decoherence) [Pachón and Brumer, 2012; Chenu and Scholes, 2015; May and Kühn, 2011; Valkunas et al., 2013]. The system and the environment are described by mixed states and are represented by density operators [Breuer and Petruccione, 2002; Weiss, 2012]. The reduced density operator of the open system is defined by taking the partial trace over the environment degrees of freedom from the global system (open system + environment) density operator (see Fig. 3).

There are different methodologies to calculate the dynamics of the reduced density operator. When the coupling between the electronic degrees of freedom of the system and the phononic degrees of freedom of the environment is weak, one can use second-order perturbation theory to find a master equation describing the dynamics of the energy transfer [Breuer and Petruccione, 2002]. In the particular case, from a basis of energy eigenstates of the Hamiltonian system, the Redfield master equation is obtained [May and Kühn, 2011; Valkunas et al., 2013; Cohen-Tannoudji et al., 1998]. The validity of the Redfield formalism in modeling energy transfer processes in different photosynthetic complexes has been widely discussed [Chenu and Scholes, 2015; Cheng and Fleming, 2009]. In some photosynthetic complexes, the energy gaps between excitonic levels are comparable to the energy of interaction with the environment. This frames the energy transfer problem in an intermediate coupling regime, in which conventional approaches such as Förster theory, or the formalism based on Redfield master equations, prove inadequate [Chenu and Scholes, 2015; Levi et al., 2015]. In these circumstances it is necessary to use non-perturbative methods such as: hierarchical equations of motion [Ishizaki and Tanimura, 2005], the time-dependent Hartree multiconfiguration method [Beck et al., 2000], the method of polaronic transformations [Jang, 2011; Wang et al., 2015], among others [Chenu and Scholes, 2015].

Experiments carried out through spectroscopic techniques using laser light (coherent light) have made it possible to discover transcendental features in the dynamics of electronic excitation energy transfer and structure of various photosynthetic complexes [Jang and Mennucci, 2018; Cao et al., 2020]. However, these are not adapted to the natural conditions under which the energy transfer process in photosynthesis occurs, i.e., under excitation by incoherent light from the sun (see Fig. 4). An extensive discussion on this topic in recent years has shed light on the type of coherences induced by incoherent light excitation and their impact on the energy transfer process [Mančal and Valkunas, 2010; Brumer and Shapiro, 2012; Tscherbul and Brumer, 2014; Sadeq and Brumer, 2014; Grinev and Brumer, 2015; Dodin et al., 2016a,b; Pachón et al., 2017; Brumer, 2018; Chenu et al., 2014, 2015; Chenu and Brumer, 2016]. It is by now clear that the dynamics induced by suddenly-turned-on incoherent sunlight are qualitatively different from coherent laser sources and also different from a bare white-noise-source provided that the spectral density of incoherent radiation has a super-Ohmic character and does not induce pure dephasing dynamics [Pachón et al., 2017; Brumer, 2018; Mančal, 2020].

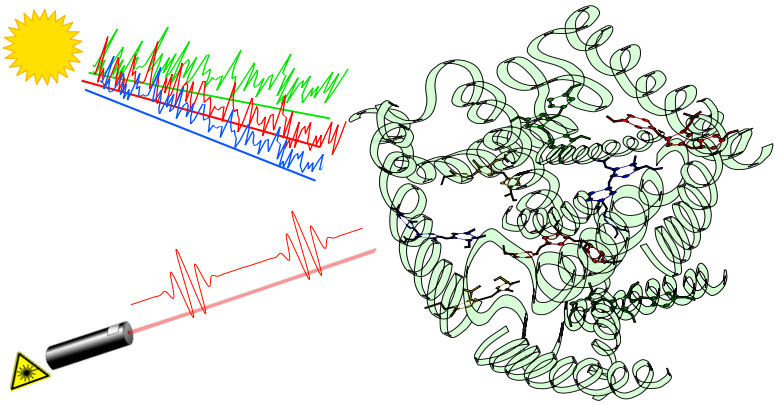

Figure 4. Light-induced processes such as energy transfer in light-harvesting systems are often studied in the laboratory using coherent pulsed laser sources, which induce a molecular response totally different than stationary incoherent thermal radiation, such as sunlight.

To account for that natural scenario in which chromophores harvest incoherent sunlight in the presence of localized (intramolecular) vibrational modes [Calderón and Pachón, 2020], in this thesis will be consider vibronic dimers formed by chromophores treated within the two-level approximation and a quantized intramolecular vibrational mode in interaction with each chromophore. The vibronic dimers are initially set up in their electronic ground and thermal equlibrium vibrational state. The excitation ignited by sunlight is then dissipated by a thermal phonon bath that accounts for the effects of the protein and solvent environments. The subsequent dynamics of the vibronic dimers are compared, in the site and exciton bases, with the dynamics of its corresponding electronic dimer with no specific intramolecular vibrational modes. Also, it will be shown that the state of intramolecular vibrations evolves devoid of non-trivial quantum correlations. As concrete examples, the two phycoerythrobilin chromophores from the protein-antenna phycoerythrin 545 and the two dihydrobiliverdin chromophores from the protein-antena phycocyanin 645 of marine cryptophyte algae are considered.

The final subject in this thesis is the discussion on whether classical light sources could induce the same effects as some quantum light sources on molecular systems confined in microcavities. The coupling of a molecular system to the confined photonic degrees of freedom in microcavities [Kavokin et al., 2007] can alter the molecular dynamics by changing the chemical landscape giving place to new photophysical [Ebbesen, 2016; Ribeiro et al., 2018; Ruggenthaler

et al., 2018; Flick et al., 2018; Dovzhenko et al., 2018; Herrera and Spano, 2018; Feist et al., 2018; Kockum et al., 2019; Hertzog et al., 2019; Herrera and Owrutsky, 2020]. It presents as a promising tool to control room-temperature photophysical processes in organic molecules. Evidence of these new phenomena has been discussed in the context of singlet fission [Martínez-Martínez et al., 2018], triplet harvesting [Martínez-Martínez et al., 2019], energy transfer [Zhong et al., 2016, 2017; Sáez-Blázquez et al., 2018; Du et al., 2018; Sáez-Blázquez et al., 2019], remote control of chemical reactions [Du et al., 2019], and nonadiabatic effects [Galego et al., 2015; Kowalewski et al., 2016a; Gu and Mukamel, 2020].

However, despite the nonadiabatic effects in the adiabatic ground state populations, evidence in the NaI molecule [Kowalewski et al., 2016a; Csehi et al., 2017] points to the lack of noticeable difference between the ignited by classical laser radiation and cavity-induced dynamics. In classical control theory [Shapiro and Brumer, 2003], light properties such as intensity and phase are utilized to modify the intrinsic dynamics of molecular reactions with classical laser-control schemes. While in quantum cavity chemistry, the quantum nature of light becomes essential for controlling the chemical landscape of molecular reactions [Ribeiro et al., 2018]. This situation has raised the interest in analyzing under what conditions classical radiation fields can produce the same molecular dynamics as light quantum states [Csehi et al., 2019]. In the present thesis, a second-order quantum-classical master equation formalism will be developed to address the direct comparison with a full quantum second-order master equation for the molecular system dynamics [Calderón and Pachón, 2021].

This thesis is organized as follows: Chapter 1 introduces the basic concepts and generalities of open quantum systems required to discuss the light-harvesting system dynamics. Chapter 2 discusses the relevance of intramolecular vibrational modes under sunlight illumination by analyzing the density matrix dynamics in the exciton and site bases of vibronic dimers. Chapter 3 analyzed the non-classical features of the reduced dynamics of intramolecular vibrational modes, comparing the illumination by coherent and incoherent light sources. Chapter 4 introduces a quantum-classical projection operator formalism to deduce a quantum-classical second-order master equation for a molecular system treating the light degrees of freedom classically, to explore the conditions to generate cavity chemistry effects without

cavities. Chapter 5 summarizes the findings.

1. Open quantum systems

This chapter addresses the generalities and main concepts of the theory of open quantum systems necessary for developing the next chapters. After it is realized that none physical system in nature is entirely isolated, the importance of open quantum systems theory is evident [Kubo et al., 1985; Gardiner, 1991; Mandel and Wolf, 1995; Cohen-Tannoudji et al., 1998; Breuer and Petruccione, 2002; Nitzan, 2006; Schlosshauer, 2007; May and Kühn, 2011; Weiss, 2012; Rivas and Huelga, 2012; Valkunas et al., 2013]. Thus, in the last decades, different methods, theoretical insights, and numerical techniques have been developed to describe more realistic open quantum system dynamics that account for non-markovian effects, strong coupling, structured environments, and low-temperature regimes [Xiong et al., 2015; Breuer et al., 2016; De Vega and Alonso, 2017].

Many research areas as quantum computing, condensed matter, quantum biology, chemical physics, and quantum optics have made significant progress due to advances in open quantum systems theory [De Vega and Alonso, 2017]. In the context of light-harvesting systems, such as photosynthetic complexes, the interplay of the pigment molecules with intra/inter-molecular vibrations and the incoherent sunlight radiation is critical to determine the electronic energy transfer dynamics [Pachón and Brumer, 2012; Huelga and Plenio, 2013; Levi et al., 2015; Jang and Mennucci, 2018; Mančal, 2020]. Thus, the system of pigment molecules represents an open quantum system in interaction with a low temperature (300 K) phonon bath (intermolecular vibrations) and a high temperature (5600 K) blackbody radiation bath [Pachón et al., 2017; Brumer, 2018; Calderón and Pachón, 2020]. Usually, intramolecular vibrational degrees of freedom, as those considered in the next chapter, are treated explicitly within the Hamiltonian of the open system. The energy of these intramolecular vibrations is comparable to the excitonic splitting. Thus, their energy is higher than the intermolecular degrees of freedom modeled in the phonon bath [Malý et al., 2016; Yeh et al., 2019; Calderón and Pachón, 2020].

This chapter is organized as follows: In the first section, the primary concepts related to the statistical operator will be established. In the second section, the basic concepts in the open quantum systems theory will be briefly discussed. The third section will focus on analyzing a second-order master equation, named the Redfield master

equation [May and Kühn, 2011; Pachón et al., 2017; Calderón and Pachón, 2020]. Finally, at the end of this chapter, a second-order quantum-classical master equation formalism will be developed to treat the environment degrees of freedom classically [Calderón and Pachón, 2021].

1.1. Density operator

The Schrödinger equation determines the time evolution of a closed system, i.e., one that is isolated from its environment

$$\mathrm{i}\hbar\frac{\partial\left|\psi(t)\right\rangle}{\partial t}=\hat{H}(t)\left|\psi(t)\right\rangle, \tag{1}$$

where $\hat{H}$ is the Hamiltonian of the closed system. All the physical information of this kind of systems is entirely encoded by a pure state $\left|\psi(t)\right\rangle$.

If a quantum system is in a mixed state, that is, in a statistical mixture of numbered pure states $\left\{\left|\psi_n(t)\right\rangle\right\}$, with probabilities $\{p_n\}$, it can be characterized by the density operator [Cohen-Tannoudji et al., 1992] defined as

$$\hat{\rho}(t)=\sum_n p_n\left|\psi_n(t)\right\rangle\left\langle\psi_n(t)\right|, \tag{2}$$

where the coefficients $p_n\geq 0$ satisfy the normalization condition $\sum_n p_n=1$. When all the coefficients $p_n=0$, except one of them $p_m=1$, the system is found in a pure state. The main properties of the density operator are:

- $\hat{\rho}^\dagger=\hat{\rho}$ (Hermiticity).
- $\mathrm{Tr}\,\hat{\rho}=1$ (Normalization)[1].
- $\mathrm{Tr}\,\hat{\rho}^2=1$ (Valid for pure states).
- $\mathrm{Tr}\,\hat{\rho}^2<1$ (Valid for mixed states).

---

[1] The symbol Tr refers to the trace of the operator analyzed and corresponds to the sum of the diagonal elements in a matrix representation for a complete orthonormal basis $\left|n\right\rangle$. $\mathrm{Tr}\hat{A}=\sum_n\left\langle n\right|\hat{A}\left|n\right\rangle=\sum_n A_{nn}$ [Breuer and Petruccione, 2002; May and Kühn, 2011].

- $\rho_{aa} \geq 0$ (Non-negative diagonal elements in any representation, see Eq. 4).
- $\rho_{aa}\rho_{bb} \geq |\rho_{ab}|^2$ (Schwartz inequality).

In terms of the density operator, the expected value of an operator $\hat{\mathcal{O}}$ reads $\langle\hat{\mathcal{O}}\rangle = \mathrm{Tr}\{\hat{\rho}\hat{\mathcal{O}}\}$. Differentiating Eq. (2) with respect to time and making use of the Schrödinger equation, the temporal evolution of the density operator obeys the von Neumann equation [Cohen-Tannoudji et al., 1992]

$$\frac{\mathrm{d}\hat{\rho}(t)}{\mathrm{d}t} = -\frac{\mathrm{i}}{\hbar}\left[\hat{H}(t), \hat{\rho}(t)\right]. \tag{3}$$

1.1.1. Populations and coherences: elements of the density matrix.

For a complete orthonormal basis of states $|a\rangle$, the density operator can be represented as

$$\hat{\rho} = \sum_{a,b}\langle a|\hat{\rho}|b\rangle|a\rangle\langle b| = \sum_{a,b}\rho_{ab}|a\rangle\langle b|. \tag{4}$$

The diagonal elements of the density matrix operator

$$\rho_{aa} = \langle a|\hat{\rho}|a\rangle = \langle a|\sum_n p_n|\psi_n\rangle\langle\psi_n|a\rangle = \sum_n p_n\left|\langle a|\psi_n\rangle\right|^2, \tag{5}$$

are interpreted as the probability of finding the state $|a\rangle$ in the statistical mixture described by the density operator $\hat{\rho}$. For the above, ρ_{aa} it is called the population of the state $|a\rangle$, that is, if the same measurement is carried out N times under the same conditions, N being a large number, $N\rho_{aa}$ systems will be in the state $|a\rangle$ [May and Kühn, 2011; Cohen-Tannoudji et al., 1992].

The non-diagonal elements of the density matrix operator

$$\rho_{ab} = \langle a|\hat{\rho}|b\rangle = \langle a|\sum_n p_n|\psi_n\rangle\langle\psi_n|b\rangle = \sum_n p_n\langle a|\psi_n\rangle\langle\psi_n|b\rangle = \sum_n p_n c_a(n)c_b^*(n), \tag{6}$$

are associated with the effects of quantum interference between the $|a\rangle$ and $|b\rangle$ states, when these are part of a coherent

linear superposition in the $|\psi_n\rangle$ state, i.e., ρ_{ab} corresponds to the average of the interference terms $c_a(n)c_b^*(n)$ over the statistical mixture described by the $\hat{\rho}$ operator. For this reason, the terms ρ_{ab} are called coherences [May and Kühn, 2011; Cohen-Tannoudji et al., 1992].

It is important to point out that the classification into populations and coherences for the matrix elements of the $\hat{\rho}$ density operator depends on the adopted basis $|a\rangle$. In particular, in the context of photosynthetic light-harvesting complexes, the site and exciton bases are important to discussing the relevance of long-lived quantum coherences reported with pulsed-laser sources in the context of the natural light-excitation scenario by incoherent sunlight [Pachón and Brumer, 2012; Levi et al., 2015; Mančal, 2020].

1.2. Open quantum systems: basic concepts

An open quantum system S couples to another system with many degrees of freedom, which represents the environment B. These two systems are part of a global system S + B, which is considered isolated. Occasionally, the open system S is called as the relevant system. As a consequence of the system-environment coupling, the system S dissipates part of its energy to the environment B and suffers a decay in its quantum correlations, named decoherence [Breuer and Petruccione, 2002; Nitzan, 2006; Weiss, 2012; May and Kühn, 2011; Schlosshauer, 2007]. The open quantum system theory plays a transcendental role in many applications of quantum physics, where isolation of the system is unfeasible, and a complete microscopic description or control of the degrees of freedom of the environment is not possible or only partially [Breuer and Petruccione, 2002; De Vega and Alonso, 2017; Weiss, 2012; Schlosshauer, 2007].

In the description of the problem using the system-reservoir approach [Breuer and Petruccione, 2002; May and Kühn, 2011; Weiss, 2012; Schlosshauer, 2007; Valkunas et al., 2013], the Hilbert space of the global system S + B is given by the tensor product $\mathscr{H}_{\mathrm{SB}} = \mathscr{H}_{\mathrm{S}} \otimes \mathscr{H}_{\mathrm{B}}$, where $\mathscr{H}_{\mathrm{S}}$ and $\mathscr{H}_{\mathrm{B}}$ represent the Hilbert spaces of the system S and the environment B, respectively. The Hamiltonian of the global system S + B can be written in the form

$$\hat{H} = \hat{H}_{\mathrm{S}} + \hat{H}_{\mathrm{B}} + \hat{H}_{\mathrm{SB}}, \tag{7}$$

where $\hat{H}_{\mathrm{S}}$ represents the free Hamiltonian for the system S, $\hat{H}_{\mathrm{B}}$ the free Hamiltonian for the environment B, and $\hat{H}_{\mathrm{SB}}$ the interaction Hamiltonian, which describes the coupling between the open quantum system S and the environment B [Breuer and Petruccione, 2002; Rivas and Huelga, 2012; Weiss, 2012; Schlosshauer, 2007].

The quantum state of the global system $\mathrm{S}+\mathrm{E}$ is described by the density operator $\hat{\rho}_{\mathrm{SB}}$ and follows the von Neumann equation

$$\frac{\mathrm{d}}{\mathrm{d}t}\hat{\rho}_{\mathrm{SB}}(t) = -\frac{\mathrm{i}}{\hbar}\left[\hat{H}, \hat{\rho}_{\mathrm{SB}}(t)\right]. \tag{8}$$

Usually, the open quantum system has few degrees of freedom, while the environment has many degrees of freedom, generally considered infinitely large. In statistical mechanics the environment represents a reservoir, if its degrees of freedom are infinite. Moreover, if it is in a state of thermal equilibrium, such a reservoir is considered as a thermal bath [Breuer and Petruccione, 2002; Rivas and Huelga, 2012; May and Kühn, 2011; Valkunas et al., 2013].

The primary purpose in the theory of open quantum systems is to avoid the integration of the global system, that is, the open quantum system of interest S together with its environment B, due to the enormous number of degrees of freedom involved. Additionally, the physical effects of interest, both their identification and interpretation, are associated with the dynamics of the open quantum system S, so the explicit dynamics of the environment is not relevant, but its effect on the system S. It is achieved by describing the dynamics of the open quantum system S in terms of the reduced density operator, as it will be analyzed later [Breuer and Petruccione, 2002; Rivas and Huelga, 2012; May and Kühn, 2011; Weiss, 2012; Schlosshauer, 2007; Valkunas et al., 2013].

1.2.1. Reduced density operator.

The global system $\mathrm{S}+\mathrm{B}$ described by the density operator $\hat{\rho}_{\mathrm{SB}}(t)$, evolves according to the von Neumann equation (3) through the Hamiltonian of Eq. (7) [Breuer and Petruccione, 2002; Rivas and Huelga, 2012; Weiss, 2012; Schlosshauer, 2007]. The dynamics of the open quantum system S is described by means of the reduced density operator, which is calculated tracing over the degrees of freedom of the environment B of the global system density operator $\mathrm{S}+\mathrm{B}$. Thus, the reduced density operator of the open quantum system S is given by

$$\hat{\rho}_{\mathrm{S}}(t) = \mathrm{Tr}_{\mathrm{B}}\,\hat{\rho}_{\mathrm{SB}}(t) = \mathrm{Tr}_{\mathrm{B}}\{\hat{U}(t,t_0)\hat{\rho}_{\mathrm{SB}}(t_0)\hat{U}^{\dagger}(t,t_0)\}, \tag{9}$$

where $\hat{U}$ represents the evolution operator of the global system $S+B$.

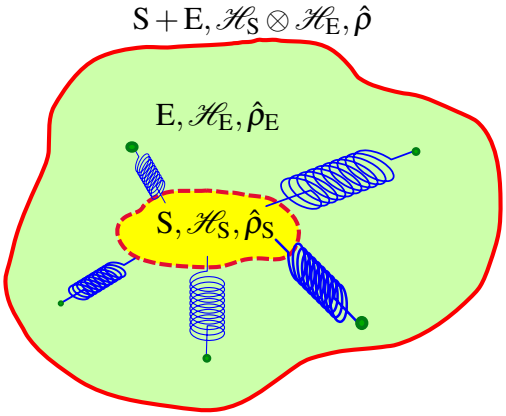

Figure 5. Open system-Environment representation.

The influence of the environment B over the system S leads to a non-unitary dynamics, which is evidenced through dissipation and decoherence [Breuer and Petruccione, 2002; Rivas and Huelga, 2012; May and Kühn, 2011; Weiss, 2012; Schlosshauer, 2007]. The expected value of an operator $\hat{\mathscr{A}}$ defined in the Hilbert space $\mathscr{H}_S$ of the open quantum system S is computed by means of reduced density operator

$$\langle \hat{\mathscr{A}} \rangle = \mathrm{Tr}_S\{\hat{\mathscr{A}}\hat{\rho}_S\}. \tag{10}$$

1.2.2. Quantum dynamical maps.

Considering there is no initial correlations between the system and the environment, the initial state of the global system S + B is given by

$$\hat{\rho}_{SB}(0) = \hat{\rho}_S(0) \otimes \hat{\rho}_B(0). \tag{11}$$

The reduced density operator of the open quantum system S as a function of time $t \geq 0$ reads

$$\hat{\rho}_S(t) = \mathrm{Tr}_B\{\hat{U}(t)\hat{\rho}_S(0) \otimes \hat{\rho}_B(0)\hat{U}^\dagger(t)\}. \tag{12}$$

For an fixed initial environment state $\hat{\rho}_{\mathrm{B}}(0)$, Eq. (12) defines a lineal map $\Phi(t,0)$ over the open quantum system Hilbert space $\mathscr{H}_{\mathrm{S}}$, that transforms the initial state $\hat{\rho}_{\mathrm{S}}(0)$ to the state $\hat{\rho}_{\mathrm{S}}(t)$ at the time t

$$\hat{\rho}_{\mathrm{S}}(0) \mapsto \hat{\rho}_{\mathrm{S}}(t) = \Phi(t,0)\hat{\rho}_{\mathrm{S}}(0). \tag{13}$$

Φ is named quantum dynamical map. This map preserves the hermiticity $(\Phi(t,0)\hat{\mathscr{A}})^{\dagger} = \Phi(t,0)\hat{\mathscr{A}}^{\dagger}$ and the trace of operators $\mathrm{Tr}_{\mathrm{S}}\{\Phi(t,0)\hat{\mathscr{A}}\} = \mathrm{Tr}_{\mathrm{S}}\{\hat{\mathscr{A}}\}$. Aditionally, $\Phi(t,0)$ represents a positive map, i.e., which transforms positive operators to positive operators $\hat{\mathscr{A}} \geq 0 \Longrightarrow \Phi(t,0)\hat{\mathscr{A}} \geq 0$, which means a transformation of physical states to physical states, therefore, the probabilities remain positive under the map [Breuer, 2012; Rivas et al., 2014]. The dynamical map $\Phi(t,0)$ is also completely positive. The dynamical map $\Phi(t,0)$ is completely positive if and only if admits a Kraus representation, such that $\Phi\hat{\mathscr{A}} = \sum_i \hat{\Omega}_i \hat{\mathscr{A}} \hat{\Omega}_i^{\dagger}$, for operators $\hat{\Omega}_i$ of the Hilbert space $\mathscr{H}_{\mathrm{S}}$, where the trace is preserved if and only if the normalization condition $\sum_i \hat{\Omega}_i^{\dagger}\hat{\Omega}_i = \hat{1}_{\mathrm{S}}$ is satisfied [Breuer, 2012; Rivas et al., 2014].

The complete positivity guarantees that not only all the physical states of S are transformed to physical states of S, but, also that all the physical states of the global system $\mathrm{S}+\mathrm{R}$ are transformed to physical states of the global system $\mathrm{S}+\mathrm{R}$ [Breuer, 2012; Rivas et al., 2014]. If the t parameter in $\Phi(t,0)$ is allowed to vary, keeping the initial state of the environment fixed $\hat{\rho}_{\mathrm{B}}(0)$, it gets a one-parameter family of completely positive dynamic maps that preserve the trace

$$\{\Phi(t,0) \mid t \geq 0, \Phi(0,0) = \hat{1}\}. \tag{14}$$

This family defines a *quantum process* for the opem system S.

Assuming a smooth temporal dependence and differentiating Eq. (13) with respect to time

$$\frac{\mathrm{d}\hat{\rho}_{\mathrm{S}}(t)}{\mathrm{d}t} = \dot{\Phi}(t,0)\hat{\rho}_{\mathrm{S}}(0), \tag{15}$$

where the dot indicates the derivative with respect to time of $\Phi(t,0)$. In order to obtain a time-local master equation,

the map defined in Eq. (13) can be inverted, so Eq. (15) can be expressed in the form

$$\frac{\mathrm{d}\hat{\rho}_{\mathrm{S}}(t)}{\mathrm{d}t} = \dot{\Phi}(t,0)\Phi(t,0)^{-1}\hat{\rho}_{\mathrm{S}}(t). \tag{16}$$

The linear application $\mathscr{K}(t) = \dot{\Phi}(t,0)\Phi(t,0)^{-1}$ can be defined as a time-dependent generator for the reduced density operator dynamics $\hat{\rho}_{\mathrm{S}}$, which leads to a local master time equation for the open quantum system S

$$\frac{\mathrm{d}\hat{\rho}_{\mathrm{S}}(t)}{\mathrm{d}t} = \mathscr{K}(t)\hat{\rho}_{\mathrm{S}}(t). \tag{17}$$

The above equation does not imply an integration over the past history of the reduced density operator, as in the case of the Nakajima-Zwanzig master equation [Breuer and Petruccione, 2002]. The generator $\mathscr{K}(t)$ of the time-local master equation must preserve hermiticity $(\mathscr{K}(t)\hat{\mathscr{A}})^{\dagger} = \mathscr{K}(t)\hat{\mathscr{A}}^{\dagger}$ and the trace $\mathrm{Tr}_{\mathrm{S}}\{\mathscr{K}(t)\hat{\mathscr{A}}\} = 0$ [Breuer, 2012]. Using the method of projection operators without time convolution [Breuer and Petruccione, 2002] it is possible to obtain an equation in the form (17) for small and intermediate couplings in the case of an initial state not correlated between system and environment. Equation (17) represents an ideal starting point for a perturbative expansion of the generator $\mathscr{K}(t)$ in powers with respect to a coupling parameter α. In this way, the generator can be expanded in the form

$$\mathscr{K}(t) = \sum_{n=1}^{\infty} \alpha^n \mathscr{K}_n(t). \tag{18}$$

1.2.3. Markovian quantum processes. A family of dynamical quantum maps $\Phi(t,0)$ corresponds to a Markovian (divisible) process if [Rivas and Huelga, 2012; De Vega and Alonso, 2017; Rivas et al., 2014] for all $t_2 \geq t_1 \geq 0$ exits a dynamical map $\Phi(t_2,t_1)$ completely positive that preserves the trace, such that the next relation is satisfied

$$\Phi(t_2,0) = \Phi(t_2,t_1)\Phi(t_1,0). \tag{19}$$

An operator $\mathscr{L}$ represents the generator of a Markovian quantum process for the system S if and only if can be written as [Rivas and Huelga, 2012; Rivas et al., 2014]

$$\frac{\mathrm{d}\hat{\rho}_{\mathrm{S}}(t)}{\mathrm{d}t} = \mathscr{L}[\hat{\rho}_{\mathrm{S}}(t)] = -i\left[\hat{H}_{\mathrm{S}}, \hat{\rho}_{\mathrm{S}}\right] + \sum_i \gamma_i(t)\left(\hat{\mathscr{A}}_i \hat{\rho}_{\mathrm{S}}(t)\hat{\mathscr{A}}_i^{\dagger} - \frac{1}{2}\left\{\hat{\mathscr{A}}_i^{\dagger}\hat{\mathscr{A}}_i, \hat{\rho}_{\mathrm{S}}(t)\right\}\right), \tag{20}$$

where $\hat{H}_{\mathrm{S}}$ is a self-adjont Hamiltonian operator of the system S which not necessarily coincides with the one considered in Eq. (7), $\hat{\mathscr{A}}_i$ represent Lindblad operators of the system S, and $\gamma_i(t) \geq 0$ for all i and time t, are the relaxation coefficients [Breuer and Petruccione, 2002; Rivas and Huelga, 2012; Breuer, 2012; Rivas et al., 2014]. Equation 20 is known as the Lindblad master equation and represents one the cornerstones in the theory of open quantum systems.

From the classical random processes theory, Markovian processes are defined as memory-less processes. To understand this interpretation from the open quantum system viewpoint, it considers that the open quantum system S and the environment B interact through a sequence of individual collisions at times $t_1, t_2, \ldots, t_n$ as considered by Rivas et. al. [Rivas et al., 2014] Each collision produces a change in the state of the system $\hat{\rho}_{\mathrm{S}}$ given by

$$\hat{\rho}_{\mathrm{S}}(t_{n+1}) = \mathrm{Tr}_{\mathrm{B}}\left[\hat{U}(t_{n+1}, t_n)\hat{\rho}_{\mathrm{S}}(t_n) \otimes \hat{\rho}_{\mathrm{B}}\hat{U}^{\dagger}(t_{n+1}, t_n)\right] = \Phi(t_{n+1}, t_n)\hat{\rho}_{\mathrm{S}}(t_n), \tag{21}$$

where $\hat{\rho}_{\mathrm{B}}$ it is considered invariant under each collision. Since $\Phi(t_{n+1}, t_n)$ represents a completely positive map. The successive concatenations of the collisions lead to a quantum markovian process in such a way that if

$$\hat{\rho}_{\mathrm{S}}(t_{n+2}) = \Phi(t_{n+2}, t_n)\hat{\rho}_{\mathrm{S}}(t_n), \tag{22}$$

then

$$\hat{\rho}_{\mathrm{S}}(t_{n+2}) = \Phi(t_{n+2}, t_{n+1})\hat{\rho}_{\mathrm{S}}(t_n + 1) = \Phi(t_{n+2}, t_{n+1})\Phi(t_{n+1}, t_n)\hat{\rho}_{\mathrm{S}}(t_n), \tag{23}$$

Therefore, it is concluded that

$$\Phi(t_{n+2}, t_n) = \Phi(t_{n+2}, t_{n+1})\Phi(t_{n+1}, t_n). \tag{24}$$

In this way, a completely positive process $\Phi\hat{\rho}_{\mathrm{S}}$ can be understood as the reduced dynamics of some unitary evolution acting on a global system $\hat{\rho}_{\mathrm{S}} \otimes \hat{\rho}_{\mathrm{B}}$, where $\hat{\rho}_{\mathrm{B}}$ is invariant and independent of $\hat{\rho}_{\mathrm{S}}$. Therefore, in the context of open quantum systems, Markovian quantum processes can be understood as a sequence of interactions without memory, where the state of the environment is the same, that is, the environment B has no memory of the interaction with the system S, and the state of the global system $\mathrm{S}+\mathrm{B}$ is uncorrelated in each interaction as if there were no previous interaction [Rivas et al., 2014].

1.2.4. Non-Markovian quantum processes. In many circumstances the correlation time of the environment is not small compared to the relaxation time of the system, so it is not correct to consider a Markovian approach. This may be due to strong coupling between the system and the environment, finite or structured environments, low temperatures, or strong initial correlations between the system and the environment [De Vega and Alonso, 2017; Breuer et al., 2016]. In these cases, where there is a substantial deviation from the dynamics of a Markovian quantum process, it is considered as a non-Markovian process.

Non-Markovian quantum processes dynamics based on equations for the reduced density operator, some techniques stand out, such as: the formalism of Nakajima-Zwanzig projection operators, derivation of local master equations in time using the method of projection operators without time convolution, the functional of influence method by means of trajectory integrals [Grabert et al., 1988], among others [De Vega and Alonso, 2017]. Although recently there have been significant advances in the quantification of non-Markovian dynamics through the structuring of different measures of non-Markovianity, the study of non-Markovian processes represents a field in constant development and with great challenges to be solved [Breuer et al., 2016; De Vega and Alonso, 2017; Rivas et al., 2014].

To quantify the non-markovian character of a quantum process, in recent years have been introduced different measures of non-markovianity based on the deviation from a divisible application and the quantification of the return of information from the environment to during the system dynamics, through functions that assign a positive number or zero, so that the zero value is obtained if and only if the process is markovian [De Vega and Alonso, 2017; Rivas et al., 2014; Breuer et al., 2016].

1.3. Dynamics of open quantum systems

In this section, it will be discussed the time evolution equations for the reduced density operator, which will determine the dynamics of the open quantum system S, these equations are called master equations. Several techniques have been developed to deduce master equations that account for the main physical effects due to the influence of the environment over the open quantum system [Kubo et al., 1985; Gardiner, 1991; Mandel and Wolf, 1995; Cohen-Tannoudji et al., 1998; Nitzan, 2006; Schlosshauer, 2007; May and Kühn, 2011; Weiss, 2012; Rivas and Huelga, 2012; Valkunas et al., 2013; Breuer and Petruccione, 2002]. Here, the focus will be on the projection operator techniques.

From the von Neumann equation (Eq. 8) and the reduced density operator definition Eq. (9), it follows

$$\frac{\mathrm{d}\hat{\rho}_{\mathrm{S}}(t)}{\mathrm{d}t} = -\frac{\mathrm{i}}{\hbar}\,\mathrm{Tr}_{\mathrm{B}}\left[\hat{H},\hat{\rho}_{\mathrm{SB}}(t)\right], \tag{25}$$

with the Hamiltonian of the global system $\hat{H} = \hat{H}_{\mathrm{S}} + \hat{H}_{\mathrm{B}} + \hat{H}_{\mathrm{SB}}$.

$$\frac{\mathrm{d}\hat{\rho}_{\mathrm{S}}(t)}{\mathrm{d}t} = -\frac{\mathrm{i}}{\hbar}\left[\hat{H}_{\mathrm{S}},\hat{\rho}_{\mathrm{S}}\right] - \frac{\mathrm{i}}{\hbar}\,\mathrm{Tr}_{\mathrm{B}}\left[\hat{H}_{\mathrm{SB}},\hat{\rho}_{\mathrm{SB}}\right], \tag{26}$$

The above equation is not a closed equation for the reduced density operator, since the global density operator $\hat{\rho}_{\mathrm{SB}}$ still appears. In the following sections, this problem will tackle through projection operator techniques that lead to master equations that describe the dynamics of the reduced density operator only. If $\hat{H}_{\mathrm{SB}} = 0$, the equation of motion for the reduced density operator correspond to the von Neumann equation, describing the isolated dynamics of the open system S.

1.3.1. Projection operator techniques.

The projection operator techniques allow to obtain an equation of motion for the reduced density operator of the open quantum system S by making a projection onto the relevant part of the global density operator [Mandel and Wolf, 1995; Breuer and Petruccione, 2002; Nitzan, 2006; May and Kühn, 2011; Weiss, 2012; Rivas and Huelga, 2012; Valkunas et al., 2013; De Vega and Alonso, 2017] . Therefore,

the operation of tracing of the environment degrees of freedom is achieved as a formal projection $\hat{\rho} \mapsto \mathcal{P}\hat{\rho}$ in the state space of the global system. Thus, the projection operator $\mathcal{P}$ is defined in such a way that the relevant part of the global density operator is given by

$$\mathcal{P}\hat{\rho}_{\mathrm{SB}} = \hat{\rho}_{\mathrm{B}}(t_0)\,\mathrm{Tr}_{\mathrm{B}}\{\hat{\rho}_{\mathrm{SB}}\}, \tag{27}$$

where $\hat{\rho}_{\mathrm{B}}(t_0)$ is the initial state of the environment.

The projection operator $\mathcal{P}$ is defined according to the physical situation analyzed, that in most cases corresponds to an environment modeled as a reservoir of infinite degrees of freedom in a thermal equilibrium state, i.e., a thermal bath [Breuer and Petruccione, 2002; De Vega and Alonso, 2017], and described by the density operator

$$\hat{\rho}_{\mathrm{B,eq}} = \frac{\mathrm{e}^{-\beta\hat{H}_{\mathrm{B}}}}{\mathrm{Tr}_{\mathrm{B}}\,\mathrm{e}^{-\beta\hat{H}_{\mathrm{B}}}}, \tag{28}$$

where $\beta = 1/k_{\mathrm{B}}T$, k_{B} represents the Boltzmann constant, and T the temperature of the bath. In this scenario, the projection operator $\mathcal{P}$ is defined as

$$\mathcal{P}\hat{\rho}_{\mathrm{SB}} = \hat{\rho}_{\mathrm{B,eq}}\,\mathrm{Tr}_{\mathrm{B}}\,\hat{\rho}_{\mathrm{SB}}. \tag{29}$$

This projection operator is know as the thermal projector [Nitzan, 2006], since the choice of the thermal equilibrium state for the environment initial state. Therefore, the reduced density operator for the system S corresponds to $\hat{\rho}_{\mathrm{S}} = \mathrm{Tr}_{\mathrm{B}}\,\mathcal{P}\hat{\rho}_{\mathrm{SB}}$, since $\mathrm{Tr}_{\mathrm{B}}\,\hat{\rho}_{\mathrm{B,eq}} = 1$. The complementary projector $\mathcal{Q}$ satisfies

$$\mathcal{Q}\hat{\rho}_{\mathrm{SB}} = \hat{\rho}_{\mathrm{SB}} - \mathcal{P}\hat{\rho}_{\mathrm{SB}}, \tag{30}$$

and defines the irrelevant part $\mathcal{Q}\rho$ (environment) of the global system. Since $\mathrm{Tr}_{\mathrm{B}}\,\hat{\rho}_{\mathrm{B,eq}} = 1$ and $\mathrm{Tr}_{\mathrm{S}}\,\hat{\rho}_{\mathrm{S}} = 1$, the projector operators are idempotent, $\mathcal{P}^2 = \mathcal{P}$ and $\mathcal{Q}^2 = \mathcal{Q}$. Besides, by construction they satisfy $\mathcal{P}\mathcal{Q} = \mathcal{Q}\mathcal{P} = 0$, and $\mathcal{P} + \mathcal{Q} = 1$.

In the interaction picture [Cohen-Tannoudji et al., 1992; Weinberg, 2015; May and Kühn, 2011] the von

Neumann equation for the global system (Eq 8) reads

$$\frac{\mathrm{d}\hat{\rho}_{\mathrm{SB}}^{(\mathrm{I})}(t)}{\mathrm{d}t} = -i\mathcal{L}_{\mathrm{SB}}^{(\mathrm{I})}(t)\hat{\rho}_{\mathrm{SB}}^{(\mathrm{I})}(t). \tag{31}$$

Here the Liouvillian operator is given by $\mathcal{L}_{\mathrm{SB}}^{(\mathrm{I})}(t)\bullet = \frac{1}{\hbar}\left[\hat{H}_{\mathrm{SB}}^{(\mathrm{I})}(t), \bullet\right]$. The superindex (I) denotes operators in the interaction picture. By means of the property $\mathcal{P}+\mathcal{Q}=1$, and the the application of the projection operators over the von Neumann equation (31) leads to equations of motion for both subspaces relevant (open system) and irrelevant (environment)

$$\frac{\mathrm{d}}{\mathrm{d}t}\mathcal{P}\hat{\rho}_{\mathrm{SB}}^{(\mathrm{I})} = -\mathrm{i}\mathcal{P}\mathcal{L}_{\mathrm{SB}}^{(\mathrm{I})}(t)\hat{\rho}_{\mathrm{SB}}^{(\mathrm{I})} = -\mathrm{i}\mathcal{P}\mathcal{L}_{\mathrm{SB}}^{(\mathrm{I})}(t)\mathcal{P}\hat{\rho}_{\mathrm{SB}}^{(\mathrm{I})} - \mathrm{i}\mathcal{P}\mathcal{L}_{\mathrm{SB}}^{(\mathrm{I})}(t)\mathcal{Q}\hat{\rho}_{\mathrm{SB}}^{(\mathrm{I})}, \tag{32}$$

$$\frac{\mathrm{d}}{\mathrm{d}t}\mathcal{Q}\hat{\rho}_{\mathrm{SB}}^{(\mathrm{I})} = -\mathrm{i}\mathcal{Q}\mathcal{L}_{\mathrm{SB}}^{(\mathrm{I})}(t)\hat{\rho}_{\mathrm{SB}}^{(\mathrm{I})} = -\mathrm{i}\mathcal{Q}\mathcal{L}_{\mathrm{SB}}^{(\mathrm{I})}(t)\mathcal{P}\hat{\rho}_{\mathrm{SB}}^{(\mathrm{I})} - \mathrm{i}\mathcal{Q}\mathcal{L}_{\mathrm{SB}}^{(\mathrm{I})}(t)\mathcal{Q}\hat{\rho}_{\mathrm{SB}}^{(\mathrm{I})}. \tag{33}$$

Solving this set of coupled equations leads to the the Nakajima-Zwanzig master equation [Mandel and Wolf, 1995; Breuer and Petruccione, 2002; Nitzan, 2006; May and Kühn, 2011; Weiss, 2012; Rivas and Huelga, 2012; Valkunas et al., 2013; Nakajima, 1958; Zwanzig, 1960]

$$\begin{aligned}\frac{\mathrm{d}}{\mathrm{d}t}\hat{\rho}_{\mathrm{S}}^{(\mathrm{I})}(t) = &-\mathrm{i}\,\mathrm{Tr}_{\mathrm{B}}\left\{\mathcal{L}_{\mathrm{SB}}^{(\mathrm{I})}(t)\hat{\rho}_{\mathrm{B,eq}}\right\}\hat{\rho}_{\mathrm{S}}^{(\mathrm{I})}(t) - \mathrm{i}\mathcal{P}\mathcal{L}_{\mathrm{SB}}^{(\mathrm{I})}(t)\mathscr{G}(t,t_0)\mathcal{Q}\rho_{\mathrm{SB}}(t_0)\\ &-\int_{t_0}^{t}\mathrm{d}t'\,\mathrm{Tr}_{\mathrm{B}}\left\{\mathcal{L}_{\mathrm{SB}}^{(\mathrm{I})}(t)\mathscr{G}(t,t')\mathcal{Q}\mathcal{L}_{\mathrm{SB}}^{(\mathrm{I})}(t')\hat{\rho}_{\mathrm{B,eq}}\right\}\hat{\rho}_{\mathrm{S}}^{(\mathrm{I})}(t),\end{aligned} \tag{34}$$

where $\mathscr{G}(t,t') = \mathscr{T}\exp\left\{-\mathrm{i}\int_{t'}^{t}\mathrm{d}\tau\mathcal{Q}\mathcal{L}_{\mathrm{SB}}^{(\mathrm{I})}(\tau)\right\}$. The time-ordered operator $\mathscr{T}$ denotes chronological time ordering of any product of operators such that the time arguments increase from right to left The first term of the right-hand side of Eq. (34) describe the mean field contribution to the unitary dynamics of the open system S, (see Eq. 38 below). The second term takes into account the initial correlations between the open system and the environment. Thus, For a factorizing initial condition $\hat{\rho}_{\mathrm{SB}}(t_0) = \hat{\rho}_{\mathrm{S}}(t_0)\otimes\hat{\rho}_{\mathrm{B}}(t_0)$, i.e., an uncorrelated initial state of the global system, the second term of the Nakajima Zwanzig master equation vanishes. The last term describes the non-Markovian memory effects on the open system dynamics derive from the coupling to the environment.

The Nakajima-Zwanzig master equation (34) is an exact integro-differential equation that encompass a time integration over the history of the open quantum system [Breuer and Petruccione, 2002]. Because of that, it is challenging to solve, almost as much as solving the entire global dynamics of the open system and the environment on the whole. Nevertheless, it represents a starting reference to develop a perturbative analysis (see section 1.3.2). Alternatively to the Nakajima-Zwanzig master equation, it has been developed a time-convolutionless projection operator technique that results in a first-order differential time-local equation [Breuer and Petruccione, 2002; May and Kühn, 2011; Valkunas et al., 2013; Rivas and Huelga, 2012; De Vega and Alonso, 2017].

1.3.2. Second-order quantum master equation. The projection operator formalism analyzed above can be employed to perform a perturbation expansion at second-order of the system-environment interaction Hamiltonian $\hat{H}_{\mathrm{SB}}$ (*weak coupling limit / Born approximation*) for the reduced density operator dynamics [May and Kühn, 2011; Breuer and Petruccione, 2002; Nitzan, 2006]. This represents a good approximation if the coupling between the system and the environment is weaker than the energy scales within the open system S. Rewriting the equations of motion 32 and 33 for the relevant and irrelevant subspaces

$$\mathrm{Tr}_{\mathrm{B}}\left[\frac{\mathrm{d}}{\mathrm{d}t}\mathcal{P}\hat{\rho}_{\mathrm{SB}}^{(\mathrm{I})}(t)\right] = -\frac{\mathrm{i}}{\hbar}\,\mathrm{Tr}_{\mathrm{B}}\left[\hat{H}_{\mathrm{SB}}^{(\mathrm{I})}(t), \hat{\rho}_{\mathrm{B,eq}}\hat{\rho}_{\mathrm{S}}^{(\mathrm{I})}(t) + \mathcal{Q}\hat{\rho}_{\mathrm{SB}}^{(\mathrm{I})}(t)\right], \tag{35}$$

$$\frac{\mathrm{d}}{\mathrm{d}t}\mathcal{Q}\hat{\rho}_{\mathrm{SB}}^{(\mathrm{I})}(t) = -\frac{\mathrm{i}}{\hbar}\mathcal{Q}\left[\hat{H}_{\mathrm{SB}}^{(\mathrm{I})}(t), \hat{\rho}_{\mathrm{B,eq}}\hat{\rho}_{\mathrm{S}}^{(\mathrm{I})}(t) + \mathcal{Q}\hat{\rho}_{\mathrm{SB}}^{(\mathrm{I})}(t)\right], \tag{36}$$

where the trace over the environment degrees of freedom was taken in the equation of motion of $\mathcal{P}\hat{\rho}_{\mathrm{SB}}^{(\mathrm{I})}$, so that $\frac{\mathrm{d}}{\mathrm{d}t}\hat{\rho}_{\mathrm{S}}^{(\mathrm{I})} = \mathrm{Tr}_{\mathrm{B}}\left\{\frac{\mathrm{d}}{\mathrm{d}t}\mathcal{P}\hat{\rho}_{\mathrm{SB}}^{(\mathrm{I})}\right\}$. Equations (35) and (36) allow for a systematic perturbative approach in terms of the strength of the interaction term $\hat{H}_{\mathrm{SB}}$. Since the contribution of $\mathcal{Q}\hat{\rho}_{\mathrm{SB}}^{(\mathrm{I})}$ in $\mathrm{Tr}_{\mathrm{B}}\,\mathcal{Q}\hat{\rho}_{\mathrm{SB}}^{(\mathrm{I})}$ is of second orden in $\hat{H}_{\mathrm{SB}}^{(\mathrm{I})}$, the first order contribution corresponds to neglect the term $\mathcal{Q}\hat{\rho}_{\mathrm{SB}}^{(\mathrm{I})}$ in Eq. (35). To explore more concretely this approximation, assume that the system-environment interaction Hamiltonian $\hat{H}_{\mathrm{SB}}$ can be written in the general form [May and Kühn, 2011; De Vega and Alonso, 2017]

$$\hat{H}_{\mathrm{SB}}^{(\mathrm{I})}(t) = \sum_{u}\hat{K}_{u}^{(\mathrm{I})}(t)\hat{\Phi}_{u}^{(\mathrm{I})}(t), \tag{37}$$

being $\left\{\hat{K}_u\right\}$ observables of the open system and $\left\{\hat{\Phi}_u\right\}$ observables of the environment.

At first-order approximation, the reduced density operator evolves according

$$\frac{\mathrm{d}}{\mathrm{d}t}\hat{\rho}_{\mathrm{S}}^{(\mathrm{I})(1)}(t) = -\frac{\mathrm{i}}{\hbar}\sum_u \left[\hat{K}_u^{(\mathrm{I})}(t)\left\langle\hat{\Phi}_u\right\rangle_{\mathrm{B}}, \hat{\rho}_{\mathrm{S}}^{(\mathrm{I})}(t)\right] = -\frac{\mathrm{i}}{\hbar}\left[\hat{H}_{\mathrm{mf}}^{(\mathrm{I})}(t), \hat{\rho}_{\mathrm{S}}^{(\mathrm{I})}(t)\right], \tag{38}$$

with $\hat{H}_{\mathrm{mf}}^{(\mathrm{I})}(t) = \sum_u \hat{K}_u^{(\mathrm{I})}(t)\left\langle\hat{\Phi}_u^{(\mathrm{I})}\right\rangle_{\mathrm{B}}$ being the mean field contribution. The expected value of the environment observables is given by $\left\langle\hat{\Phi}_u\right\rangle_{\mathrm{B}} = \left\langle\hat{\Phi}_u^{(\mathrm{I})}(t)\right\rangle_{\mathrm{B}} = \mathrm{Tr}_{\mathrm{B}}\left\{\hat{\Phi}_u\hat{\rho}_{\mathrm{B,eq}}\right\}$. Since the thermal equilibrium state of the environment has identical form in the Schrödinger and interaction pictures $\hat{\rho}_{\mathrm{B,eq}} = \hat{\rho}_{\mathrm{B,eq}}^{(\mathrm{I})}$. The mean field contribution introduces an overall energy shift to the system Hamiltonian $\hat{H}_{\mathrm{S}}$ [May and Kühn, 2011; Nitzan, 2006]. Usually, this contribution is neglected or taking into account by redefining the system Hamiltonian $\hat{H}_{\mathrm{S}}$.

The second-order contribution is calculated by inserting a first-order solution of Eq. (36) in $\hat{H}_{\mathrm{SB}}$, which is obtained by neglecting the term $\mathcal{Q}\hat{\rho}^{(\mathrm{I})}$ in the right hand side of Eq. (36)

$$\mathcal{Q}\hat{\rho}_{\mathrm{SB}}^{(\mathrm{I})}(t) = -\frac{\mathrm{i}}{\hbar}\int_{t_0}^{t}\mathrm{d}\tau\mathcal{Q}\left[\hat{H}_{\mathrm{SB}}^{(\mathrm{I})}(\tau), \hat{\rho}_{\mathrm{B,eq}}\hat{\rho}_{\mathrm{S}}^{(\mathrm{I})}(\tau)\right], \tag{39}$$

where it has taken $\mathcal{Q}\hat{\rho}_{\mathrm{SB}}^{(\mathrm{I})}(t_0) = 0$, since initially the relevant system and the environment are decoupled, i.e., $\hat{\rho}_{\mathrm{SB}}(t_0) = \hat{\rho}_{\mathrm{S}}(t_0)\otimes\hat{\rho}_{\mathrm{B,eq}}$ (*uncorrelated initial global state*). Replacing the Eq. (39) in the Eq. (35), and introducing the environmental correlation functions $C_{uv}(t,\tau)$, the second-order reduced master equation for the open system reads [Breuer and Petruccione, 2002; May and Kühn, 2011; Nitzan, 2006; Valkunas et al., 2013]

$$\begin{aligned}\frac{\mathrm{d}}{\mathrm{d}t}\hat{\rho}_{\mathrm{S}}^{(\mathrm{I})(2)}(t) = &-\frac{\mathrm{i}}{\hbar}\sum_u\left\langle\hat{\Phi}_u\right\rangle\left[\hat{K}_u^{(\mathrm{I})}(t), \hat{\rho}_{\mathrm{S}}^{(\mathrm{I})}(t)\right] \\ &-\sum_{uv}\int_{t_0}^{t}\mathrm{d}\tau\left(C_{uv}(t-\tau)\left[\hat{K}_u^{(\mathrm{I})}(t), \hat{K}_v^{(\mathrm{I})}(\tau)\hat{\rho}_{\mathrm{S}}^{(\mathrm{I})}(\tau)\right] - C_{vu}(\tau-t)\left[\hat{K}_u^{(\mathrm{I})}(t), \hat{\rho}_{\mathrm{S}}^{(\mathrm{I})}(\tau)\hat{K}_v^{(\mathrm{I})}(\tau)\right]\right).\end{aligned} \tag{40}$$

This master equation is a time non-local integro-differential equation, that link the change of the state of S at time t $\rho_{\mathrm{S}}(t)$ with its state at previous times $t_0 < \tau < t$. Then, the integral of the right-hand side of Eq. (40) accounts for memory effects in the open system dynamics as a consequence of the interaction with the environment, and quantified

through the environment correlation functions.

The environmental correlation functions are given by

$$\begin{aligned} C_{uv}(t-\tau) &= \frac{1}{\hbar^2}\left\langle \hat{\Phi}_u(t)\hat{\Phi}_v(\tau)\right\rangle_{\mathrm{B}} - \frac{1}{\hbar^2}\left\langle \hat{\Phi}_u\right\rangle_{\mathrm{B}}\left\langle \hat{\Phi}_v\right\rangle_{\mathrm{B}} \\ &= \frac{1}{\hbar^2}\left\langle \hat{\Phi}_u(t-\tau)\hat{\Phi}_v(0)\right\rangle_{\mathrm{B}} - \frac{1}{\hbar^2}\left\langle \hat{\Phi}_u\right\rangle_{\mathrm{B}}\left\langle \hat{\Phi}_v\right\rangle_{\mathrm{B}} = \frac{1}{\hbar^2}\left\langle \Delta\hat{\Phi}_u(t)\Delta\hat{\Phi}_v(0)\right\rangle_{\mathrm{B}}, \end{aligned} \tag{41}$$

where $\left\langle \hat{\Phi}_u^{(\mathrm{I})}(t)\hat{\Phi}_v^{(\mathrm{I})}(\tau)\right\rangle_{\mathrm{B}} = \mathrm{Tr}_{\mathrm{B}}\left\{\hat{\Phi}_u^{(\mathrm{I})}(t)\hat{\Phi}_v^{(\mathrm{I})}(\tau)\hat{\rho}_{\mathrm{B,eq}}\right\}$ is the two-time correlation function. Since the state $\hat{\rho}_{\mathrm{B,eq}}$ is stationary, the correlation functions are time-homogeneous $C_{uv}(t,\tau) = C_{uv}(t-\tau)$, i.e., depend only on the difference $t-\tau$. The quantity $\Delta\hat{\Phi}_u^{(\mathrm{I})}(t) = \hat{\Phi}_u^{(\mathrm{I})}(t) - \left\langle \hat{\Phi}_u^{(\mathrm{I})}\right\rangle_{\mathrm{B}}$ accounts for the fluctuations of the observables of the environment. Therefore, the environmental correlation function measures the correlations between the fluctuations of the environment observables $\left\{\hat{\Phi}_u\right\}$. These correlations decay according to the correlation time τ_{B} [Cohen-Tannoudji et al., 1998; May and Kühn, 2011; Nitzan, 2006; Valkunas et al., 2013]. The correlation time τ_{B} provide information about for how long the environment observables recall the effect of the interaction with the open system S [Levi et al., 2015; Cohen-Tannoudji et al., 1998].

If the environment equilibrates quickly from its interaction with the system S, i.e., the dynamics of the environment is much faster than that the system, the correlation functions decay to zero much faster that any characteristic system timescale. This allows to consider a *Markovian approximation* in Eq. (40), asssuming that the timescale of relaxation of the system τ_{S} is much larger than τ_{B}. Thus, it is acceptable approximate $\hat{\rho}_{\mathrm{S}}^{(\mathrm{I})}(\tau)$ by $\hat{\rho}_{\mathrm{S}}^{(\mathrm{I})}(t)$ in Eq. (40), provided that $\tau_{\mathrm{S}} \gg \tau_{\mathrm{B}}$. By means of this approximation Eq. (40) is local in time, i.e., the variation in time of $\hat{\rho}_{\mathrm{S}}^{(\mathrm{I})}(t)$ rely on its state at time t only, there is no contributions from previous times. Also, the integrand of Eq. (40) is negligible for $t \gg \tau$, it is feasible to extend the limit of integration to infinity after a change of variables leading to the Markovian second-order master equation in Schrödinger picture [May and Kühn, 2011; Nitzan, 2006; Levi et al., 2015]

$$\begin{aligned} \frac{\mathrm{d}}{\mathrm{d}t}\hat{\rho}_{\mathrm{S}}^{(2)}(t) = &-\frac{\mathrm{i}}{\hbar}\left[\hat{H}_{\mathrm{S}} + \sum_u \left\langle \hat{\Phi}_u\right\rangle_{\mathrm{B}}\hat{K}_u(t), \hat{\rho}_{\mathrm{S}}(t)\right] \\ &-\sum_{uv}\int_0^\infty \mathrm{d}\tau\left(C_{uv}(\tau)\left[\hat{K}_u, \hat{U}_{\mathrm{S}}(\tau)\hat{K}_v\hat{U}_{\mathrm{S}}^\dagger(\tau)\hat{\rho}_{\mathrm{S}}(t)\right] - C_{vu}(-\tau)\left[\hat{K}_u, \hat{\rho}_{\mathrm{S}}(t)\hat{U}_{\mathrm{S}}(\tau)\hat{K}_v\hat{U}_{\mathrm{S}}^\dagger(\tau)\right]\right). \end{aligned} \tag{42}$$

1.3.3. The environment as an ensemble of harmonic oscillators.

The effect of the environment over the open system dynamics is encoded in the correlation functions $C_{uv}(t,\tau)$. However, the specific calculation of these correlations functions is not achievable due to the lack of information of the state of the environment [May and Kühn, 2011], which in practice corresponds to a macroscopic reservoir [Weiss, 2012; Breuer and Petruccione, 2002; May and Kühn, 2011; Nitzan, 2006; Valkunas et al., 2013]. In order to gain physical insigths regarding environmental correlations it is convenient to consider phenomenological system-plus-reservoir models [Weiss, 2012], which allow to compute the correlation functions, and reach the expected classical limit [Weiss, 2012; May and Kühn, 2011; Schlosshauer, 2007].

A widespread approach consists in modeling the environment as a collection of independent harmonic oscillators [Ullersma, 1966; Caldeira and Leggett, 1983; Weiss, 2012] described by the Hamiltonian

$$\hat{H}_{\mathrm{B}} = \sum_n \hbar\omega_n \left(\hat{b}_n^\dagger \hat{b}_n + \frac{1}{2}\right), \tag{43}$$

where $\hat{b}_n^\dagger$ ($\hat{b}_n$) represents the creation (annihilation) operator, and ω_n is the frequency of the n^{th} environmental harmonic oscillator. It is considered that the interaction between the open system S and each oscillator of the environment is weak for a macroscopic environment [Weiss, 2012], which no means that necessarily the influence of the whole environment being weak [Caldeira and Leggett, 1983]. Therefore, it makes sense to consider a linear coupling function of the environment coordinates, which also allows eliminate the environment in an exact way [Ingold, 2002; Weiss, 2012]. The above is equivalent to linearizing a nonlinear coupling in the weak limit of coupling to the environment degrees of freedom, performing a Taylor expansion of the interaction Hamiltonian $\hat{H}_{\mathrm{SB}}$ around the equilibrium positions of the environmental oscillators [May and Kühn, 2011; Ingold, 2002].

Consequently, the interaction Hamiltonian $\hat{H}_{\mathrm{SB}}$ reads

$$\hat{H}_{\mathrm{SB}} = \sum_n \hbar g_n \hat{K}_n q_n; \quad q_n = \sqrt{\tfrac{\hbar}{2m_n\omega_n}}\left(\hat{b}_n^\dagger + \hat{b}_n\right), \tag{44}$$

where g_n the coupling strength between the operator system $\hat{K}_n$ and the environmental oscillators, and q_n represents the position of the n^{th} environmental harmonic oscillator. Considering that only a single system operator $\hat{K}$ is coupled to the environment, the correlation function $C_{uv}(t)$ is replaced by [May and Kühn, 2011]

$$C(t) = \int_0^\infty \mathrm{d}\omega \Big[\coth\left(\tfrac{1}{2}\hbar\omega\beta\right)\cos(\omega t) - \mathrm{i}\sin(\omega t)\Big]\omega^2 J(\omega), \tag{45}$$

where $J(\omega)$ represents the spectral density

$$J(\omega) = \sum_n g_n^2 \delta(\omega - \omega_n), \tag{46}$$

which characterizes the frequency-dependent effect of the environment on the system S, and represents the bridge with experiments[Pachón and Brumer, 2014], fundamental quantum chemistry calculations, and molecular dynamics simulations [Levi et al., 2015; Pachón and Brumer, 2012; De Vega and Alonso, 2017]. The spectral density determines the environmental correlations functions, that ultimately determine the effect of the environment on the open system dynamics. Although, the spectral density is defined as a discrete quantity, when describing realistic physical environment adopts a continuous behavior. In the next chapter, it will be discussed the specific form that adopts the spectral density in the context of light harvesting systems that are in contact with phonon and photon environments [Pachón et al., 2017; Calderón and Pachón, 2020].

1.3.4. Redfield master equation. The second-order master equation 42 is also known as the Redfield master equation [Redfield, 1957; May and Kühn, 2011; Nitzan, 2006; Weiss, 2012]. Considering the eigenstate basis $\{|a\rangle\}$ of the Hamiltonian $\hat{H}_{\mathrm{S}}$, that satisfy the relation $\hat{H}_{\mathrm{S}}|a\rangle = E_a|a\rangle$, Eq. (42) reads:

$$\frac{\mathrm{d}\rho_{ab}(t)}{\mathrm{d}t} = -\mathrm{i}\omega_{ab}\rho_{ab}(t) - \sum_{cd} R_{ab,cd}\,\rho_{cd}(t), \tag{47}$$

where $\omega_{ab} = (E_a - E_b)/\hbar$ is the transition frequency between the eigenstates $|a\rangle$ and $|b\rangle$, $\rho_{ab}(t) = \langle a|\hat{\rho}_{\mathrm{S}}^{(2)}(t)|b\rangle$, and $R_{ab,cd}$ is the Redfield relaxation tensor. The first term of the right-hand side of Eq. (47) accounts for the unitary

dynamics, and the Redfield relaxation tensor $R_{ab,cd}$ describes the dephasing and relaxation energy processes due to the interaction with the environment [Redfield, 1957; Breuer and Petruccione, 2002; Nitzan, 2006; Weiss, 2012; May and Kühn, 2011].

From the considerations made above, the Redfield master equation considers three approximations: first, absence of initial correlations between the system S and the environment B. Second, weak coupling assumption between the system S and the environment B. Third, the dynamics of $\rho(t)$ is slow compared to the time scale of relaxation of the environment B [Breuer and Petruccione, 2002; Nitzan, 2006; May and Kühn, 2011]. Through the formalism of Redfield, four different kinds of processes associated with the relaxation tensor can be identified: population transfer ($a = b,\ c = d$), coherence decay ($a = c,\ b = d, a \neq b$), exchange between populations and coherences ($a = b,\ c \neq d, c = d, a \neq b$) and coherence exchange (none of the above combinations) [May and Kühn, 2011]. The Redfield relaxation tensor is time-independent and contains non-secular terms [Pachón et al., 2013; Dodin et al., 2018]

$$R_{ab,cd} = \delta_{ac}\sum_{e}\Gamma_{be,ed}(\omega_{de}) + \delta_{bd}\sum_{e}\Gamma_{ae,ec}(\omega_{ce}) - \Gamma_{ca,bd}(\omega_{db}) - \Gamma_{db,ac}(\omega_{ca}). \tag{48}$$

The damping matrix elements that determine the time span for correlations are defined by

$$\Gamma_{ab,cd}(\omega) = \sum_{u,v}\int_{0}^{\infty} \mathrm{d}\tau \mathrm{e}^{\mathrm{i}\omega\tau} C_{u,v}(\tau)\hat{K}_{u,ab}\hat{K}_{v,cd}. \tag{49}$$

Here, $\hat{K}_{u,ab}$ denote the observables of the system of interest that are coupled to the environment. Thus, the system-environment interaction can be written as $\sum_u \hat{\Phi}_{u,ab} \otimes \hat{K}_{u,ab}$, where $\hat{\Phi}_{u,ab}$ represent the observables of environment that are coupled to the system. The bath correlation function is defined by $C_{u,v}(t) = \frac{1}{\hbar^2}\left\langle \hat{\Phi}_{u,ab}(t)\hat{\Phi}_{v,ab}(0)\right\rangle_{\mathrm{B}}$, title = Coherent one-photon phase control in closed and open quantum systems: A general where $\left\langle \hat{\Phi}_{u,ab}\right\rangle = 0$ is assumed [May and Kühn, 2011; Nitzan, 2006; Breuer and Petruccione, 2002]. The real part of $\Gamma_{ab,cd}$ describes an irreversible redistribution of the amplitudes contained in the various parts of reduced density matrix. The imaginary part introduces terms that can be interpreted as a modification of the transition frequencies of the respective mean-field matrix elements

[May and Kühn, 2011; Nitzan, 2006; Breuer and Petruccione, 2002].

2. Nonadiabatic sunlight harvesting

In the last three decades, new experimental, theoretical and computational techniques have been developed to resolve the interplay between the multiple electronic and vibrational degrees of freedom, together with the variety of energy scales involved in molecular-aggregates energy-transfer-processes. [Pachón and Brumer, 2012; Chenu and Scholes, 2015; Brunk and Rothlisberger, 2015; Curutchet and Mennucci, 2016; De Vega and Alonso, 2017; Jang and Mennucci, 2018; Brumer, 2018]. In doing so, two-dimensional-electronic-spectroscopy experiments have revealed long-lived oscillations in two-dimensional spectra of several photosynthetic light-harvesting complexes [Engel et al., 2007; Collini et al., 2010; Panitchayangkoon et al., 2010] that pointed out to the potential existence of quantum superpositions related to the interplay of the electronic and vibrational degrees of freedom [Ishizaki et al., 2010; Pachón and Brumer, 2011, 2012; Huelga and Plenio, 2013; Chenu and Scholes, 2015]. In particular, the coupling between the electronic degrees of freedom and intramolecular vibrations in quasi-resonance to excitonic transitions (vibronic coupling) has been proposed as a consistent physical design principle that could explain the origin of long-lived oscillations observed in two-dimensional spectra, and possibly related to the high efficiency of the energy transfer process [Christensson et al., 2012; Kolli et al., 2012; Tiwari et al., 2013; Chin et al., 2013; Chenu et al., 2013; Novelli et al., 2015; Malý et al., 2016; Dean et al., 2016; Yeh et al., 2019]. Unexpectedly, during the course of potentially being supporting long-lived oscillations, the state of the intramolecular vibrations evolve from a thermal state with non-quantum correlations into a state provided with genuinely quantum correlations even at room temperature [Schlosshauer, 2007; O'Reilly and Olaya-Castro, 2014; Scholak and Brumer, 2017].

Two-dimensional-electronic-spectroscopy is a laser-pulsed non-linear technique [Mukamel, 1995] and therefore, the extent to which their results are representative for natural conditions with continuous incoherent light sources has been intensively addressed in the literature [Mančal and Valkunas, 2010; Brumer and Shapiro, 2012; Tscherbul and Brumer, 2014; Sadeq and Brumer, 2014; Grinev and Brumer, 2015; Dodin et al., 2016a,b; Pachón et al., 2017; Brumer, 2018; Chenu et al., 2014, 2015; Chenu and Brumer, 2016]. It is by now clear that the dynamics induced by

suddenly-turned-on incoherent sunlight are qualitatively different from coherent laser sources and also different from a bare white-noise-source provided that incoherent light has a super-Ohmic character and does not induce pure dephasing dynamics [Pachón and Brumer, 2013; Pachón et al., 2017]. The relevance of intramolecular vibrational modes, their impact on the energy transfer, as well as their non-classical behaviour are explored in this thesis for the natural scenario of illumination by sunlight. In this chapter will be consider vibronic dimers formed by two chromophores treated within the two-level approximation and a quantized intramolecular vibrational mode in interaction with each chromophore.

Under sunlight illumination, it is found that the introduction of intramolecular vibrational modes may increase the population amplitudes in the vibronic dimers compared to the electronic ones. The amplitude of the single exciton coherence increases up to one order of magnitude with the inclusion of the intramolecular vibrational modes, but coherence between site states is of the same order for both electronic and vibronic dimers. To account for the assistance of intramolecular vibrational modes to long-decoherence times, the decoherence rate of vibronic single exciton state superpositions is systematically analyzed in a broad regime of the dimer parameter space. It is shown that the decoherence rate displays a non-trivial behavior and that neither the nonadiabatic regime nor the values of electronic and vibronic couplings of the dynamics analyzed lead to the lowest value in the decoherence rate.

2.1. Vibronic antenna systems under sunlight illumination

To model energy transfer dynamics in a light-harvesting complex under sunlight illumination, consider a molecular aggregate (light-harvesting system) immersed within a protein and solvent environment, that is excited by incoherent thermal radiation. From an open quantum systems perspective, the entire system (i.e., molecular aggregate + protein/solvent environment + thermal radiation), can be described by a global system-bath Hamiltonian [Pachón and Brumer, 2012; Pachón et al., 2017] (see section 1.2)

$$\hat{H} = \hat{H}_{\mathrm{S}} + \hat{H}_{\mathrm{SB}} + \hat{H}_{\mathrm{B}}. \tag{50}$$

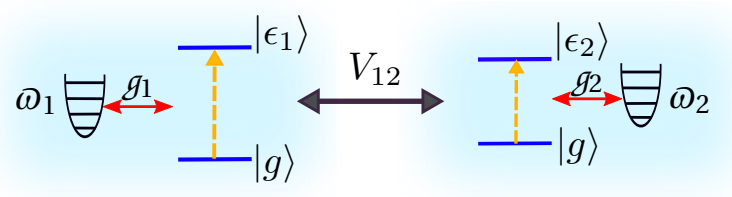

Figure 6. Pictorial representation of a vibronic dimer described by the Hamiltonian of Eq. 51.

2.1.1. Light-harvesting system . For simplicity, the light-harvesting system (molecular aggregate) corresponds to a set of N chromophores (sites) that interact through an inter-chromophore Coulomb coupling. Each chromophore is modeled as a two-level system coupled to a quantized intramolecular vibrational mode of frequency ϖ_i. Thus, the molecular aggregate is described by the Hamiltonian

$$\hat{H}_{\rm S} = \sum_{i=1}^{N} \left(E_{{\rm g}_i} \hat{1}_i + \varepsilon_i \hat{\sigma}_i^+ \hat{\sigma}_i^- \right) + \sum_{i \neq j}^{N} V_{ij} \hat{\sigma}_i^+ \hat{\sigma}_j^- + \sum_{i=1}^{N} \hbar g_i \hat{\sigma}_i^+ \hat{\sigma}_i^- \left(\hat{b}_i^\dagger + \hat{b}_i \right) + \sum_{i=1}^{N} \hbar \varpi_i \hat{b}_i^\dagger \hat{b}_i, \tag{51}$$

being $E_{{\rm g}_i}$ the ground state energy, ε_i the electronic energy of the $i^{\rm th}$ site, $\hat{\sigma}_i^+$ ($\hat{\sigma}_i^-$) creates (annihilates) an electronic excitation in the $i^{\rm th}$ site, V_{ij} is the electronic coupling between the $i^{\rm th}$ and the $j^{\rm th}$ site. Here, $\hat{b}_i^\dagger$ ($\hat{b}_i$) is the creation (annihilation) operator of the $i^{\rm th}$ intramolecular vibrational mode, and $g_i = \sqrt{S_i}\varpi_i$ represents the coupling between the $i^{\rm th}$ excited electronic state and the $i^{\rm th}$ intramolecular vibrational mode, and S_i is the Huang-Rhys factor. This model assumed that the chromophores are sufficiently far apart that the intermolecular states do not overlap; thus, the electron transfer between chromophores is neglected [Pachón and Brumer, 2012]. Also, the ground and the first electronic states (two-level approximation) suffice for describing the weak incoherent light-induced dynamics, and that the intramolecular vibrational modes can be treated within the harmonic approximation [Pachón and Brumer, 2012; Pachón et al., 2017].

The action of the operators $\hat{\sigma}_i^+$ and $\hat{b}_i^\dagger$ allows for defining, in a bare electronic-vibratio-nal basis, the vibronic states (i.e., product of bare electronic and vibrational states). The electronic ground state with arbitrary vibrational excitations reads $\left|g_i, v_i\right\rangle = \left(\hat{b}_i^\dagger\right)^{v_i} / \sqrt{v_i!} \left|g_i, 0_i\right\rangle$, where $\left|g_i\right\rangle$ denotes the electronic ground state, and $\left|v_i\right\rangle = \left(\hat{b}_i^\dagger\right)^{v_i} / \sqrt{v_i!} \left|0_i\right\rangle$ stands for the vibrational excited state with quantum number v_i and $\left|0_i\right\rangle$ the vibrational ground

state of the i^{th} site. The electronic singly excited state $\left|\varepsilon_i\right\rangle$ of the i^{th} site with arbitrary vibrational excitations reads $\left|\varepsilon_i,\nu_i\right\rangle = \hat{\sigma}_i^{+}\left(\hat{b}_i^{\dagger}\right)^{\nu_i}/\sqrt{\nu_i!}\left|g_i,0_i\right\rangle$, where $\left|\varepsilon_i\right\rangle = \hat{\sigma}_i^{+}\left|g_i\right\rangle$.

The eigenstates of the Hamiltonian $\hat{H}_{\text{S}}$ correspond to the vibronic exciton states $\left\{\left|\psi_n\right\rangle\right\}$ defined by $\hat{H}_{\text{S}}\left|\psi_n\right\rangle = \xi_n\left|\psi_n\right\rangle$. The vibronic single exciton states[2] are defined by

$$\left|\psi_n^{(e)}\right\rangle = \sum_{i=1}^{N}\sum_{\nu_i} C_{i,\nu_i}^{n}\left|\varepsilon_i,\nu_i\right\rangle. \tag{52}$$

The localization of the n^{th} vibronic single exciton state on the k^{th} site is given by

$$l_{\varepsilon_k}(\psi_n^{(e)}) = \left\langle \psi_n^{(e),k}|\psi_n^{(e)}\right\rangle = \sum_{\nu_k}\left|C_{k,\nu_k}^{n}\right|^2, \tag{53}$$

with $\left|\psi_n^{(e),k}\right\rangle = \sum_{\nu_k} C_{k,\nu_k}^{n}\left|\varepsilon_k,\nu_k\right\rangle$ a vibronic single exciton state completely localized on the k^{th} site.

For the case of vibronic dimers (two chromophores) considered here, the intersite mixing ratio for a superposition between the n^{th} and the m^{th} vibronic single exciton states is defined by [Malý et al., 2016] $\zeta_{nm} = l_{\varepsilon_1}(\psi_n^{(e)})l_{\varepsilon_2}(\psi_m^{(e)}) + l_{\varepsilon_1}(\psi_m^{(e)})l_{\varepsilon_2}(\psi_n^{(e)})$. This ratio characterizes the type of coherence in the vibronic single exciton basis: $\zeta_{nm} = 1$ for a pure electronic coherence (superposition between vibronic single exciton states localized each one on different sites), and $\zeta_{nm} = 0$ for a pure vibrational coherence (superposition between vibronic single exciton states localized on the same site).

2.1.2. Protein/solvent and incoherent radiation environments.

The protein and solvent environment surrounding the light-harvesting system can be treated as a local phonon bath [May and Kühn, 2011; Mukamel, 1995] that module the electronic energies and electronic couplings and represent the primary source of decoherence and dissipation in the electronic-energy-transfer-process. Due to the highly mixed character of electronic-

---

[2] For clarity in then notation, the superindex makes reference to the electronic ground state (g), electronic single excited state (e) and electronic double excited state (f).

vibrational coherences, it is then necessary to consider the coupling of the intramolecular vibrational modes to the phonon bath, provoking vibrational relaxation [Yeh et al., 2019].

The sunlight is formally described as a blackbody radiation photon bath at 5600 K [Pachón et al., 2017; Brumer, 2018; Blankenship, 2014]. The system-bath and (phonon+photon) baths Hamiltonians are given by

$$\hat{H}_{\mathrm{SB}} = \sum_{i,l}^{N,\infty} \hbar g_{il}^{(\mathrm{e})} \hat{\sigma}_i^{+} \hat{\sigma}_i^{-} \left(\hat{b}_l^{(i)} + \hat{b}_l^{(i)\dagger} \right) + \sum_{i,m}^{N,\infty} \hbar g_{im}^{(\mathrm{v})} (\hat{b}_i^{\dagger} + \hat{b}_i) \left(\hat{b}_m^{(i)} + \hat{b}_m^{(i)\dagger} \right) - \sum_{j}^{N} \hat{\mu}_j \cdot \hat{\mathbf{E}}(t), \tag{54}$$

$$\hat{H}_{\mathrm{B}} = \sum_{i,l}^{N,\infty} \hbar \omega_l^{(i)} \hat{b}_l^{(i)\dagger} \hat{b}_l^{(i)} + \sum_{\mathbf{k},s} \hbar c k \hat{a}_{\mathbf{k},s}^{\dagger} \hat{a}_{\mathbf{k},s} + \sum_{i,m}^{N,\infty} \hbar \omega_m^{(i)} \hat{b}_m^{(i)\dagger} \hat{b}_m^{(i)}. \tag{55}$$

Here, $g_{il}^{(\mathrm{e})}$ ($g_{im}^{(\mathrm{v})}$) represent the coupling between the electronic single excited state of the i^{th} site (i^{th} intramolecular vibrational mode) and the l^{th} (m^{th}) phonon mode. $\hat{b}_l^{(i)\dagger}$ $\left(\hat{b}_l^{(i)}\right)$ is the creation (annihilation) operator of a l^{th} phonon mode of frequency $\omega_l^{(i)}$ which interacts with the electronic single excited state of the i^{th} site. $\hat{b}_m^{(i)\dagger}$ $\left(\hat{b}_m^{(i)}\right)$ is the creation (annihilation) operator of a m^{th} phonon mode of frequency $\omega_m^{(i)}$ which interacts with the i^{th} intramolecular vibrational mode.

The dipole operator of the i^{th} site is represented by $\hat{\mu}_j$, and the electric field of the radiation is given by [Mandel and Wolf, 1995]

$$\hat{\mathbf{E}}(t) = \hat{\mathbf{E}}^{(+)}(t) + \hat{\mathbf{E}}^{(-)}(t); \quad \hat{\mathbf{E}}^{(+)}(t) = \mathrm{i} \sum_{\mathbf{k},s} \left(\frac{\hbar \omega}{2\varepsilon_0 V} \right)^{1/2} \hat{a}_{\mathbf{k},s} (\boldsymbol{\varepsilon}_{\mathbf{k},s}) \mathrm{e}^{-\mathrm{i}\omega t}, \tag{56}$$

where $\hat{\mathbf{E}}^{(-)}(t) = \left[\hat{\mathbf{E}}^{(+)}(t) \right]^{\dagger}$, and $\hat{a}_{\mathbf{k},s}^{\dagger}$ ($\hat{a}_{\mathbf{k},s}$) being the creation (annihilation) operator for the $\mathbf{k}^{\mathrm{th}}$ radiation field mode in the s^{th} polarization state.

The effect of the incoherent radiation environment (blackbody bath) and the vibrational environment (phonon bath) is encoded in the spectral densities $J_j^{\mathrm{BB}}(\omega)$ and $J_j^{\mathrm{PB}}(\omega)$, respectively. The blackbody radiation bath is character-

ized by the super-Ohmic spectral density [Pachón et al., 2017]

$$\omega^2 J_j^{\mathrm{BB}}(\omega) = \frac{2\hbar\omega^3}{3(4\varepsilon_0\pi^2c^3)}. \tag{57}$$

This spectral density generates long-lasting coherent dynamics (see Fig. 8, $\Lambda^{(\mathrm{e,v})} = 0$ case) provided by the lack of pure dephasing dynamics and the strong dependence of the decoherence rate on the system level spacing [Pachón et al., 2017] (see Fig. 10 A and B).

The spectral density of the phonon-baths reads

$$\omega^2 J_j^{\mathrm{PB}}(\omega) = \frac{2\Omega_j^{(\mathrm{e,v})}\Lambda_j^{(\mathrm{e,v})}\omega}{\hbar(\omega^2 + \Omega_j^{(\mathrm{e,v})2})}, \tag{58}$$

where $\Omega^{(\mathrm{e,v})}$ represents the cutoff frequency and $\Lambda^{(\mathrm{e,v})}$ the reorganization energy of the phonon baths coupled to the electronic (e) and intramolecular vibrational (v) degrees of freedom. The dynamics of light-harvesting systems with spectral densities of the form (58) are commonly solved with the nonperturbative hierarchical equations of motion (HEOM) method [Tanimura and Kubo, 1989; Ishizaki and Tanimura, 2005; Ishizaki and Fleming, 2009], since usually the energy transfer dynamics remains in an intermediate coupling regime, where the electronic coupling between chromophores is comparable to the reorganization energy of the phonon bath. However, this method does not readily adapt to super-ohmic spectral densities, such as blackbody radiation. To circumvent this, the HEOM method has been used to treat the phonon bath, whereas the non-unitary effect of the incoherent light has been accounted for by a Lindblad dissipator [Fassioli et al., 2012; Chan et al., 2018]. However, this hybrid approach does not properly take into account the influence of the super-Ohmic spectral density in the density matrix dynamics since it does not consider the dependence of the decoherence rates on the system level spacing.

To adequately describe the correlations induced by the super-Ohmic spectral density of the blackbody radiation together with the phonon bath effects, the dynamics are solved in the vibronic exciton basis $\{|\psi_n\rangle\}$, i.e., in the eigenstates of the Hamiltonian in Eq. (51), by using the standard Redfield master equation (second-order and non-secular) [May and Kühn, 2011; Pachón et al., 2017]. Recent works on energy transfer dynamics of vibronic dimers

excited with coherent light have considered the Redfield approach and have shown similar results to the HEOM method under parameters used in experimental conditions [Romero et al., 2014; Novoderezhkin and van Grondelle, 2017; Bennett et al., 2018]. Further details about both methods and comparison between them are presented in the Appendix 1. However, the Redfield master equation approach provides accurate results for weak coupling to the phonon bath (second-order approximation), i.e., low reorganization energies compared to the electronic coupling.

In consequence, the Redfield master equation that take into account the effects of the phonon baths and blackbody radiation reads

$$\frac{\mathrm{d}\rho_{ab}(t)}{\mathrm{d}t} = -\mathrm{i}\omega_{ab}\rho_{ab}(t) - \sum_{c,d}\left(R^{\mathrm{PB}}_{ab,cd} + R^{\mathrm{BB}}_{ab,cd}\right)\rho_{cd}(t). \tag{59}$$

Here, the first term of the right-hand side accounts for the unitary dynamics, and the Redfield relaxation tensors $R^{\mathrm{PB}}_{ab,cd}$ and $R^{\mathrm{BB}}_{ab,cd}$ describe the dephasing and relaxation energy processes due to the vibrational environment (phonon baths) and the incoherent radiation environment (blackbody bath), respectively. These are given by

$$R^{\mathrm{PB,BB}}_{ab,cd} = \delta_{ac}\sum_{e}\Gamma^{\mathrm{PB,BB}}_{be,ed}(\omega_{de}) + \delta_{b,d}\sum_{e}\Gamma^{\mathrm{PB,BB}}_{ae,ec}(\omega_{ce}) - \Gamma^{\mathrm{PB,BB}}_{ca,bd}(\omega_{db}) - \Gamma^{\mathrm{PB,BB}}_{db,ac}(\omega_{ca}). \tag{60}$$

The damping matrix elements that determine the time span for correlations are defined by

$$\Gamma^{\mathrm{PB,BB}}_{ab,cd}(\omega) = \sum_{u,v}\int_0^\infty \mathrm{d}\tau \mathrm{e}^{\mathrm{i}\omega\tau} C^{\mathrm{PB,BB}}_{u,v}(\tau)\hat{K}^{\mathrm{PB,BB}}_{u,ab}\hat{K}^{\mathrm{PB,BB}}_{v,cd}. \tag{61}$$

Here, $\hat{K}^{\mathrm{PB,BB}}_{u,ab}$ denote the observables of the system of interest that are coupled to the phonon and blackbody baths (see Eq. 54). Thus, the system-phonon bath and system-blackbody bath can be written as $\sum_u \hat{\Phi}^{\mathrm{PB,BB}}_{u,ab}\otimes\hat{K}^{\mathrm{PB,BB}}_{u,ab}$, where $\hat{\Phi}^{\mathrm{PB,BB}}_{u,ab}$ represent the observables of the phonon and blackbody baths that are coupled to the vibronic dimer (see Eq. 54). The bath correlation function is defined by $C^{\mathrm{PB,BB}}_{u,v}(\tau) = \frac{1}{\hbar^2}\left\langle\hat{\Phi}^{\mathrm{PB,BB}}_{u,ab}(t)\hat{\Phi}^{\mathrm{PB,BB}}_{v,ab}(0)\right\rangle_{\mathrm{PB,BB}}$, where $\left\langle\hat{\mathscr{O}}\right\rangle_{\mathrm{PB,BB}} = \mathrm{Tr}\left[\hat{\rho}^{\mathrm{PB,BB}}_{\mathrm{equi}}\hat{\mathscr{O}}\right]$ and $\left\langle\hat{\Phi}^{\mathrm{PB,BB}}_{u,ab}\right\rangle_{\mathrm{PB,BB}} = 0$. The real part of $\Gamma_{ab,cd}$ describes an irreversible redistribution of the amplitudes contained in the various parts of reduced density matrix. The imaginary part introduces terms that can be interpreted as a modification of the transition frequencies and of the respective mean-field matrix elements. The correlation function for each

environment phonon/photon mode is given by

$$C_i^{\mathrm{PB,BB}}(t) = \int_0^\infty \mathrm{d}\omega\,\omega^2 J_i^{\mathrm{PB,BB}}(\omega)\left[\coth\left(\frac{\hbar\omega\beta}{2}\right)\cos(\omega t) - \mathrm{i}\sin(\omega t)\right]. \tag{62}$$

2.2. Light-harvesting system dynamics in the presence of blackbody radiation and phonon baths

Due to the exponential scaling of the dimension of the full Hilbert space, for all simulations below, only the first four states (ground state and three excited levels) of each intramolecular vibrational mode are considered. Convergence of the density matrix time evolution was verified with the case of four excited levels. For the vibronic dimers considered here (two monomers and two intramolecular vibrations), the vibronic exciton manifold has then dimension 64: 16 vibronic ground exciton states $\{|\psi_1^{(g)}\rangle,\ldots,|\psi_{16}^{(g)}\rangle\}$, 32 vibronic single exciton states $\{|\psi_{17}^{(e)}\rangle,\ldots,|\psi_{48}^{(e)}\rangle\}$ and 16 vibronic double exciton states $\{|\psi_{49}^{(f)}\rangle,\ldots,|\psi_{64}^{(f)}\rangle\}$.

The comparison with the case of an electronic dimer with no specific intramolecular vibrational modes, in the site states $\{|\varepsilon_1\rangle,|\varepsilon_2\rangle\}$ and in the single exciton states $\{|e\rangle,|e'\rangle\}$, follows after tracing over the intramolecular vibrational degrees of freedom in the density matrix of the vibronic dimer. For electronic dimers, the Frenkel Hamiltonian [Van Amerongen et al., 2000; May and Kühn, 2011] corresponds to the first two terms of the Hamiltonian described in Eq. (51), with site states $\{|\tilde{\varepsilon}_1\rangle,|\tilde{\varepsilon}_2\rangle\}$ and single exciton states $\{|\tilde{e}\rangle,|\tilde{e}'\rangle\}$. Specifically, the two phycoerythrobilin ($\mathrm{PEB}_{50/61\,\mathrm{C}}$ and $\mathrm{PEB}_{50/61\,\mathrm{D}}$) chromophores from the protein-antenna phycoerythrin 545 (PE545), and the two dihydrobiliverdin ($\mathrm{DBV}_{50/61\,\mathrm{C}}$ and $\mathrm{DBV}_{50/61\,\mathrm{D}}$) chromophores from the protein-antena phycocyanin 645 (PC645) of marine cryptophyte algae are considered below.

The PEB dimer has a energy gap between excited electronic states $\Delta\varepsilon = 1042\ \mathrm{cm}^{-1}$, and due to the large spatial separation between chromophores, the electronic coupling is small compared to the energy gap between excited electronic states ($V = 92\ \mathrm{cm}^{-1}$); in consequence, each excitonic state is highly localized over a specific chromophore, with exciton energy splitting $\Delta e = 1058\ \mathrm{cm}^{-1}$. The DBV dimer has an energy gap between excited electronic states $\Delta\varepsilon = 73\ \mathrm{cm}^{-1}$, and an electronic coupling $V = 319.4\ \mathrm{cm}^{-1}$ that results in the formation of delocalized exciton states

with an exciton energy splitting $\Delta e = 643\ \mathrm{cm}^{-1}$.

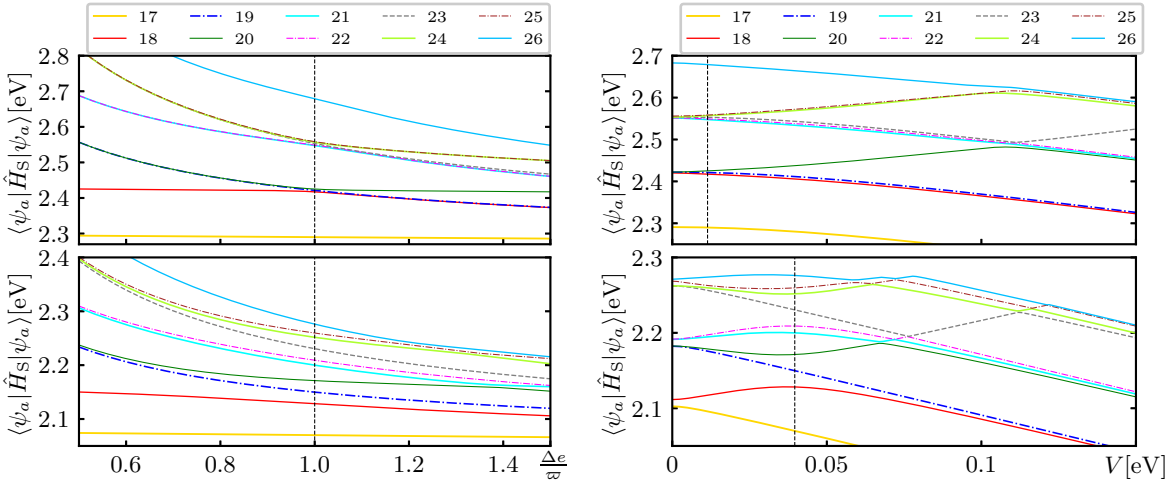

Figure 7. Left panels: $\langle\psi_a|\hat{H}_S|\psi_a\rangle$ as a function of the ratio between the exciton energy splitting Δe and the intramolecular vibrational frequency ϖ. Right panels: $\langle\psi_a|\hat{H}_S|\psi_a\rangle$ as a function of the electronic coupling V. For both panels, upper figures: PEB dimer, and bottom figures: DBV dimer. The vertical black dashed lines indicate the conditions considered in the simulations.

Figure 7 depicts the functional dependence of $\langle\psi_a|\hat{H}_S|\psi_a\rangle$ on the ratio between the exciton energy splitting and the intramolecular vibrational frequency $\Delta e/\varpi$, and on the electronic coupling V for the first ten vibronic single exciton states $(|\psi_{17}\rangle,\ldots,|\psi_{26}\rangle)$[3] for the PEB (top panels) and DBV (bottom panels) dimers. The vertical dashed lines indicate the conditions considered in the simulations below, and corresponds to a nonadiabatic framework [Tiwari et al., 2013; Yeh et al., 2019] that has been related to an enhancement of energy transfer process and the appearance of non-classical correlations driven by strong vibronic interactions [O'Reilly and Olaya-Castro, 2014; Novelli et al., 2015; Scholes et al., 2017].

Energy transfer starts with the rapid incoherent excitation of the electronic sites in their electronic ground states with transition dipole moments of 11.87 D ($\mathrm{PEB}_{50/61\,\mathrm{D}}$), 12.17 D ($\mathrm{PEB}_{50/61\,\mathrm{C}}$), 13.1 D ($\mathrm{DBV}_{50/61\,\mathrm{D}}$) and 13.2 D ($\mathrm{DBV}_{50/61\,\mathrm{C}}$). Initially, the intramolecular vibrational modes

[3] Since the analysis below will focus only on the vibronic single exciton states manifold, the superindex (e) will be drop.

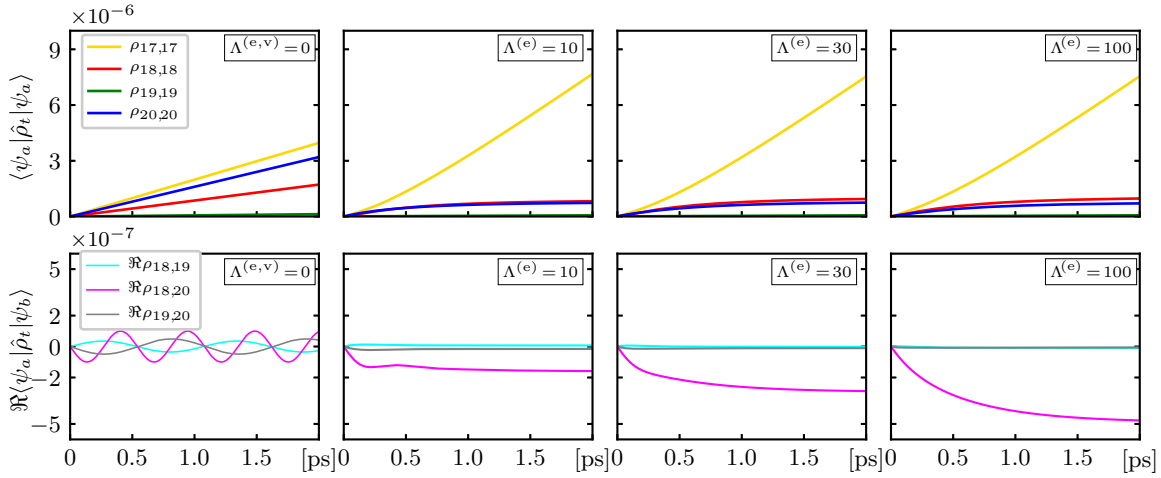

Figure 8. Time evolution of vibronic single exciton states populations $\rho_{aa} = \langle \psi_a | \hat{\rho} | \psi_a \rangle$ and coherences (inset figures) $\mathbb{R}\rho_{ab} = \mathbb{R}\langle \psi_a | \hat{\rho} | \psi_b \rangle$ (color coding is shown on top) in the PEB dimer for the reorganization energies $\Lambda^{(\mathrm{e})} = 0, 10, 30, 100\ \mathrm{cm}^{-1}$ and $\Lambda^{(\mathrm{v})} = 10\ \mathrm{cm}^{-1}$. Baths parameters are $T_{\mathrm{PB}}^{(\mathrm{e,v})} = 300\,\mathrm{K}$, $T_{\mathrm{BB}} = 5600\,\mathrm{K}$

of frequency $\varpi_1 = \varpi_2 = 1058\ \mathrm{cm}^{-1}$ for the PEB dimer and $\varpi_1 = \varpi_2 = 643\ \mathrm{cm}^{-1}$ for the DBV dimer are in thermal equilibrium at $T = 300\,\mathrm{K}$. After the dynamics begin, the vibronic dimer remains coupled to the incident blackbody radiation [Pachón and Brumer, 2013; Pachón et al., 2017]; this is in sharp contrast to the pulsed laser excitation conditions [Brumer, 2018]. The frequency of the two intramolecular vibrational modes is in full resonance with the exciton splitting, i.e., $\varpi_1 = \varpi_2 = \Delta e$. The vibronic coupling strength to each monomer is the same, i.e., $g_1 = g_2 = g$, specifically, $g = 267.1\ \mathrm{cm}^{-1}$ for the PEB dimer and $g = 250\ \mathrm{cm}^{-1}$ for the DBV dimer. For the simulations below, same spectral densities on each monomer are taken, with $\Omega_j^{(\mathrm{e})} = 100\ \mathrm{cm}^{-1}$ (for various values of the reorganization energy $\Lambda_j^{(\mathrm{e})}$), and with $\Omega_j^{(\mathrm{v})} = 50\ \mathrm{cm}^{-1}$ (for $\Lambda_j^{(\mathrm{v})} = 10\ \mathrm{cm}^{-1}$ provided that $\Lambda_j^{(\mathrm{e})} \neq 0$).

2.2.1. Vibronic single exciton basis. Consider first the dynamics of the vibronic dimer in interaction with blackbody radiation only, i.e., turning off the non-unitary effects related to the phonon baths and assume that the system and the blackbody radiation are initially decoupled, i.e., $\hat{\rho}(t_0) = \hat{\rho}_{\mathrm{S}}(t_0) \otimes \hat{\rho}_{\mathrm{BB}}(t_0)$. The transition dipole moments are considered parallel to the incident electric field and constant in time so that the effect of different orientations of the transition dipole moments is neglected.

Figure 8 ($\Lambda^{(\mathrm{e,v})} = 0$ case) shows vibronic single exciton states with populations higher than 10^{-6}, i.e., those

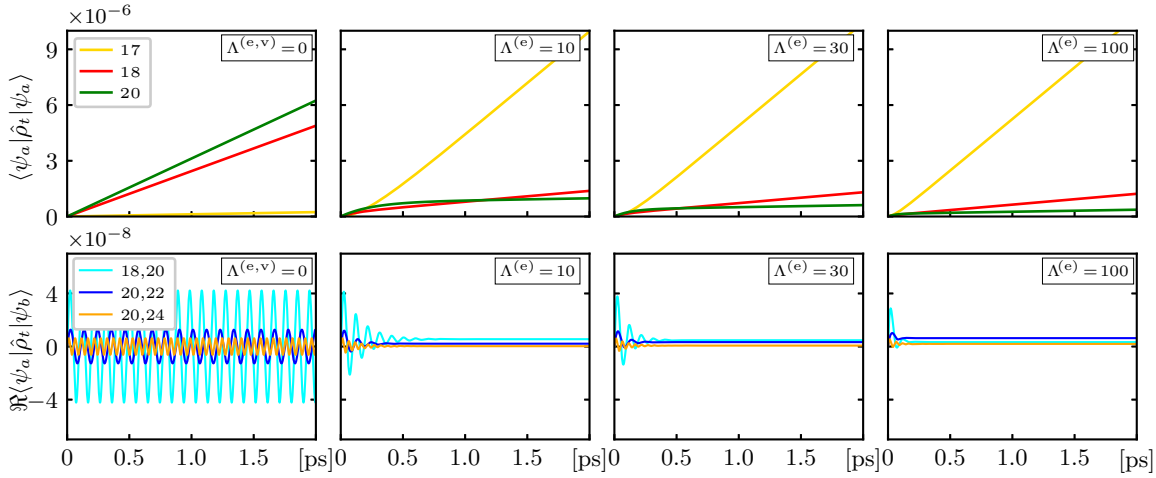

Figure 9. Time evolution of vibronic single exciton states populations $\rho_{aa} = \langle \psi_a | \hat{\rho} | \psi_a \rangle$ and coherences (inset figures) $\mathbb{R}\rho_{ab} = \mathbb{R}\langle \psi_a | \hat{\rho} | \psi_b \rangle$ (color coding is shown on top) in the DBV dimer for the reorganization energies $\Lambda^{(\mathrm{e})} = 0, 10, 30, 100\,\mathrm{cm}^{-1}$ and $\Lambda^{(\mathrm{v})} = 10\,\mathrm{cm}^{-1}$. Baths parameters are $T_{\mathrm{PB}}^{(\mathrm{e,v})} = 300\,\mathrm{K}$, $T_{\mathrm{BB}} = 5600\,\mathrm{K}$.

with higher oscillator strength, and the coherent superpositions arising between them in the PEB dimer after suddenly-turning-on the incoherent radiation. The linear increase of the populations is expected in low-intensity incoherent radiation [Pachón et al., 2017]. In chromophores isolated from the vibrational phonon environment, suddenly turned-on incoherent-light-induced-dynamics are effectively coherent and last for hundreds of picoseconds [Pachón et al., 2017]. Nevertheless, the amplitude of the vibronic coherences ($\sim 10^{-8}$) is approximately two orders of magnitude smaller than the populations; hence, they turn out to quickly become irrelevant for the dynamics of populations [Sadeq and Brumer, 2014].

Most of these vibronic coherences display a highly mixed electronic-vibrational character, characteristic of a nonadiabatic framework [Tiwari et al., 2013, 2017; Yeh et al., 2019], and quantified through the intersite mixing ratio [Malý et al., 2016]. Specifically, for the coherences depicted in Fig. 8, $\zeta_{18,19} = 0.52$, $\zeta_{18,20} = 0.50$ and $\zeta_{19,20} = 0.48$. Therefore, vibronic coherence dynamics are influenced by the decoherence and dissipation of the electronic as well as intramolecular degrees of freedom. This is the reason for introducing a thermal bath of each intramolecular vibrational mode in Eqs. (54) and (55).

To incorporate the effect of the phonon bath ($\Lambda^{(\mathrm{e,v})} \neq 0$), assume that it is initially decoupled from the dimers

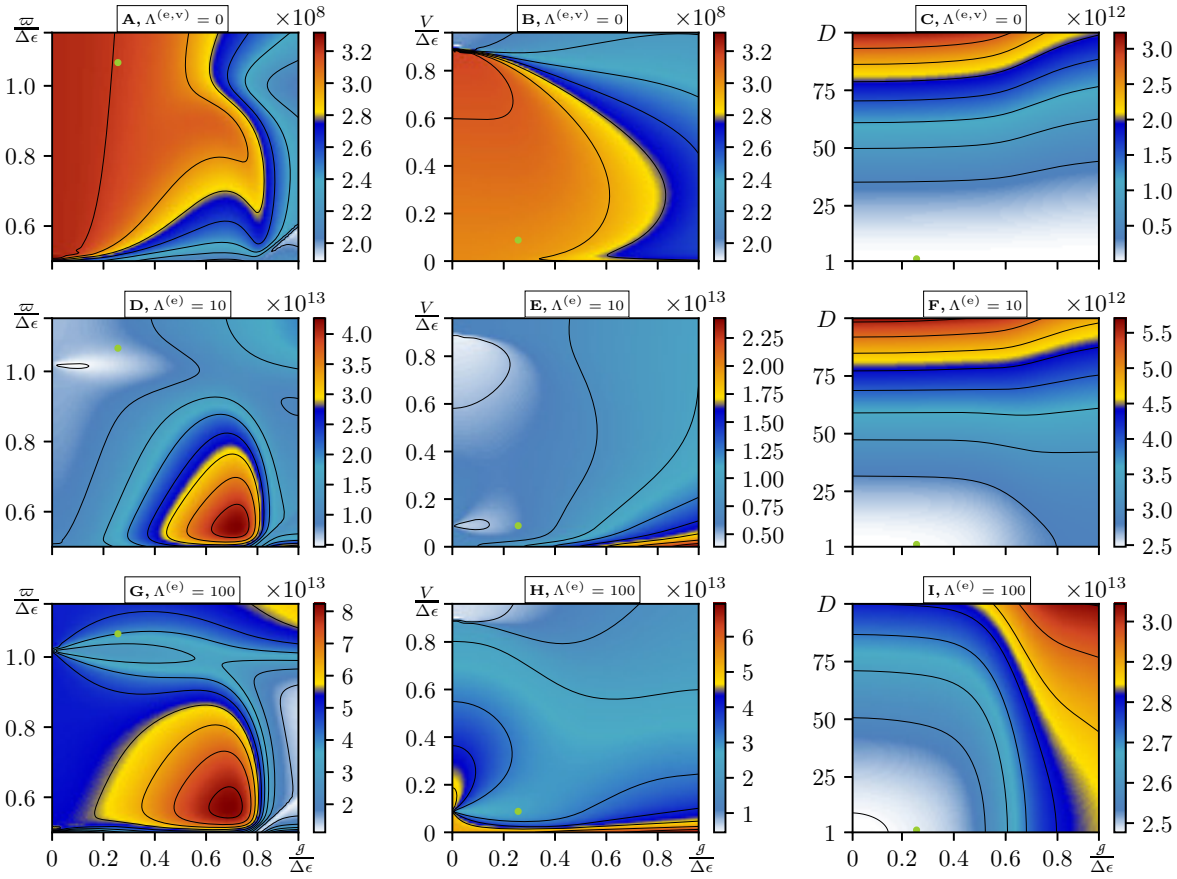

Figure 10. Decoherence rate $\gamma_{18,20}\,[\mathrm{s}^{-1}]$ (color map) for the PEB dimer with the reorganization energies $\Lambda^{(\mathrm{e,v})} = 0\,\mathrm{cm}^{-1}$ (top panels), $\Lambda^{(\mathrm{e})} = 10\,\mathrm{cm}^{-1}$, $\Lambda^{(\mathrm{v})} = 10\,\mathrm{cm}^{-1}$ (middle panels) and $\Lambda^{(\mathrm{e})} = 100\,\mathrm{cm}^{-1}$, $\Lambda^{(\mathrm{v})} = 10\,\mathrm{cm}^{-1}$ (bottom panels), as a function of the ratios $g/\Delta\varepsilon$, $\varpi/\Delta\varepsilon$, $V/\Delta\varepsilon$ and the transition dipole moment amplitude D, where $\Delta\varepsilon$ represents the site energy difference. Green points represent the values adopted for the simulations of the density matrix dynamics in the vibronic single exciton, exciton and sites bases, discussed in this chapter. Baths parameters are $T_{\mathrm{PB}}^{(\mathrm{e,v})} = 300\,\mathrm{K}$, $T_{\mathrm{BB}} = 5600\,\mathrm{K}$.

$\hat{\rho}(t_0) = \hat{\rho}_{\mathrm{S}}(t_0) \otimes \hat{\rho}_{\mathrm{BB}}(t_0) \otimes \hat{\rho}_{\mathrm{PB}}(t_0)$. Figure 8 depicts the populations of vibronic single exciton states for different values of the reorganization energy $\Lambda^{(\mathrm{e})} = 10, 30, 100\,\mathrm{cm}^{-1}$. Specifically, the population of the lowest energy vibronic single exciton state $\left|\psi_{17}\right\rangle$ of the PEB dimer increases for increasing values of the reorganization energy. In the case of the DBV dimer, there is an increase of two orders of magnitude in the population of the state $\left|\psi_{17}\right\rangle$, see Fig. 9 . This is a consequence of the intricate interplay between bath-enhanced rates and nonadiabatic dynamics of vibronic single

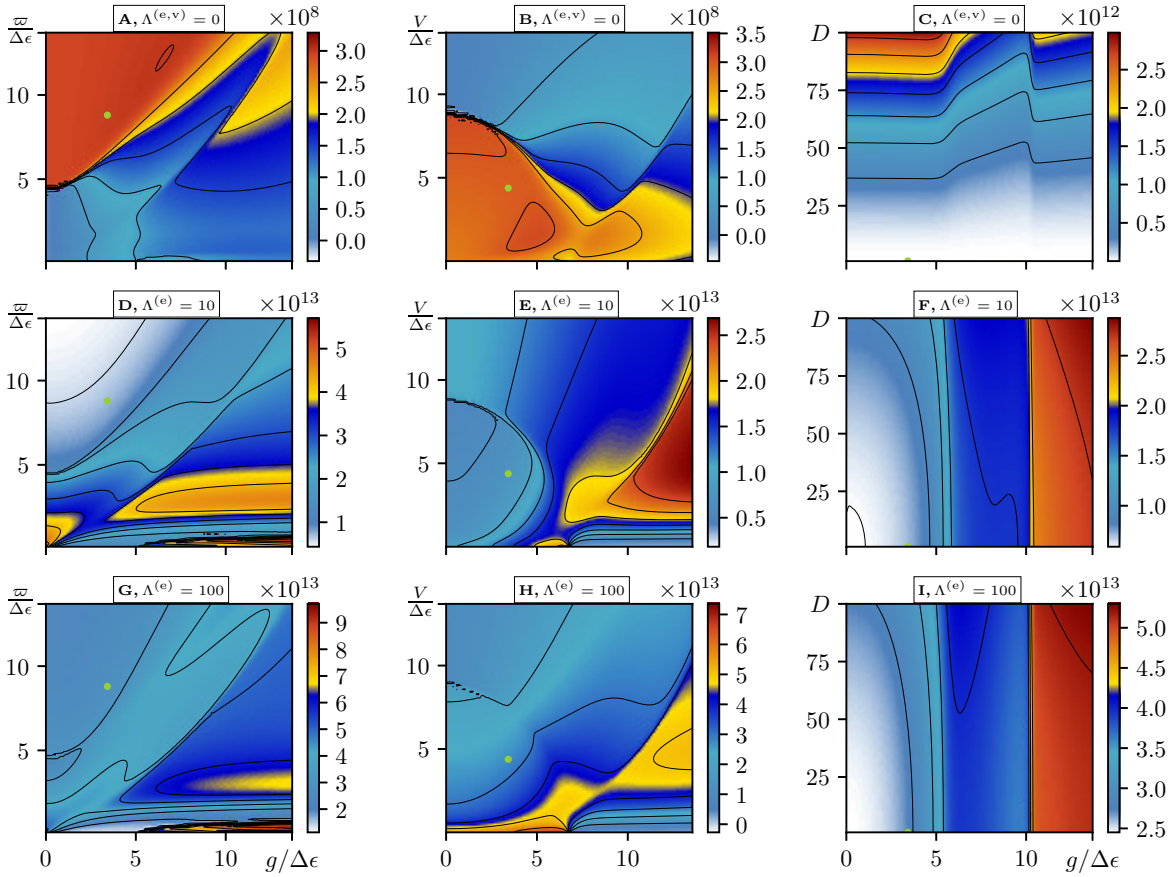

Figure 11. Decoherence rate $\gamma_{18,20}\,[\mathrm{s}^{-1}]$ (color map) for the DBV dimer with the reorganization energies $\Lambda^{(\mathrm{e,v})} = 0\,\mathrm{cm}^{-1}$ (top panels), $\Lambda^{(\mathrm{e})} = 10\,\mathrm{cm}^{-1}$, $\Lambda^{(\mathrm{v})} = 10\,\mathrm{cm}^{-1}$ (middle panels) and $\Lambda^{(\mathrm{e})} = 100\,\mathrm{cm}^{-1}$, $\Lambda^{(\mathrm{v})} = 10\,\mathrm{cm}^{-1}$ (bottom panels), as a function of the ratios $g/\Delta\varepsilon$, $\varpi/\Delta\varepsilon$, $V/\Delta\varepsilon$ and the transition dipole moment amplitude D, where $\Delta\varepsilon$ represents the site energy difference. Green points represent the values adopted for the simulations of the density matrix dynamics in the vibronic single exciton, exciton and sites bases, discussed in this chapter. Baths parameters are $T_{\mathrm{PB}}^{(\mathrm{e,v})} = 300$ K, $T_{\mathrm{BB}} = 5600$ K.

exciton states with small energy gaps.

Figure 8 also depicts the dynamics of superpositions between vibronic single exciton states (vibronic coherences). The vibronic coherences, originated by the turning-on of the incoherent radiation, decay due to the interaction with the phonon bath. Their influence on the population of the vibronic single exciton states is negligible, owing to the amplitude of the vibronic coherences is approximately one (PEB dimer) and two (DBV dimer) orders of magnitude

smaller than the populations of vibronic single exciton states.

To explore the role of the vibronic coupling and the incoherent light excitation process on the lifetime of quantum superpositions between vibronic single exciton states, the decoherence rate of the highest amplitude vibronic coherence $\mathbb{R}\rho_{18,20}(t)$ in the PEB dimer is analyzed (see Fig. 8). Figure 10 depicts the functional dependence of the decoherence rate $\gamma_{18,20}$ on the ratio between the vibronic coupling and the site energy difference $g/\Delta\varepsilon$, the ratio between the intramolecular vibrational frequency and the site energy difference $\varpi/\Delta\varepsilon$, the ratio between the electronic coupling and the site energy difference $V/\Delta\varepsilon$, and the dipole moment amplitude D. The green points in Fig. 10 depict the specific values for the PEB dimer, $g/\Delta\varepsilon = 0.26$, $\varpi/\Delta\varepsilon = 1.02$, $V_{12}/\Delta\varepsilon = 0.09$ and $D = 1$ (For the DBV dimer case, see Fig. 11).

In absence of thermal baths for the intra-molecular vibrational modes (not shown), the decoherence rate $\gamma_{18,20}$ decreases for increasing values of the vibronic coupling g. However, in the more realistic scenario depicted in Fig. 10, increasing the vibronic coupling may lead to regions of parameter space with higher decoherence rates. Thus, the decoherence rate $\gamma_{18,20}$ displays a non-trivial behavior under the variation of the physical quantities defined above and neither the vibronic resonance condition $\varpi_1 = \varpi_2 = \Delta e$ (i.e., nonadiabatic regime) nor the values of electronic and vibronic couplings of the dynamics discussed (see green points in Fig. 10) lead to the lowest value in the decoherence rate. Thus, the longest decoherence time for vibronic single exciton state superpositions is not reached under the physical conditions considered usually in two-dimensional-electronic-spectroscopy studies [Yeh et al., 2019; Duan et al., 2019].

For natural light-matter coupling strengths (Figs. 10 A, B, D, E, G and H): (i) increasing the reorganization energy increases the decoherence rate $\gamma_{18,20}$ for $\Lambda^{(\mathrm{e})} = 0, 10, 100\,[\mathrm{cm}^{-1}]$ as $\gamma_{18,20} \sim 10^{8}, 10^{13}, 10^{13}\,[\mathrm{s}^{-1}]$, respectively. (ii) For $\Lambda^{(\mathrm{e})} = 0$, the decoherence rate $\gamma_{18,20}$ is at least five orders of magnitude smaller than for cases with $\Lambda^{(\mathrm{e})} \neq 0$. This follows from the low intensity of sunlight and the energy-gap dependence of blackbody radiation decoherence rates $\gamma^{\mathrm{BB}}_{e,e'} \sim \left(\mu^2_{e,e'}\omega^3_{e,e'}/3\hbar\pi\varepsilon_0 c^3\right)\coth(\hbar\omega_{e,e'}/2k_{\mathrm{B}}T^{\mathrm{BB}})$. Thus, for small energy gaps $\hbar\omega_{e,e'}$, the decoherence rate $\gamma^{\mathrm{BB}}_{e,e'}$ may be considerably smaller than the case of an Ohmic thermal phonon bath $\gamma^{\mathrm{BB}}_{e,e'} \sim 4k_{\mathrm{B}}T^{\mathrm{PB}}\Lambda/\hbar^2\Omega$, which is energy-gap independent [Pachón et al., 2017]. For the values of the reorganization energy considered in Fig. 10, the increase

of the transition dipole moment amplitude leads to higher values in the decoherence rate $\gamma_{18,20}$ (see Fig. 10 C, F and I). Increasing of the vibronic coupling g in Fig. 10 for the values of the reorganization energy considered does not leads to decrease of the decoherence rate.

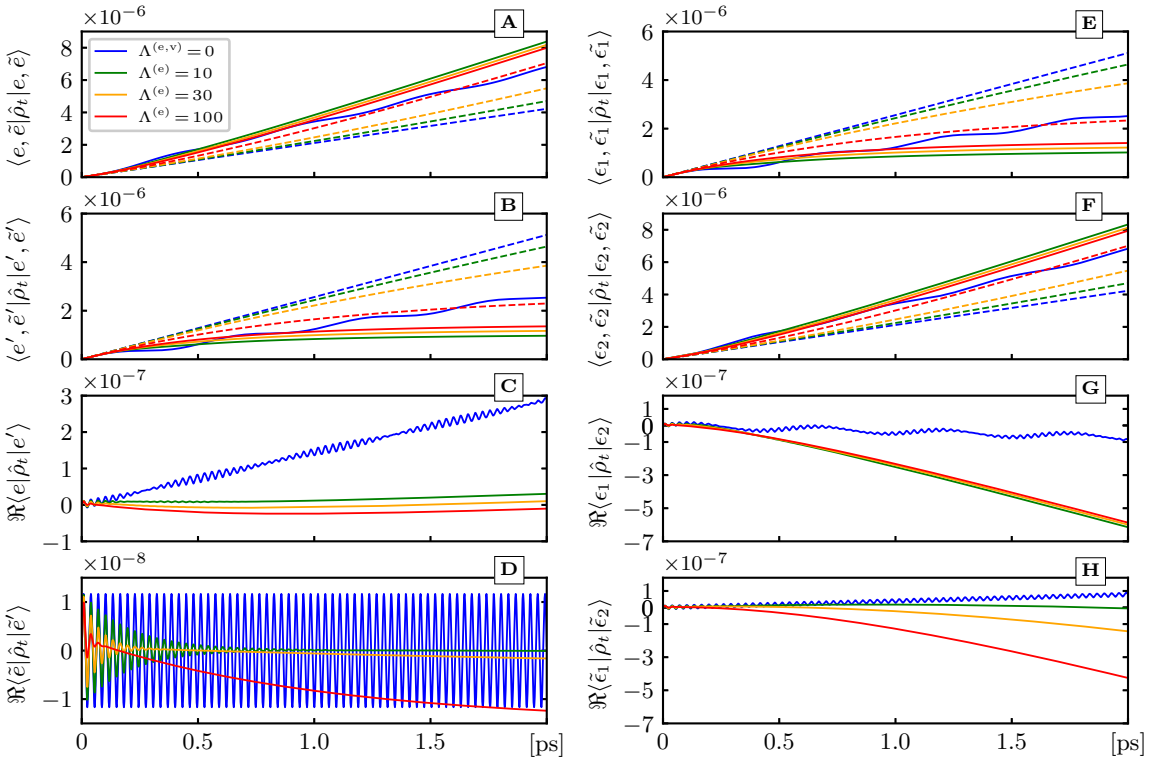

Figure 12. Left panels—Dynamics in the single exciton basis for the vibronic dimer case $\{|e\rangle, |e'\rangle\}$, and the electronic dimer case $\{|\tilde{e}\rangle, |\tilde{e}'\rangle\}$ varying the reorganization energy $\Lambda^{(e)}$ [cm^{-1}] ($\Lambda^{(v)} = 10$ cm^{-1}) in the PEB dimer (color coding is shown on the top left box): A,B) Populations of the lowest and highest energy single exciton states (solid and dashed lines represent the vibronic and electronic dimer cases, respectively). C) Single exciton coherence in the vibronic dimer model. D) Single exciton coherence in the electronic dimer model. Right panels—Dynamics in the site basis $\{\text{PEB}_{50/61\,\text{D}}, \text{PEB}_{50/61\,\text{C}}\}$ (vibronic dimer case $\{|\varepsilon_1\rangle, |\varepsilon_2\rangle\}$, and electronic dimer $|\tilde{\varepsilon}_1\rangle, |\tilde{\varepsilon}_2\rangle$) varying the reorganization energy $\Lambda^{(e)}$ [cm^{-1}] ($\Lambda^{(v)} = 10$ cm^{-1}) in the PEB dimer (same color coding as the top panels): E,F) Populations of the two site states in the vibronic dimer (solid lines) and the electronic dimer (dashed lines). G) Coherence between site states in the vibronic dimer model. H) Coherence between site states in the electronic dimer model. Baths parameters are $T_{\text{PB}}^{(e,v)} = 300$ K, $T_{\text{BB}} = 5600$ K.

2.2.2. Reduced exciton and site bases. The role of the high frequency intramolecular vibrational modes is explored by comparing the reduced electronic dynamics (tracing over the intramolecular vibrations) of the vibronic dimers considered above with their corresponding electronic dimer dynamics (no specific intramolecular vibrational modes). Figures 12 and 13 show the populations and coherences in the exciton (top panels) and site bases (bottom panels), with (vibronic dimer) and without (electronic dimer) intramolecular vibrational modes for the PEB and DBV dimers, respectively.

In the exciton basis, and in the absence of the phonon baths ($\Lambda^{(e,v)} = 0$ cm^{-1}), the population of the lowest energy exciton state of the vibronic dimer is higher than that of its corresponding electronic dimer case: one and half times for the PEB dimer (see Fig. 12 A), and two orders of magnitude for the DBV dimer (see Fig. 13 A). The amplitude of the coherence between single exciton states in the vibronic dimer model (see Fig. 12 C) is one order of magnitude higher than in the electronic dimer case (see Fig. 12 D) for the PEB dimer, and two orders of magnitude in the case of DBV dimer (see Fig. 13 C and D). The increase in population and coherence can be understood as the result of the smaller energy gaps [Pachón and Brumer, 2011, 2012] induced by intramolecular vibrations, i.e., a consequence of the nonadiabatic character of the dynamics (see Fig. 7). Hence, for $\Lambda^{(e,v)} = 0$, the population of the lowest energy exciton state and the coherence between single exciton states increase with the inclusion of intramolecular vibrational modes.

In the presence of the phonon bath ($\Lambda^{(e,v)} \neq 0$), the behavior of populations are similar to $\Lambda^{(e,v)} = 0$. The amplitude of the coherences increases slightly in the PEB dimer (see Fig. 12 C and D) and by up to one order of magnitude in the DBV dimer (see Fig. 13 C and D). The population of the lowest energy exciton state of the PEB dimer has higher amplitudes in the vibronic dimer than in the electronic dimer; however, as the value of the reorganization increases, this population difference decreases. Moreover, the population rate of the reduced vibronic dimer barely changes by increasing the reorganization energy, thus being robust against the fluctuations of the phonon environment (see Figs. 12 A and 13 A). For small values of the reorganization energy ($\Lambda^{(e)} \sim 10$cm^{-1}), a similar population trend is found for the DBV dimer; however, for moderate ($\Lambda^{(e)} \sim 30$cm^{-1}) and large values ($\Lambda^{(e)} \sim 100$cm^{-1}) of the reorganization energy, the population of the lowest energy exciton state has slightly higher amplitudes in the case

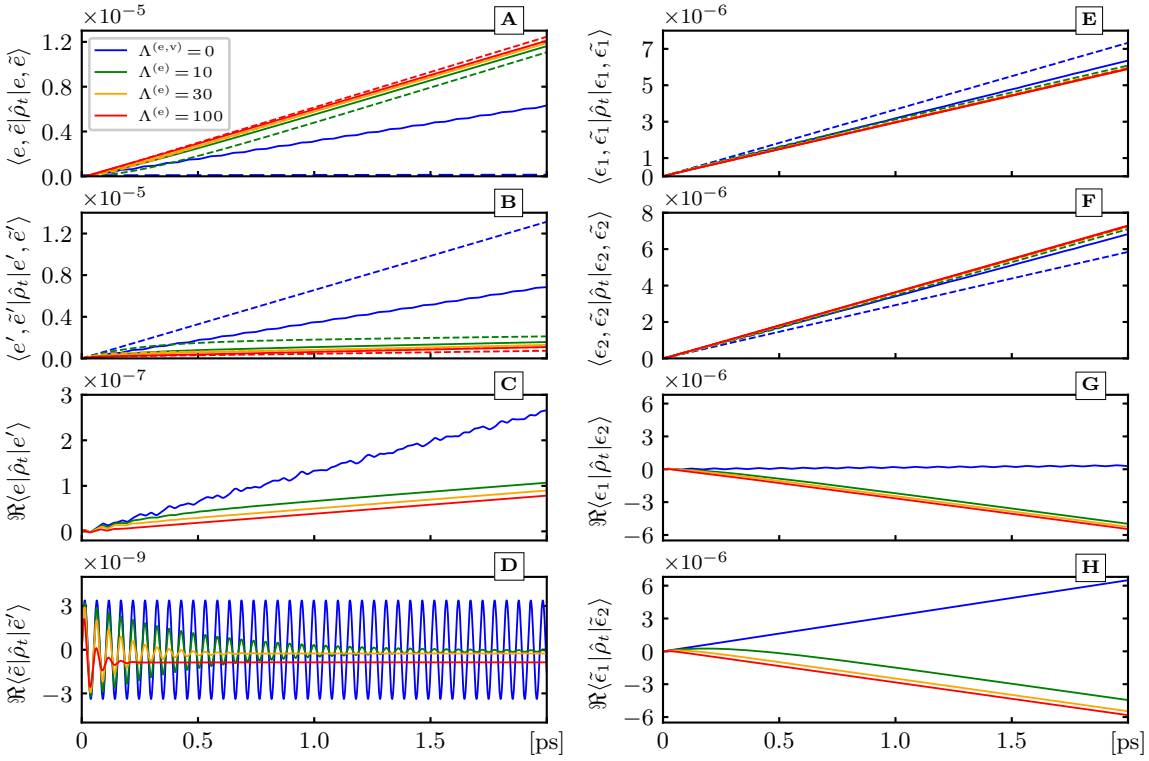

Figure 13. Left panels—Dynamics in the single exciton basis for the vibronic dimer case $\{|e\rangle, |e'\rangle\}$, and the electronic dimer case $\{|\tilde{e}\rangle, |\tilde{e}'\rangle\}$ varying the reorganization energy $\Lambda^{(e)}$ [cm^{-1}] ($\Lambda^{(v)} = 10$ cm^{-1}) in the DBV dimer (color coding is shown on the top left box): A,B) Populations of the lowest and highest energy single exciton states (solid and dashed lines represent the vibronic and electronic dimer cases), respectively. C) Single exciton coherence in the vibronic dimer model. D) Single exciton coherence in the electronic dimer model. Right panels—Dynamics in the site basis $\{\mathrm{DBV}_{50/61\,\mathrm{D}}, \mathrm{DBV}_{50/61\,\mathrm{C}}\}$ (vibronic dimer case $\{|\varepsilon_1\rangle, |\varepsilon_2\rangle\}$, and electronic dimer $\{|\tilde{\varepsilon}_1\rangle, |\tilde{\varepsilon}_2\rangle\}$) varying the reorganization energy $\Lambda^{(e)}$ [cm^{-1}] ($\Lambda^{(v)} = 10$ cm^{-1}) in the DBV dimer (same color coding as the top panels): E,F) Populations of the two site states in the vibronic dimer (solid lines) and the electronic dimer (dashed lines). G) Coherence between site states in the vibronic dimer model. H) Coherence between site states in the electronic dimer model. Baths parameters are $T_{\mathrm{PB}}^{(e,v)} = 300$ K, $T_{\mathrm{BB}} = 5600$ K.

of the electronic dimer than the vibronic dimer (see Fig. 13 A). This clearly shows the highly non-trivial interplay between bath-enhanced population rates and nonadiabatic dynamics for highly localized (PEB) and highly delocalized (DBV) excitons.

In the site basis, and for all values of the reorganization energy considered, the population of the chromophores

$\mathrm{PEB}_{50/61\,\mathrm{C}}$ and $\mathrm{DBV}_{50/61\,\mathrm{C}}$ is higher than that of $\mathrm{PEB}_{50/61\,\mathrm{D}}$ and $\mathrm{DBV}_{50/61\,\mathrm{D}}$, respectively, in the case of the vibronic dimer than in the electronic dimer case (see Fig. 12 E and F, and Fig. 13 E and F). Since population is pumped from the ground state and the transition dipole moments favor excitation to singly excited exciton states with low energy, the population difference occurs due the localization l_{ε_i} of the vibronic single exciton states on those chromophores; specifically, $l_{\varepsilon_1}(\psi_{17}) = 0.007, l_{\varepsilon_2}(\psi_{17}) = 0.993$, $l_{\varepsilon_1}(\psi_{18}) = 0.524, l_{\varepsilon_2}(\psi_{18}) = 0.476$, $l_{\varepsilon_1}(\psi_{19}) = 0.007, l_{\varepsilon_2}(\psi_{19}) = 0.993$, and $l_{\varepsilon_1}(\psi_{20}) = 0.475, l_{\varepsilon_2}(\psi_{20}) = 0.525$. Here, $\mathrm{PEB}_{50/61\,\mathrm{D}}$ and $\mathrm{DBV}_{50/61\,\mathrm{D}}$ are sites 1 whereas $\mathrm{PEB}_{50/61\,\mathrm{C}}$ and $\mathrm{DBV}_{50/61\,\mathrm{C}}$ are sites 2.

For the PEB dimer, the amplitude of the coherence between site states of the vibronic dimer is higher than that of its corresponding electronic dimer case. Also, the coherence between site states decreases with the coupling to the phonon bath and shows to be robust against the fluctuations of the phonon environment. For the DBV dimer, the coherence between site states increases with the coupling to the phonon bath and remains of the same order for electronic and vibronic dimers. Therefore, for the vibronic dimers analyzed here, and for the highest values of the reorganization energy, quantized vibrational modes barely enhance populations or coherences in the site basis.

The role of intramolecular vibrations resonant with excitonic transitions in light-harvesting systems was analyzed under natural sunlight illumination. The inclusion of the intramolecular vibrational modes reinforces the exciton coherence by up to one order of magnitude, as was shown for the DBV dimer. However, the comprehensive analysis shows that the populations of single exciton and site states of vibronic dimers are not significantly affected as compared to their corresponding electronic dimers. There is no direct evidence of an enhancement in the energy transport mediated by the inclusion of resonant intramolecular vibrational degrees of freedom under natural conditions, as it was analyzed in the previous chapter. Recently, similar conclusions were elucidated on the impact of the vibronic coupling in the electronic and vibrational coherences observed in two-dimensional-electronic-spectroscopies [Duan et al., 2019].

3. Intramolecular vibrational modes dynamics under sunlight illumination

More than a decade ago, the coherent oscillations in nonlinear spectra of photosynthetic light-harvesting complexes ignited an intense debate on the existence of non-trivial quantum effects in light-initiated reactions in

biology [Engel et al., 2007; Sarovar et al., 2010; Collini et al., 2010; Panitchayangkoon et al., 2010; Pachón and Brumer, 2011; Huelga and Plenio, 2013; Chenu and Scholes, 2015; Curutchet and Mennucci, 2016; Scholes et al., 2017]. Despite the conceptual difference between excitation by coherent (lab conditions) and incoherent light (natural conditions) [Brumer, 2018; Mančal, 2020], the discussion on the quantum/classical character of energy transport has focused either on modeling light-harvesting system by classical formulations or on measuring quantum fluctuations of the protein-complex states. By a consistent quantum formulation of the natural conditions, it will be shown in this chapter that the state of intramolecular vibrations evolves devoid of non-trivial quantum correlations [O'Reilly and Olaya-Castro, 2014]. Therefore, energy transport in light-harvesting complexes under natural conditions is not driven by non-classical intramolecular vibrational processes [Calderón and Pachón, 2020].

Despite the fact that incoherent sources are expected to induce incoherent dynamics [Brumer and Shapiro, 2012], the *suddenly-turning-on* of incoherent radiation generates effectively coherent dynamics in the vibronic single exciton basis. This may equivocally leads to the conclusion that the temporal coherence of the light source plays a minor role on the energy-transfer process. By focusing on the non-classical behaviour of the states of intramolecular vibrational degrees of freedom, it is unambiguously shown that under sunlight illumination conditions, the state of the two vibrational modes and that of the anticorrelated vibrational mode evolve devoid of non-classical correlations. This is in sharp contrast to the case of illumination by coherent light sources [O'Reilly and Olaya-Castro, 2014] and can be considered as a genuine and experimentally verifiable difference between natural and in-lab conditions, *independent of the suddenly-turning-on condition*.

In the first section of this chapter, it will be introduce the basic concepts of single mode quantum optics states, namely, number and coherent states [Mandel and Wolf, 1995; Gerry and Knight, 2005; Grynberg et al., 2010; Agarwal, 2013]. The diagonal coherent state representation will be analyzed, with the purpose to define the Mandel parameter, which allows for quantifying the non-trivial quantum character of a bosonic state by comparing the occupation number distribution for a given bosonic state with the occupation number distribution of a coherent state [Mandel and Wolf, 1995; Gerry and Knight, 2005; Agarwal, 2013]. The concepts developed in Section 3.1 will not be applied in the context of quantum optics, i.e, for electromagnetic field states, but phonon states, i.e., intramolecular vibrational

modes in photosynthetic dimers, in order to discuss their non-classical character. Coherent (Sec. 3.2) and incoherent (Sec. 3.3) excitation conditions will be analyzed for the intramolecular vibrational modes dynamics. [Calderón and Pachón, 2020].

3.1. Non-classicality of bosonic states

In quantum optics has been developed different methods to quantify theoretically and experimentally the quantum character of the electromagnetic field, that follows a bosonic statistics [Mandel and Wolf, 1995; Gerry and Knight, 2005; Grynberg et al., 2010; Agarwal, 2013]. It is possible to represent the density operator by means of distribution functions in phase space [Hillery et al., 1984; Carmichael, 2009; Agarwal, 2013]. In particular, the $P(\alpha)$ distribution introduced by Glauber and Sudarshan [Glauber, 1963; Sudarshan, 1963], allows for a diagonal coherent state representation, that results useful to evaluate correlations with normal ordering [Carmichael, 2009]. The phase space content all the variables associated with the real and imaginary parts of α. The density operator can be represented by means of the $P(\alpha)$ distribution as

$$\hat{\rho} = \int P(\alpha)\,|\alpha\rangle\langle\alpha|\,\mathrm{d}^2\alpha, \quad \int P(\alpha)\mathrm{d}^2\alpha = 1. \tag{63}$$

The $P(\alpha)$ distribution does not have all the classical probability distribution properties since it can adopt negative values or display singularities for some bosonic quantum states. Quantum states with $P(\alpha) \geq 0$ are considered "classical" since their expected values can be simulated by averaging over random classical fields with probability distribution $P(\alpha)$ [Gerry and Knight, 2005; Garrison and Chiao, 2008]. Quantum states with $P(\alpha) < 0$ in some region of the phase space are considered "non-classical" [Scully and Zubairy, 1997; Gerry and Knight, 2005; Agarwal, 2013]. The distribution $P(\alpha)$ is given by [Scully and Zubairy, 1997; Gerry and Knight, 2005; Agarwal, 2013]

$$P(\alpha) = \frac{1}{\pi^2}\mathrm{e}^{|\alpha|^2}\int \langle -\beta|\hat{\rho}|\beta\rangle\,\mathrm{e}^{|\beta|^2-(\beta\alpha^*-\beta^*\alpha)}\mathrm{d}^2\beta. \tag{64}$$

The expected value of normally-ordered moments of the boson field, that is, all creation operators to the left of

annihilation operators, can be expressed in the form

$$\left\langle \hat{a}^{\dagger m}\hat{a}^{n}\right\rangle = \int P(\alpha)\alpha^{*m}\alpha^{n}\mathrm{d}^{2}\alpha = \left\langle \alpha^{*m}\alpha^{n}\right\rangle_{P}. \tag{65}$$

3.1.1. Mandel parameter. The Mandel parameter Q_M allows characterizing non-classicality in the case of bosonic fields. Mandel established that the photon number distribution for the case of a coherent state corresponds to a Poisson distribution, and therefore any distribution that is narrower than this must correspond to a non-classical state [Agarwal, 2013; Mandel, 1979]. The Mandel parameter reads

$$Q_M = \frac{\left\langle \hat{n}^2\right\rangle - \left\langle \hat{n}\right\rangle^2}{\left\langle \hat{n}\right\rangle} - 1 = \frac{\left\langle (\hat{a}^\dagger\hat{a})^2\right\rangle - \left\langle \hat{a}^\dagger\hat{a}\right\rangle^2 - \left\langle \hat{a}^\dagger\hat{a}\right\rangle}{\left\langle \hat{a}^\dagger\hat{a}\right\rangle}. \tag{66}$$

For a coherent state the Mandel parameter readas $Q_M = 0$. For a Fock (number) state $Q_M = -1$. A negative value of Q_M represents a sufficient condition for a state to be considered non-classical. If $Q_M > 0$, nothing can be concluded about non-classicality [Gerry and Knight, 2005; Agarwal, 2013]. To prove that a negative value of Q_M implies non-classicality in a quantum state, it can be related to the distribution $P(\alpha)$ using Eq. (65)

$$Q_M = \frac{\left\langle \hat{a}^{\dagger 2}\hat{a}^2\right\rangle - \left\langle \hat{a}^\dagger\hat{a}\right\rangle^2}{\left\langle \hat{a}^\dagger\hat{a}\right\rangle} = \frac{\left\langle \alpha^{*2}\alpha^2\right\rangle_P - \left\langle \alpha^*\alpha\right\rangle_P^2}{\left\langle \alpha^*\alpha\right\rangle_P} = \frac{\left\langle (\alpha^*\alpha - \left\langle \alpha^*\alpha\right\rangle_P)^2\right\rangle_P}{\left\langle \alpha^*\alpha\right\rangle_P}. \tag{67}$$

The value of Q_M will always be positive if the distribution $P(\alpha)$ corresponds to a classical probability distribution. Therefore, if the value of Q_M is negative, it is due to the non-classicality of the distribution $P(\alpha)$ [Agarwal, 2013].

3.2. Intramolecular vibrational dynamics ignited by coherent light excitation

The vibronic dimers considered in the previous chapter are described by the Hamiltonian (see Eq. 105)

$$\begin{aligned}\hat{H}_{\mathrm{S}} = {} & \varepsilon_1\hat{\sigma}_1^+\hat{\sigma}_1^- + \varepsilon_2\hat{\sigma}_2^+\hat{\sigma}_2^- + V_{12}\left(\hat{\sigma}_1^+\hat{\sigma}_2^- + \hat{\sigma}_2^+\hat{\sigma}_1^-\right) + \hbar\varpi\left(\hat{b}_1^\dagger\hat{b}_1 + \hat{b}_2^\dagger\hat{b}_2\right) \\ & + \hbar g\left[\hat{\sigma}_1^+\hat{\sigma}_1^-\left(\hat{b}_1^\dagger + \hat{b}_1\right) + \hat{\sigma}_2^+\hat{\sigma}_2^-\left(\hat{b}_2^\dagger + \hat{b}_2\right)\right].\end{aligned} \tag{68}$$

Initially, the intramolecular vibrational modes of frequency $\varpi_1 = \varpi_2 = \varpi = 1058\ \mathrm{cm}^{-1}$ for the PEB dimer and $\varpi_1 = \varpi_2 = \varpi = 643\ \mathrm{cm}^{-1}$ for the DBV dimer are in thermal equilibrium at $T = 300\,\mathrm{K}$. The frequency of the two intramolecular vibrational modes is in full resonance with the exciton splitting, i.e., a nonadiabatic scenario where $\varpi = \Delta e$ (see Fig. 7). The vibronic coupling strength to each monomer is the same, i.e., $g_1 = g_2 = g$, specifically, $g = 267.1\ \mathrm{cm}^{-1}$ for the PEB dimer and $g = 250\,\mathrm{cm}^{-1}$ for the DBV dimer.

In the seminal contribution discussed in Ref. [Tiwari et al., 2013] was analyzed the importance of the anti-correlated vibrational mode in the nonadiabatic dynamics of the FMO complex. The correlated (+) and anticorrelated (−) vibrational modes of frequencies $\varpi_+ = \varpi_- = \varpi$ are defined through the creation and annihilation operators

$$\hat{b}_+ = \frac{1}{\sqrt{2}}(\hat{b}_1 + \hat{b}_2), \quad \hat{b}_+^\dagger = \frac{1}{\sqrt{2}}(\hat{b}_1^\dagger + \hat{b}_2^\dagger), \tag{69}$$

$$\hat{b}_- = \frac{1}{\sqrt{2}}(\hat{b}_1 - \hat{b}_2), \quad \hat{b}_-^\dagger = \frac{1}{\sqrt{2}}(\hat{b}_1^\dagger - \hat{b}_2^\dagger). \tag{70}$$

In terms of the correlated and anticorrelated vibrational modes, i.e., delocalized vibrational coordinates, the vibronic dimer Hamiltonian of Eq. (68) reads

$$\begin{aligned}\hat{H}_\mathrm{S} = {} & \varepsilon_1 \hat{\sigma}_1^+ \hat{\sigma}_1^- + \varepsilon_2 \hat{\sigma}_2^+ \hat{\sigma}_2^- + V_{12}\left(\hat{\sigma}_1^+ \hat{\sigma}_2^- + \hat{\sigma}_2^+ \hat{\sigma}_1^-\right) + \hbar\varpi\left(\hat{b}_+^\dagger \hat{b}_+ + \hat{b}_-^\dagger \hat{b}_-\right) \\ & + \frac{\hbar g}{\sqrt{2}}\left[\left(\hat{\sigma}_1^+ \hat{\sigma}_1^- - \hat{\sigma}_2^+ \hat{\sigma}_2^-\right)\left(\hat{b}_-^\dagger + \hat{b}_-\right) + \left(\hat{\sigma}_1^+ \hat{\sigma}_1^- + \hat{\sigma}_2^+ \hat{\sigma}_2^-\right)\left(\hat{b}_+^\dagger + \hat{b}_+\right)\right].\end{aligned} \tag{71}$$

The correlated vibrational mode (center of mass mode) does not influence the energy transfer between the chromophores [Tiwari et al., 2013, 2017]. On the other hand, the anticorrelated vibrational mode (tuning mode) allows nonadiabatic energy transfer by tuning the electronic energy gap between chromophores [Tiwari et al., 2013, 2017].

The initial thermal state ($T = 300\,\mathrm{K}$) of the intramolecular vibrations in the PEB dimer has no non-classical character [Agarwal, 2013], the populations of the first four quantized levels are $\langle \nu_i = 0|\hat{\rho}(t=0)|\nu_i = 0\rangle = 0.993769$, $\langle \nu_i = 1|\hat{\rho}(t=0)|\nu_i = 1\rangle = 6.19244 \times 10^{-3}$, $\langle \nu_i = 2|\hat{\rho}(t=0)|\nu_i = 2\rangle = 3.85868 \times 10^{-5}$, $\langle \nu_i = 3|\hat{\rho}(t=0)|\nu_i = 3\rangle = 2.40444 \times 10^{-7}$. Considering a coherent excitation initial condition for the electronic degrees of freedom of the chromophores in photosynthetic complexes, usually assumed in simulations of pulsed-laser-spectroscopic-setups [Brumer,

2018], the intramolecular vibrational dynamics turn out to display a non-classical character [O'Reilly and Olaya-Castro, 2014].

In Fig. 14, the PEB dimer is assumed to have been prepared in the excitation of the electronic site 1 (first two rows) and an exciton state [O'Reilly and Olaya-Castro, 2014] (last two rows). Thus, under pulsed-laser-excitation conditions, the dimer is initially prepared in a coherent superposition of vibronic exciton states provided that the chromophore-chromophore dipole interaction is finite. For these excitation conditions, the Mandel parameter adopts negative values, indicating that during the dynamics, the state of the intramolecular vibrational modes of frequencies ϖ_1 and ϖ_2, and the state of the anticorrelated vibrational mode of frequency ϖ_- has a nonclassical character. In this simulations, the dynamics are unitary, so it is to be expected that this nonclassical character will be diminished by the presence of decoherence interactions with the phonon baths [O'Reilly and Olaya-Castro, 2014].

Fig. 14 shows the changes in the population dynamics of the intramolecular vibrational modes quantized levels. The deviation from his initial thermal equilibrium state is a consequence of the transient formation of vibronic exciton states using the coherent initial excitation condition that also generates coherences between vibrational states (see Fig. 15, second and third columns).

3.3. Classicality of intramolecular vibrations dynamics under sunlight illumination

In the previous section, it was well established that intramolecular quantized vibrational modes initially in a thermal state could develop a genuinely non-classical character due to coherent exciton-vibration interactions [O'Reilly and Olaya-Castro, 2014]. The detailed analysis of the potential generation of non-classicality, in the context of incoherent light excitation, allows to conclude that the quantized vibrational modes do not display non-classical correlations quantified by the Mandel parameter [Mandel and Wolf, 1995].

As it was discussed above the Mandel parameter identifies the non-classical character of bosonic states through the comparison of occupation number distribution for a given bosonic state with the occupation number distribution of a coherent state [Mandel and Wolf, 1995]. For the case of a coherent state the occupation number distribution corresponds to a Poisson distribution $Q = 0$. Thus, for any occupation number distribution narrower than a Poisson distribution, i.e., with $Q < 0$, the associated bosonic state has a quantum character with no classical analog.

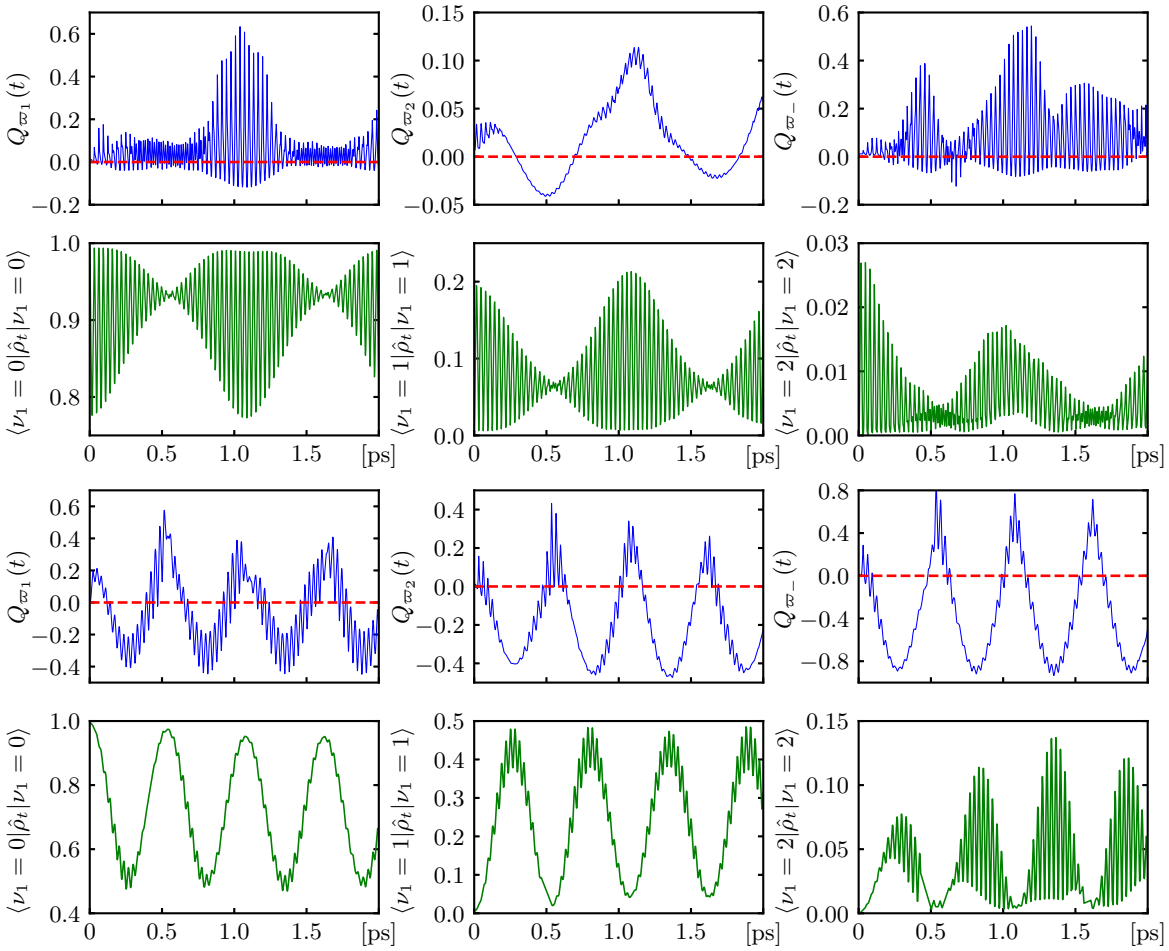

Figure 14. Values of the Mandel parameter Q for the vibrational modes of frequencies ϖ_1, ϖ_2, and ϖ_- and populations of the first three quantized levels of the intramolecular vibrational mode of frequency ϖ_1 localized in chromophore $\text{PEB}_{50/61\,\text{D}}$. Different initial electronic excitation conditions are considered: coherent excitation of the electronic site 1 $\langle\varepsilon_1|\hat{\rho}(t=0)|\varepsilon_1\rangle = 1$ (first two rows), coherent excitation of the highest energy excitonic state $\langle e'|\hat{\rho}(t=0)|e'\rangle = 1$ (last two rows). The effect of the phonon baths has not been considered, so the dynamics is unitary.

For different values of the reorganization energy and under sunlight illumination conditions, Fig. 16 depicts the Mandel parameter for the two vibrational modes of frequencies ϖ_1 and ϖ_2 considered in the vibronic model of the PEB and DBV dimers. The reduced dynamics of the anticorrelated vibrational mode of frequency ϖ_-, previously analyzed in the seminal contribution in Ref.[Tiwari et al., 2013], and responsible for the nonadiabatic character of the dynamics (see Fig. 7), is also considered. For every case considered, the Mandel parameter adopt positive values,

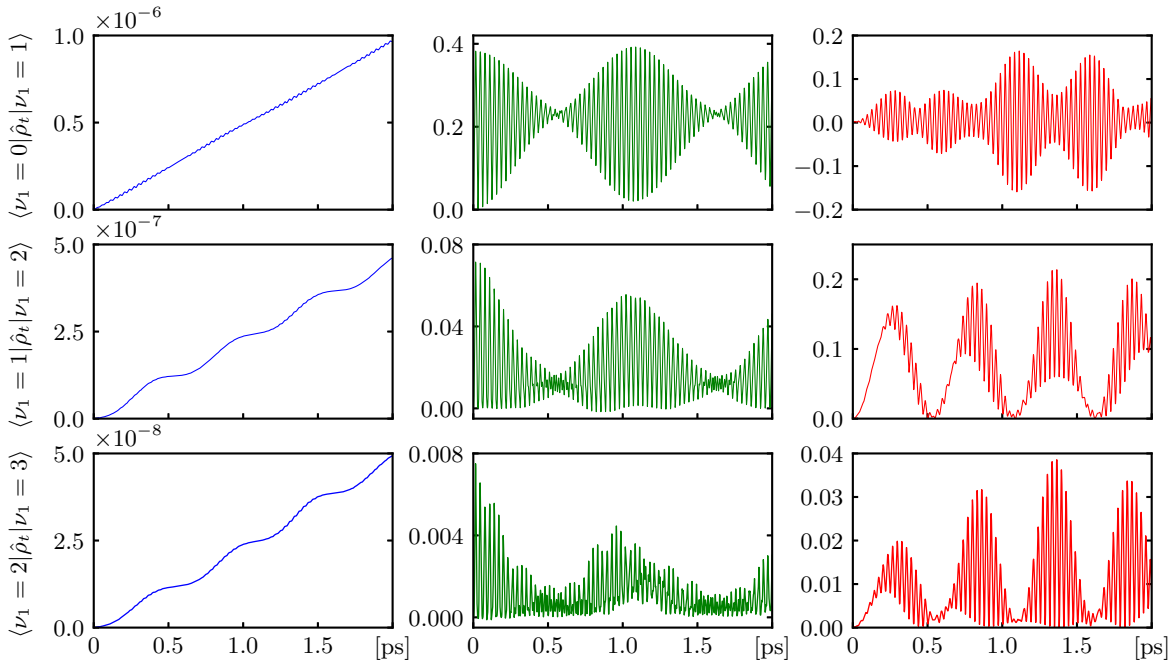

Figure 15. Coherences between the first four quantized levels ($n = 0, 1, 2, 3$) of the intramolecular vibrational mode of frequency ϖ_1 localized in chromophore $\mathrm{PEB}_{50/61\,\mathrm{D}}$ under different initial electronic excitation conditions: incoherent light excitation (first column), coherent excitation of the electronic site 1 $\langle \varepsilon_1 | \hat{\rho}(t=0) | \varepsilon_1 \rangle = 1$ (second column), and coherent excitation of the highest energy excitonic state $\langle e' | \hat{\rho}(t=0) | e' \rangle = 1$ (third column). The effect of the phonon baths has not been considered, so the dynamics is unitary.

indicating that during the dynamics, the state of the intramolecular vibrations modes has a classical character. Even, in the case of absence of phonon bath ($\Lambda^{(\mathrm{e,v})} = 0$), the value of the Mandel parameter remains positive [Calderón and Pachón, 2020].

Under sunlight illumination conditions, dimers are initially in their the electronic ground state while intramolecular vibrations, that are decoupled from the ground state, are initially at thermal equilibrium; therefore, the initial condition is devoid of quantum superpositions. Under pulsed-laser-excitation conditions, vibrations are also assumed to be at thermal equilibrium; however, in sharp contrast to natural conditions, the dimer is assumed to have been prepared in, e.g., an exciton state. Therefore, under pulsed-laser-excitation conditions, the dimer is initially prepared in a coherent superposition of vibronic exciton states provided that the chromophore-chromophore dipole interaction is finite.

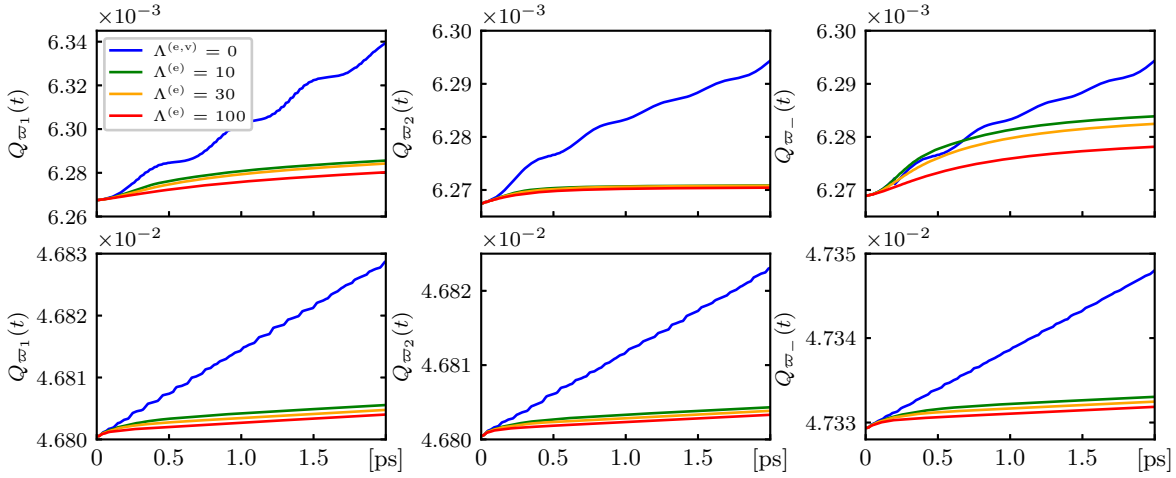

Figure 16. Values of the Mandel parameter Q for the vibrational modes of frequencies ϖ_1, ϖ_2, and ϖ_{ac} (top pannels: PEB dimer, bottom panels: DBV dimer), for different values of the reorganization energies $\Lambda^{(e)}\,[\mathrm{cm}^{-1}]$ and $\Lambda^{(v)} = 10\,\mathrm{cm}^{-1}$ (color coding is shown on the top left). Baths parameters are $T_{PB}^{(e,v)} = 300\,\mathrm{K}$, $T_{BB} = 5600\,\mathrm{K}$.

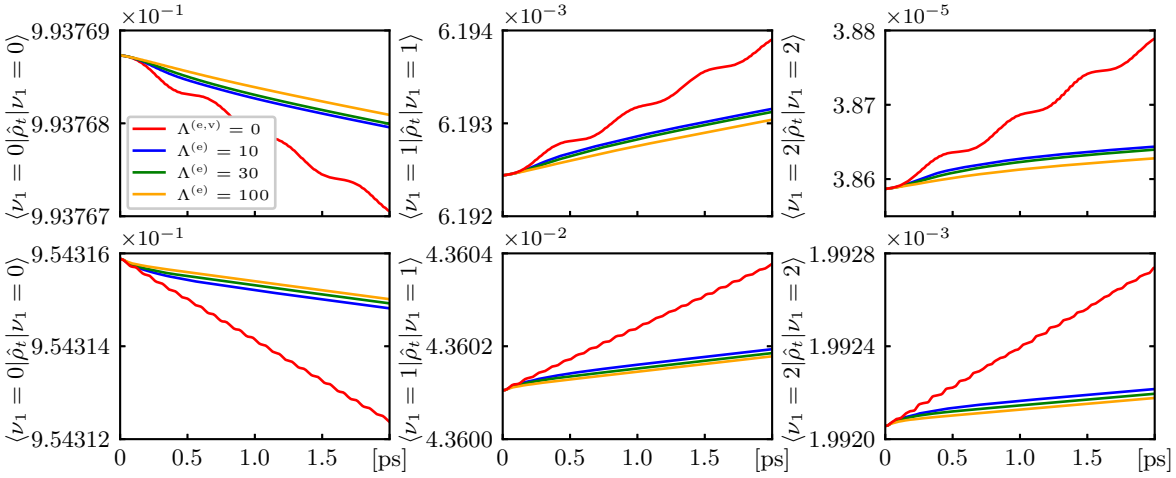

Figure 17. Populations of the first three quantized levels of the intramolecular vibrational mode of frequency ϖ_1 localized in chromophore $\mathrm{PEB}_{50/61\,\mathrm{D}}$ (top pannels), and chromophore $\mathrm{DBV}_{50/61\,\mathrm{D}}$ (bottom panels), for different values of the reorganization energies $\Lambda^{(e)}\,[\mathrm{cm}^{-1}]$ and $\Lambda^{(v)} = 10\,\mathrm{cm}^{-1}$ (color coding is shown on the top left). Baths parameters are $T_{PB}^{(e,v)} = 300\,\mathrm{K}$, $T_{BB} = 5600\,\mathrm{K}$.

Fig. 17 depicts the populations of the first three quantized levels of the intramolecular vibrations mode of frequency ϖ_1 localized in chromophores $\mathrm{PEB}_{50/61\,\mathrm{D}}$ and $\mathrm{DBV}_{50/61\,\mathrm{D}}$, under sunlight illumination conditions. Considering that the initial state for the intramolecular vibrations is a thermal one, it is clear from the quantized levels

populations dynamics that the state will remain thermal. Nevertheless, in sharp contrast to the pulsed-laser-excitation scenario depicted in Fig. 14. Fig. 15 (first column) shows the coherences between the first four quantized levels of the intramolecular vibrational mode of frequency ϖ_1 localized in the chromophore $\mathrm{PEB}_{50/61\,\mathrm{D}}$. These coherences are approximately one to three orders of magnitude smaller than the populations depicted in Fig. 17 (top pannels); therefore their influence on the populations dynamics is negligible.

For vanishing chromophore-chromophore dipole interaction, the electronic and vibrational contributions to the vibronic Hamiltonian in Eq. (105) commute; thus indicating that a product state of electronic and vibrational single eigenstates will also be an eigenstate –not a coherent superposition of eigenstates– of the vibronic Hamiltonian. The fact that for this product state the Mandel parameter adopts only positive values led to conclude [O'Reilly and Olaya-Castro, 2014] that the transient formation of vibronic exciton states establishes non-classical correlations in the vibrational modes. However, the chromophore-chromophore dipole interaction is finite under sunlight illumination but no non-classical correlations are established provided lack quantum correlations in the initial state. Therefore, non-classical correlations does not emerge due to the transient formation of vibronic exciton states, but as a consequence of the initial quantum correlations established in the light-harvesting system by the pulsed-laser-preparation of the initial state.

Summarizing, the role of intramolecular vibrations resonant with excitonic transitions in light-harvesting systems was analyzed under natural sunlight illumination and the standard pulsed-laser-coherent-excitation. Under incoherent light excitation conditions, the initial state of the light-harvesting system is of incoherent nature, namely, an incoherent mixture of eigenstates. For this scenario (see Fig. 16), it was further shown that intramolecular vibrational modes evolve devoid of non-classical correlations. Therefore, the generation of non-classical correlations via the transient formation of vibronic exciton states lacks of theoretical support since the quantum correlations come from the quantum superposition encoded in the initial state. Thus, that picture should be replaced in favor of the natural dynamics of the initial quantum correlations established in the light-harvesting system by the pulsed-laser-preparation

of the initial state.

4. Quantum to classical cavity molecular electrodynamics

Quantum cavity chemistry addresses the possibility of altering the chemical landscape giving place to new photophysical phenomena [Ebbesen, 2016; Ribeiro et al., 2018; Ruggenthaler et al., 2018; Flick et al., 2018; Dovzhenko et al., 2018; Herrera and Spano, 2018; Feist et al., 2018; Kockum et al., 2019; Hertzog et al., 2019; Herrera and Owrutsky, 2020] by coupling molecular systems to the confined photonic degrees of freedom in microcavities [Kavokin et al., 2007]. It presents as a promising tool to control room-temperature photophysical processes in organic molecules. Evidence of this new phenomena have been discussed in the context of singlet fission processes [Martínez-Martínez et al., 2018], triplet harvesting [Martínez-Martínez et al., 2019], energy transfer [Zhong et al., 2016, 2017; Sáez-Blázquez et al., 2018; Du et al., 2018; Sáez-Blázquez et al., 2019], remote control of chemical reactions [Du et al., 2019], and nonadiabatic effects [Galego et al., 2015; Kowalewski et al., 2016a; Gu and Mukamel, 2020].

In classical control theory [Shapiro and Brumer, 2003], properties of light such as intensity of phase are utilized to modify the intrinsic dynamics of molecular reactions with classical laser-control schema, in quantum cavity chemistry is the quantum nature of light that becomes essential for controlling the chemical landscape of molecular reactions. However, despite the nonadiabatic effects in the populations of the adiabatic ground state, evidence in the NaI molecule [Kowalewski et al., 2016a; Csehi et al., 2017] points to the lack of noticeable difference between the ignited by classical laser radiation and cavity-induced dynamics. This situation has raised the interest in analyzing under what conditions classical radiation fields can produce the same molecular dynamics as light quantum states [Csehi et al., 2019].

Traditionally, semiclassical methods have been studied in the context of light-matter interaction by making a full quantum treatment of the molecular degrees of freedom and considering different classical dynamics schema for the photonic degrees of freedom [Hoffmann et al., 2019a,b; Chen et al., 2019; Li et al., 2020]. Recently, by using mixed quantum-classical dynamics techniques [Gerasimenko, 1982; Grunwald et al., 2009] to solve the Ehrenfest mean-field dynamics have been able to account, to some extend, for spontaneous emission, interference, strong coupling, and correlated light-matter dynamics [Hoffmann et al., 2019a,b; Chen et al., 2019; Li et al., 2020].

Here, by making use of a mixed representation of molecule operators and radiation phase-space distributions [Kapral and Ciccotti, 1999; Toutounji and Kapral, 2001; Kapral, 2015] and by tracing out the radiation degrees of freedom, an effective master equation was derived to account exclusively for the dynamics of the molecule degrees of freedom. The closeness condition of this master equation is obtained by considering contributions up to second-order-in-the-light-matter-interaction. The closed master equation allows for a direct comparison between the full quantum dynamics, the traditional semiclassical light-matter interaction and an alternative semiclassical non-local in time description. Therefore, the purpose of this chapter is not to show the implementation of trajectory methods [Hoffmann et al., 2019b; Li et al., 2020] but to discuss the influence of the photonic degrees of freedom on molecular-only dynamics in terms of statistics of the radiation field.

In a nutshell, up to second order in the light matter interaction, quantum effects can be mimic by classical light sources if the mean-field contribution, the symmetrized two-time correlation function, and the linear response function defined through the antisymmetrized two-time correlation function are equal in both scenarios. Note that this condition does not refers to the classical limit of the quantum light source but the possibility of tailoring classical light sources that mimic, up to second order, the effect of radiation on the molecule degrees of freedom.

In doing so, the impact of the quantum fluctuations of three quantum light field states, namely, a Fock state, a Fock state superposition, and a squeezed vacuum state are analyzed in system models. These states have a non-trivial quantum character [Mandel and Wolf, 1995; Gerry and Knight, 2005; Agarwal, 2013], and let to explore the effect of the vanishing and non-vanishing mean-field contribution and of the symmetrized/antisymmetrized two-time correlation functions on the molecular-only dynamics.

This chapter is organized as follows: the description of a molecular system coupled to a quantized light field is provided in Section 4.1, in close resemblance to the Section 1.3.2. Section 4.2 introduces a quantum-classical projection operator formalism to deduce a quantum-classical second-order master equation for the molecular system that treats the light degrees of freedom classically. Besides, the standard semiclassical approach is analyzed, together with a methodology to determine an effective electric field. Sec. 4.3 discusses numerical results comparing the quantum-classical, standard semiclassical, and the exact quantum dynamics of Hamiltonians used in theoretical

molecular polaritonics considering different light field states with a nonclassical character.

4.1. Quantum cavity molecular-only dynamics

Consider a molecular system interacting with a quantized light field and assume that the dipole approximation holds and frame the interaction in the length gauge [Flick et al., 2017; Ruggenthaler et al., 2018]. In this setup, the general correlated electron-nuclear-photon Hamiltonian consisting of n_{el} electrons, n_{nul} nuclei, and n_{ph} photon modes can be written as a sum of the electro-nuclear (bare molecular) Hamiltonian $\hat{H}_{\mathrm{bm}}$ and the photon Hamiltonian $\hat{H}_{\mathrm{ph}}$. The bare molecular Hamiltonian $\hat{H}_{\mathrm{bm}}$ comprises five terms, the kinetic energy of the electrons $\hat{T}_{\mathrm{el}}$, the kinetic energy of the nucleons $\hat{T}_{\mathrm{nuc}}$, the interaction between electrons $\hat{V}_{\mathrm{el-el}}$, between nucleons $\hat{V}_{\mathrm{nuc-nuc}}$ and the electron-nucleons interaction $\hat{V}_{\mathrm{el-nuc}}$, it reads $\hat{H}_{\mathrm{bm}} = \hat{T}_{\mathrm{el}} + \hat{T}_{\mathrm{nuc}} + \hat{V}_{\mathrm{el-el}} + \hat{V}_{\mathrm{nuc-nuc}} + \hat{V}_{\mathrm{el-nuc}}$. The photon Hamiltonian incorporates the coupling to the molecular degrees of freedom and reads

$$\begin{aligned}\hat{H}_{\mathrm{ph}} &= \frac{1}{2}\sum_{\alpha=1}^{n_{\mathrm{ph}}}\left[\hat{\mathrm{p}}_\alpha^2 + \omega_\alpha^2\left(\hat{\mathrm{q}}_\alpha + e\,\boldsymbol{\lambda}_\alpha\cdot\hat{\mathbf{R}}/\omega_\alpha\right)^2\right] \\ &= \hat{H}_{\mathrm{bph}} + \hat{H}_{\text{ph-m}} + \hat{H}_{\mathrm{rm}},\end{aligned} \tag{72}$$

with $\hat{\mathbf{R}} = \sum_{I=1}^{n_{\mathrm{nuc}}} Z_I\hat{\mathbf{X}}_I - \sum_{i=1}^{n_{\mathrm{el}}}\hat{\mathbf{x}}_i$ being the total dipole operator including both sets of electronic $\{\hat{\mathbf{x}}_i\}$ and nuclear $\{\hat{\mathbf{X}}_I\}$ coordinates and Z_I stand for the nuclear charges. $\hat{H}_{\mathrm{bph}} = \frac{1}{2}\sum_{\alpha=1}^{n_{\mathrm{ph}}}(\hat{\mathrm{p}}_\alpha^2 + \omega_\alpha^2\hat{\mathrm{q}}_\alpha^2)$ denotes the bare photon Hamiltonian, $\hat{H}_{\text{ph-m}} = \sum_{\alpha=1}^{n_{\mathrm{ph}}}\omega_\alpha\hat{\mathrm{q}}_\alpha\boldsymbol{\lambda}_\alpha\cdot e\hat{\mathbf{R}}$ does so for the interaction between photons and molecular degrees of freedom, with $\boldsymbol{\lambda}$ as the dipole coupling strength. Finally, $\hat{H}_{\mathrm{rm}} = \frac{1}{2}\sum_{\alpha=1}^{n_{\mathrm{ph}}}\left(\boldsymbol{\lambda}_\alpha\cdot e\hat{\mathbf{R}}\right)^2$ accounts for the renormalization of the bare molecular Hamiltonian due to the coupling to light.

To provide a general insight into the quantum aspects of light in molecular systems, consider the molecular system-light field Hamiltonian

$$\hat{H} = \hat{H}_{\mathrm{m}} + \hat{H}_{\mathrm{bph}} + \hat{H}_{\text{ph-m}} \tag{73}$$

with the molecular Hamiltonian $\hat{H}_{\mathrm{m}} = \hat{H}_{\mathrm{bm}} + \hat{H}_{\mathrm{rm}}$. The dynamics of the state $\hat{\rho}$ of the entire system described by $\hat{H}$ follows from the von Neumann equation, $\frac{\mathrm{d}}{\mathrm{d}t}\hat{\rho} = -\frac{\mathrm{i}}{\hbar}\left[\hat{H},\hat{\rho}\right]$. Because interest here is in the influence that coupling to photons induces on the molecular systems, the partial trace over the states of the photons is applied to $\hat{\rho}$, so that the

reduced state of the molecular systems follows from $\hat{\rho}_{\rm m} = {\rm tr}_{\rm ph}\hat{\rho}$. To focus exclusively on the dynamics induced by the light-matter coupling, it is convenient to calculate the equation of motion of $\hat{\rho}_{\rm m}$ in the interaction picture by introducing the unitary transformation $\hat{\rho}^{(\rm I)}(t) = \hat{U}^{\dagger}(t-t_0)\hat{\rho}(t)\hat{U}(t-t_0)$ with $\hat{U}(t-t_0) = \exp\left[\frac{\rm i}{\hbar}\hat{H}_{\rm m}(t-t_0)\right]\exp\left[\frac{\rm i}{\hbar}\hat{H}_{\rm bph}(t-t_0)\right]$. Therefore,

$$\frac{\rm d}{{\rm d}t}\hat{\rho}_{\rm m}^{(\rm I)}(t) = -\frac{\rm i}{\hbar}{\rm tr}_{\rm ph}\left[\hat{H}_{\text{ph-m}}^{(\rm I)}(t), \hat{\rho}^{(\rm I)}(t)\right]. \tag{74}$$

By continuing the discussion in the interaction picture, the shear complexity of the intrinsic molecular dynamics is left out and the light-matter interaction becomes the focus of the description below.

To develop a perturbative approach, it is convenient to introduce the Feshbach projection formalism [Wu et al., 2009]. The traditional application of this formalism in atomic and molecular physics deals with the representation of a state in terms of its bounded $\mathscr{H}_{\rm bd}$ and continuum $\mathscr{H}_{\rm cn}$ support, i.e., it has to do Hilbert spaces of the form $\mathscr{H}_{\rm bd-cn} = \mathscr{H}_{\rm bd} \oplus \mathscr{H}_{\rm cn}$. Here, by contrast, the Hilbert space is of the form $\mathscr{H} = \mathscr{H}_{\rm m} \otimes \mathscr{H}_{\rm bph}$. The physical difference between both configurations is that in the former case, the probability is conserved in the total Hilbert space $\mathscr{H}_{\rm bd-cm}$ whereas in the latter case, probability is conserved in the each subspace $\mathscr{H}_{\rm m}$ and $\mathscr{H}_{\rm bph}$.

Define $\mathscr{P}\hat{\rho}^{(\rm I)}(t) = \hat{\rho}_{\rm ph}(t_0) \otimes {\rm tr}_{\rm ph}\hat{\rho}^{(\rm I)}(t)$, with $\hat{\rho}_{\rm ph}(t_0) = \hat{\rho}_{\rm ph}^{(\rm I)}$. Because ${\rm tr}_{\rm ph}\hat{\rho}_{\rm ph}(t_0) = 1$, then $\mathscr{P}$ is a projector super-operator with orthogonal complement $\mathscr{Q} = 1 - \mathscr{P}$. The equation of motion for both subspaces reads

$${\rm tr}_{\rm ph}\left[\mathscr{P}\frac{\rm d}{{\rm d}t}\hat{\rho}^{(\rm I)}(t)\right] = -\frac{\rm i}{\hbar}{\rm tr}_{\rm ph}\left[\hat{H}_{\text{ph-m}}^{(\rm I)}(t), \hat{\rho}_{\rm ph}(t_0)\otimes\hat{\rho}_{\rm m}^{(\rm I)}(t) + \mathscr{Q}\hat{\rho}^{(\rm I)}(t)\right], \tag{75}$$

$$\mathscr{Q}\frac{\rm d}{{\rm d}t}\hat{\rho}^{(\rm I)}(t) = -\frac{\rm i}{\hbar}\mathscr{Q}\left[\hat{H}_{\text{ph-m}}^{(\rm I)}(t), \hat{\rho}_{\rm ph}(t_0)\otimes\hat{\rho}_{\rm m}^{(\rm I)}(t) + \mathscr{Q}\hat{\rho}^{(\rm I)}(t)\right], \tag{76}$$

where the trace over the photon field was taken in the equation of motion of $\mathscr{P}\hat{\rho}^{(\rm I)}$ so that $\frac{\rm d}{{\rm d}t}\hat{\rho}_{\rm m}^{(\rm I)} = {\rm tr}_{\rm ph}\left[\mathscr{P}\frac{\rm d}{{\rm d}t}\hat{\rho}^{(\rm I)}\right]$. Equations (75) and (76) allow for a systematic perturbative approach in terms of the strength of the interaction term

$\hat{H}^{(\mathrm{I})}_{\text{ph-m}}$. Since the contribution of $\mathscr{Q}\hat{\rho}^{(\mathrm{I})}$ in $\mathrm{tr}_{\mathrm{ph}}\mathscr{Q}\hat{\rho}^{(\mathrm{I})}$ is of second-order in $\hat{H}^{(\mathrm{I})}_{\text{ph-m}}$, the first order contribution corresponds to neglect the term $\mathscr{Q}\hat{\rho}^{(\mathrm{I})}$ in Eq. (75). To explore more concretely this approximation, assume that $\hat{H}_{\text{ph-m}}$ can be written as $\hat{H}^{(\mathrm{I})}_{\text{ph-m}}(t) = \sum_u \hat{K}^{(\mathrm{I})}_u(t)\hat{\Phi}^{(\mathrm{I})}_u(t)$ being $\{\hat{K}_u\}$ observables of the molecular system and $\{\hat{\Phi}_u\}$ observables of the radiation field. To first order in the interaction, the Eq. (74) reads

$$\begin{aligned}\frac{\mathrm{d}}{\mathrm{d}t}\hat{\rho}^{(\mathrm{I})(1)}_{\mathrm{m}}(t) &= -\frac{\mathrm{i}}{\hbar}\left[\hat{H}^{(\mathrm{I})}_{\mathrm{mf}}(t), \hat{\rho}^{(\mathrm{I})}_{\mathrm{m}}(t)\right] \\ &= -\frac{\mathrm{i}}{\hbar}\sum_u \langle\hat{\Phi}^{(\mathrm{I})}_u\rangle\left[\hat{K}^{(\mathrm{I})}_u(t), \hat{\rho}^{(\mathrm{I})}_{\mathrm{m}}(t)\right],\end{aligned} \tag{77}$$

with $\hat{H}^{(\mathrm{I})}_{\mathrm{mf}}(t) = \sum_u \hat{K}^{(\mathrm{I})}_u(t)\langle\hat{\Phi}^{(\mathrm{I})}_u\rangle$ being the mean field contribution and $\langle\hat{\Phi}^{(\mathrm{I})}_u\rangle = \mathrm{Tr}_{\mathrm{ph}}\left[\hat{\Phi}^{(\mathrm{I})}_u(t)\hat{\rho}_{\mathrm{ph}}(t_0)\right]$. Therefore, up to first order, the interaction with the quantum radiation field can be mimicked by a classical field having electric field $\mathbf{E}^{\mathrm{cl}} = \langle\hat{\Phi}^{(\mathrm{I})}_u\rangle$. However, for radiation states such as Fock states $\langle\hat{\Phi}^{(\mathrm{I})}_u\rangle = 0$; thus, a classical field obtained from the assignation rule $\langle\hat{\Phi}^{(\mathrm{I})}_u\rangle \to \mathbf{E}^{\mathrm{cl}}$ fails at reproducing, e.g., the NaI molecule results [Kowalewski et al., 2016a; Csehi et al., 2017] and therefore, a higher order contribution in needed.

The second-order contribution is calculated by inserting a first order solution of Eq. (76) in $\hat{H}_{\text{ph-m}}$, which is obtained by neglecting the term $\mathscr{Q}\hat{\rho}^{\mathrm{int}}$ in the right hand side of Eq. (76). Thus,

$$\mathscr{Q}\hat{\rho}^{(\mathrm{I})}(t) = -\frac{\mathrm{i}}{\hbar}\int_{t_0}^{t}\mathrm{d}\tau\mathscr{Q}\left[\hat{H}^{(\mathrm{I})}_{\text{ph-m}}(\tau), \hat{\rho}_{\mathrm{ph}}(t_0)\otimes\hat{\rho}^{(\mathrm{I})}_{\mathrm{m}}(\tau)\right], \tag{78}$$

where it has taken $\mathscr{Q}\hat{\rho}^{(\mathrm{I})}(t_0) = 0$, since initially the matter system and the photon field are decoupled, i.e., $\hat{\rho}(t_0) = \hat{\rho}_{\mathrm{m}}(t_0)\otimes\hat{\rho}_{\mathrm{ph}}(t_0)$. Therefore, replacing the Eq. (78) in Eq. (75), the second-order reduced master equation for the molecular system reads

$$\begin{aligned}\frac{\mathrm{d}}{\mathrm{d}t}\hat{\rho}^{(\mathrm{I})(2)}_{\mathrm{m}}(t) &= -\frac{\mathrm{i}}{\hbar}\sum_u \left\langle\hat{\Phi}^{(\mathrm{I})}_u(t)\right\rangle\left[\hat{K}^{(\mathrm{I})}_u(t), \hat{\rho}^{(\mathrm{I})}_{\mathrm{m}}(t)\right] \\ &- \frac{1}{\hbar^2}\int_{t_0}^{t}\mathrm{d}t'\sum_{u,v}\left[\mathscr{C}_{u,v}(t,t') - \left\langle\hat{\Phi}^{(\mathrm{I})}_u(t)\right\rangle\left\langle\hat{\Phi}^{(\mathrm{I})}_v(t')\right\rangle\right]\left[\hat{K}^{(\mathrm{I})}_u(t), \left[\hat{K}^{(\mathrm{I})}_v(t'), \hat{\rho}^{(\mathrm{I})}_{\mathrm{m}}(t')\right]\right] \\ &- \frac{\mathrm{i}}{2\hbar}\int_{t_0}^{t}\mathrm{d}t'\sum_{u,v}\chi_{u,v}(t,t')\left[\hat{K}^{(\mathrm{I})}_u(t), \left[\hat{K}^{(\mathrm{I})}_v(t'), \hat{\rho}^{(\mathrm{I})}_{\mathrm{m}}(t')\right]_+\right].\end{aligned} \tag{79}$$

Here, $\chi_{u,v}(t,t') = \frac{2}{\hbar}\mathscr{A}_{u,v}(t,t')$ is the linear response function [May and Kühn, 2011], where the real (symmetrized) $\mathscr{C}_{u,v}(t,t') = \frac{1}{2}\left(\langle\hat{\Phi}_u^{(\mathrm{I})}(t)\hat{\Phi}_v^{(\mathrm{I})}(t')\rangle + \langle\hat{\Phi}_v^{(\mathrm{I})}(t')\hat{\Phi}_u^{(\mathrm{I})}(t)\rangle\right)$ and imaginary (antisymmetrized) $\mathscr{A}_{u,v}(t,t') = \frac{1}{2\mathrm{i}}\langle\left[\hat{\Phi}_u^{(\mathrm{I})}(t),\hat{\Phi}_v^{(\mathrm{I})}(t')\right]\rangle$ parts of two-time correlation function [Ingold, 2002; Cohen-Tannoudji et al., 1998] $g(t,t') = \langle\hat{\Phi}_u^{(\mathrm{I})}(t)\hat{\Phi}_v^{(\mathrm{I})}(t')\rangle = \mathrm{Tr}_{\mathrm{ph}}\left(\hat{\Phi}_u^{(\mathrm{I})}(t)\hat{\Phi}_v^{(\mathrm{I})}(t')\hat{\rho}_{\mathrm{ph}}(t_0)\right)$, and $[\cdot,\cdot]_+$ symbolizes an anticommutator.

States with $\langle\hat{\Phi}_u^{(\mathrm{I})}\rangle = 0$ can be now accounted for and treated by means of Eq. (79). There, it is then clear that the dynamics exhibited, e.g., by the NaI molecule [Kowalewski et al., 2016a; Csehi et al., 2017] is ignited by the quantum statistics of the Fock states encoded in $\mathscr{C}_{u,v}(t,t')$ and $\chi_{u,v}(t,t')$. To advance on discussing the ability of classical fields to mimic the dynamics induced by quantum fields, the radiation degrees of freedom are translated below into phase-space distributions and derive an equivalent expression to Eq. (79).

4.2. Quantum-classical cavity molecular-only dynamics

After tracing out the light fields, the central argument here is that as long as the reduced equation of motion of $\hat{\rho}_{\mathrm{m}}$ under quantum and classical light coincides, then it is possible to *effectively* mimic the molecule dynamics ignited by quantum light fields with classical ones. In establishing so, it is necessary to derive the analog of Eq. (79) under the action of classical fields.

To do so, first perform a partial Wigner-Weyl transform [Weyl, 1927; Wigner, 1932] on the Hilbert space of the light field so that a phase-space picture of the light field degrees of freedom is obtained. The partial Wigner-Weyl representation for the state $\hat{\rho}$ reads

$$\hat{\rho}^{\mathrm{W}}(\mathbf{q},\mathbf{p}) = \frac{1}{(2\pi\hbar)^{n_{\mathrm{p}}}}\int \mathrm{d}\mathbf{u}\langle\mathbf{q}+\frac{\mathbf{u}}{2}|\hat{\rho}|\mathbf{q}-\frac{\mathbf{u}}{2}\rangle \mathrm{e}^{-\frac{\mathrm{i}}{\hbar}\mathbf{p}\cdot\mathbf{u}}, \tag{80}$$

where the integration is performed over the entire phase-space of light field degrees of freedom $(\mathbf{q},\mathbf{p}) = (\{\mathrm{q}_\alpha\},\{\mathrm{p}_\alpha\})$. The state $\hat{\rho}^{\mathrm{W}}$ retains its operator nature since the molecular degrees of freedom still represent quantum operators in the molecule Hilbert space $\mathscr{H}_{\mathrm{m}}$. After performing the Wigner-Weyl transform, the molecule-light field dynamics is

governed by the von-Neumann–Moyal equation [J. E. Moyal, 1949; Beck and Sergi, 2013]

$$\frac{\partial \hat{\rho}^{\mathrm{W}}}{\partial t} = \left\{\hat{H}^{\mathrm{W}}, \hat{\rho}^{\mathrm{W}}\right\}_{\mathrm{M}} = -\frac{\mathrm{i}}{\hbar}(\hat{H}^{\mathrm{W}} \mathrm{e}^{\frac{\mathrm{i}\hbar}{2}\Lambda} \hat{\rho}^{\mathrm{W}} - \hat{\rho}^{\mathrm{W}} \mathrm{e}^{\frac{\mathrm{i}\hbar}{2}\Lambda} \hat{H}^{\mathrm{W}}), \tag{81}$$

where $\{\cdot,\cdot\}_{\mathrm{M}}$ symbolizes the Moyal bracket, with $\mathrm{e}^{\frac{\mathrm{i}\hbar}{2}\Lambda} = \lim_{N\to\infty} \sum_{l=0}^{N} \frac{1}{l!}(\frac{\mathrm{i}\hbar}{2}\Lambda)^l$, where $\Lambda = \sum_{\alpha=1}^{n_{\mathrm{ph}}} \frac{\overleftarrow{\partial}}{\partial \mathrm{q}_\alpha}\frac{\overrightarrow{\partial}}{\partial \mathrm{p}_\alpha} - \frac{\overleftarrow{\partial}}{\partial \mathrm{p}_\alpha}\frac{\overrightarrow{\partial}}{\partial \mathrm{q}_\alpha}$, the arrows indicate the direction in which derivates acts. In this representation there is no approximation invoked.

The classical limit for the light degrees of freedom of Eq. (81) corresponds to the von-Neumann–Poisson equation that is reached by disregarding $\mathscr{O}(\hbar^2)$ terms in the expansion of the phase-space operator $\mathrm{e}^{\frac{\mathrm{i}\hbar}{2}\Lambda}$. Thus, the quantum-classical dynamics [Kapral and Ciccotti, 1999; Kapral, 2015] of the state $\hat{\rho}^{\mathrm{W}}$ reads

$$\frac{\partial \hat{\rho}^{\mathrm{W}}}{\partial t} = -\frac{\mathrm{i}}{\hbar}\left[\hat{H}^{\mathrm{W}}, \hat{\rho}^{\mathrm{W}}\right] + \frac{1}{2}\left(\left\{\hat{H}^{\mathrm{W}}, \hat{\rho}^{\mathrm{W}}\right\}_{\mathrm{P}} - \left\{\hat{\rho}^{\mathrm{W}}, \hat{H}^{\mathrm{W}}\right\}_{\mathrm{P}}\right), \tag{82}$$

where $\{\cdot,\cdot\}_{\mathrm{P}}$ denotes the classical Poisson bracket. It is essential to point out that the dynamics generated by the quantum-classical Liouvillian superoperator $\mathscr{L}_{\mathrm{W}}$ coincides with the Moyal bracket's quantum dynamics as the light field Hamiltonian is quadratic in its quadratures. In this partial Wigner representation, the Hamiltonian of the Eq. (73) reads

$$\hat{H}^{\mathrm{W}} = \hat{H}_{\mathrm{m}} + \hat{H}^{\mathrm{W}}_{\text{ph-m}} + H^{\mathrm{W}}_{\mathrm{ph}}. \tag{83}$$

The interaction between the light field and the molecular degrees of freedom is defined by the Hamiltonian of the general form $\hat{H}^{\mathrm{W}}_{\text{ph-m}} = \sum_u \hat{K}_u \Phi^{\mathrm{W}}_u$, where $\hat{K}_u$ represents an operator in the Hilbert space of the molecular system, and Φ^{W}_u the phase-space representation of operator $\hat{\Phi}_u$ of the light field. Note that the photon Hamiltonian $H^{\mathrm{W}}_{\mathrm{ph}}$ is not an operator anymore.

The partial trace over the light degrees of freedom is obtained as

$$\hat{\rho}_{\mathrm{m}} = \mathrm{Tr}_{\mathrm{ph}}\, \hat{\rho}^{\mathrm{W}} = \int \mathrm{d}\mathbf{q}\mathrm{d}\mathbf{p}\hat{\rho}^{\mathrm{W}}. \tag{84}$$

After replacing the Hamiltonian (83) in the Eq. (82), and taking into account that $\left[H_{\rm ph}^{\rm W},\hat{\rho}^{\rm W}\right]=\left\{\hat{H}_{\rm m},\hat{\rho}^{\rm W}\right\}_{\rm P}=0$, the evolution of the reduced state of the molecular system reads

$$\frac{\partial\hat{\rho}_{\rm m}}{\partial t}=-\frac{\rm i}{\hbar}\left[\hat{H}_{\rm m},\hat{\rho}_{\rm m}\right]-\frac{\rm i}{\hbar}\sum_{u}\left[\hat{K}_{u},{\rm Tr}_{\rm ph}\left(\Phi_{u}^{\rm W}\hat{\rho}^{\rm W}\right)\right]+\frac{1}{2}\sum_{u}\left[\hat{K}_{u},{\rm Tr}_{\rm ph}\left\{\Phi_{u}^{\rm W},\hat{\rho}^{\rm W}\right\}_{\rm P}\right]_{+}+{\rm Tr}_{\rm ph}\left\{H_{\rm ph}^{\rm W},\hat{\rho}^{\rm W}\right\}_{\rm P}. \tag{85}$$

The full influence of the quantum/classical cavity into the molecular dynamics is encoded in $\Phi_{u}^{\rm W}$ provided that no approximation is involved in Eq. (85). Therefore, deviations from the quantum description can be discussed in terms of the quantum/classical correlations of $\Phi_{u}^{\rm W}$ (see below).

4.2.1. Derivation of the Reduced Master Equation in the Mixed Wigner Representation.

Since the dynamics of $\Phi_{u}^{\rm W}$, at first-order, depends on the interaction with the molecule itself, Eq. (85) is not closed from a mathematical viewpoint. This can be overcome after introducing a projection operator technique in the quantum classical Hilbert–phase-space of the entire molecular-light field system. For simplicity, consider the second-order regime in the molecule-light interaction thorough the Liouvillian superoperators in the interaction picture of the partial Wigner transform $\hat{\rho}^{\rm W(I)}(t)={\rm e}^{{\rm i}\mathscr{L}_{0}^{\rm W}t}\hat{\rho}^{\rm W}(t)$, with $\mathscr{L}_{0}^{\rm W}=\mathscr{L}_{\rm m}+\mathscr{L}_{\rm ph}^{\rm W}$. Where $\mathscr{L}_{\rm m}\bullet=\frac{1}{\hbar}\left[\hat{H}_{\rm m},\bullet\right]$, and $\mathscr{L}_{\rm ph}^{\rm W}\bullet={\rm i}\left\{H_{\rm ph}^{\rm W},\bullet\right\}_{\rm P}$.

Therefore, the quantum/classical Liouville equation in the interaction picture reads

$$\frac{\partial}{\partial t}\hat{\rho}^{\rm W(I)}(t)=-{\rm i}\mathscr{L}_{\rm ph\text{-}m}^{\rm W(I)}(t)\hat{\rho}^{\rm W(I)}(t), \tag{86}$$

where $\mathscr{L}_{\rm ph\text{-}m}^{\rm W(I)}(t)={\rm e}^{{\rm i}\mathscr{L}_{0}^{\rm W}t}\mathscr{L}_{\rm ph\text{-}m}^{\rm W}$. The factorized interaction Hamiltonian in the interaction representation assumes the time-dependent form $\hat{H}_{\rm ph\text{-}m}^{\rm W(I)}(t)=\sum_{u}\hat{K}_{u}^{\rm (I)}(t)\Phi_{u{\rm W}}^{\rm (I)}(t)$. Thus, the interaction Liouvillian in the interaction representation reads $\mathscr{L}_{\rm ph\text{-}m}^{\rm W(I)}(t)\bullet=\frac{1}{\hbar}\left[\hat{H}_{\rm ph\text{-}m}^{\rm W(I)}(t),\bullet\right]+\frac{\rm i}{2}\left(\left\{\hat{H}_{\rm ph\text{-}m}^{\rm W(I)}(t),\bullet\right\}_{\rm P}-\left\{\bullet,\hat{H}_{\rm ph\text{-}m}^{\rm W(I)}(t)\right\}_{\rm P}\right)$. Using the concept of partial trace over the phase-space light-field-degrees-of-freedom, and since ${\rm Tr}_{\rm ph}\rho_{\rm ph}^{\rm W(I)}(t_0)=\int{\rm d}\mathbf{q}{\rm d}\mathbf{p}\rho_{\rm ph}^{\rm W(I)}(t_0)=1$, it is then possible to define the quantum/classical projection superoperator

$\mathscr{P}\hat{\rho}^{\rm W(I)}(t)=\rho_{\rm ph}^{\rm W(I)}(t_0)\,{\rm Tr}_{\rm ph}\hat{\rho}^{\rm W(I)}(t)$, with orthogonal complement $\mathscr{Q}=\hat{1}-\mathscr{P}$. The equations of motion for

both subspaces read

$$\mathrm{Tr}_{\mathrm{ph}}\left(\mathscr{P}\frac{\mathrm{d}}{\mathrm{d}t}\hat{\rho}^{\mathrm{W(I)}}(t)\right)=-\mathrm{i}\,\mathrm{Tr}_{\mathrm{ph}}\left(\mathscr{P}\mathscr{L}^{\mathrm{W(I)}}_{\text{ph-m}}(t)\rho^{\mathrm{W(I)}}_{\mathrm{ph}}(t_0)\times\hat{\rho}^{(\mathrm{I})}_{\mathrm{m}}(t)+\mathscr{P}\mathscr{L}^{\mathrm{W(I)}}_{\text{ph-m}}(t)\mathscr{Q}\hat{\rho}^{\mathrm{W(I)}}(t)\right), \tag{87}$$

$$\mathscr{Q}\frac{\mathrm{d}\hat{\rho}^{\mathrm{W(I)}}(t)}{\mathrm{d}t}=-\mathrm{i}\Big(\mathscr{Q}\mathscr{L}^{\mathrm{W(I)}}_{\text{ph-m}}(t)\rho^{\mathrm{W(I)}}_{\mathrm{ph}}(t_0)\hat{\rho}^{(\mathrm{I})}_{\mathrm{m}}(t)+\mathscr{Q}\mathscr{L}^{\mathrm{W(I)}}_{\text{ph-m}}(t)\mathscr{Q}\hat{\rho}^{\mathrm{W(I)}}(t)\Big). \tag{88}$$

To second-order, the term $\mathscr{Q}\mathscr{L}^{\mathrm{W(I)}}_{\text{ph-m}}(t)\mathscr{Q}\hat{\rho}^{\mathrm{W(I)}}(t)$ is disregarded. The mixed-Wigner-representation Equations (87,88) are analog to Eqs. (75,76), respectively.

Considering the factorized initial condition $\mathscr{Q}\hat{\rho}^{\mathrm{W(I)}}(t_0)=0$, the solution of Eq. (88) reads $\mathscr{Q}\hat{\rho}^{\mathrm{W(I)}}(t)=-\mathrm{i}\int_{t_0}^{t}\mathrm{d}t'\,\mathscr{Q}\mathscr{L}^{\mathrm{W(I)}}_{\text{ph-m}}(t')\rho^{\mathrm{W(I)}}_{\mathrm{ph}}(t_0)\hat{\rho}^{(\mathrm{I})}_{\mathrm{m}}(t')$. After replacing this result in Eq. (87), the first and second-order reduced master equations for the molecular system read

$$\frac{\mathrm{d}}{\mathrm{d}t}\hat{\rho}^{(\mathrm{I})(1)}_{\mathrm{m}}(t)=-\frac{\mathrm{i}}{\hbar}\sum_{u}\left\langle\Phi^{\mathrm{W(I)}}_{u}(t)\right\rangle\left[\hat{K}^{(\mathrm{I})}_{u}(t),\hat{\rho}^{(\mathrm{I})}_{\mathrm{m}}(t)\right], \tag{89}$$

$$\begin{aligned}\frac{\mathrm{d}}{\mathrm{d}t}\hat{\rho}^{(\mathrm{I})(2)}_{\mathrm{m}}(t)=&-\frac{\mathrm{i}}{\hbar}\sum_{u}\left\langle\Phi^{\mathrm{W(I)}}_{u}(t)\right\rangle\left[\hat{K}^{(\mathrm{I})}_{u}(t),\hat{\rho}^{(\mathrm{I})}_{\mathrm{m}}(t)\right]\\&-\frac{1}{\hbar^2}\int_{t_0}^{t}\mathrm{d}t'\sum_{u,v}\left(\mathscr{C}^{\mathrm{W}}_{u,v}(t,t')-\left\langle\Phi^{\mathrm{W(I)}}_{u}(t)\right\rangle\left\langle\Phi^{\mathrm{W(I)}}_{v}(t')\right\rangle\right)\left[\hat{K}^{(\mathrm{I})}_{u}(t),\left[\hat{K}^{(\mathrm{I})}_{v}(t'),\hat{\rho}^{(\mathrm{I})}_{\mathrm{m}}(t')\right]\right]\\&-\frac{\mathrm{i}}{2\hbar}\int_{t_0}^{t}\mathrm{d}t'\sum_{u,v}\chi^{\mathrm{W}}_{u,v}(t,t')\left[\hat{K}^{(\mathrm{I})}_{u}(t),\left[\hat{K}^{(\mathrm{I})}_{v}(t'),\hat{\rho}^{(\mathrm{I})}_{\mathrm{m}}(t')\right]_{+}\right],\end{aligned} \tag{90}$$

where

$$\mathscr{C}^{\mathrm{W}}_{u,v}(t,t')=\frac{1}{2}\Big(\left\langle\Phi^{\mathrm{W(I)}}_{u}(t)\Phi^{\mathrm{W(I)}}_{v}(t')\right\rangle+\left\langle\Phi^{\mathrm{W(I)}}_{v}(t')\Phi^{\mathrm{W(I)}}_{u}(t)\right\rangle\Big), \tag{91}$$

$$\chi^{\mathrm{W}}_{u,v}(t,t')=\left\langle\left\{\Phi^{\mathrm{W(I)}}_{u}(t),\Phi^{\mathrm{W(I)}}_{v}(t')\right\}_{\mathrm{P}}\right\rangle, \tag{92}$$

represent the phase-space versions of real (symmetrized) part of the two-time correlation function $g(t,t')$ and the linear response function [Ingold, 2002; Cohen-Tannoudji et al., 1998] of the light field operator that couples to the molecular

system. $\left\langle \Phi_u^{\mathrm{W(I)}}(t)\right\rangle = \mathrm{Tr}_{\mathrm{ph}}\left[\Phi_u^{\mathrm{W(I)}}(t)\rho_{\mathrm{ph}}^{\mathrm{W(I)}}(t_0)\right]$ represents the expected value of the light field observable that couples to the molecular system.

The reduced master equation in Eq. (90) is analog to Eq. (79), but it admits analysing the influence of classical or quantum descriptions of light fields on the same foot-stage. The correlations $\mathscr{C}^{\mathrm{W}}_{u,v}(t,t')$ and $\chi^{\mathrm{W}}_{u,v}(t,t')$, derived in the quantum-classical projection operator approach, correspond to the classical limit of the quantities $\mathscr{C}_{u,v}(t,t')$ and $\chi_{u,v}(t,t')$ in the Eq. (79), respectively. The analogy can be understood in terms of the light field two-time correlation function given by

$$\begin{aligned} g^{\mathrm{W}}_{u,v}(t,t') &= \left\langle \Phi_u^{\mathrm{W(I)}}(t)\Phi_v^{\mathrm{W(I)}}(t')\right\rangle \\ &= \int \mathrm{dqdp}\,\Phi^{\mathrm{W}}(\mathrm{q},\mathrm{p};t)\Phi^{\mathrm{W}}(\mathrm{q},\mathrm{p};t')\rho_{\mathrm{ph}}^{\mathrm{W(I)}}(\mathrm{q},\mathrm{p};t_0). \end{aligned} \tag{93}$$

In the classical limit, the symmetrized correlation function coincides with the two-time correlation function $\mathscr{C}^{\mathrm{W}}_{u,v}(t,t') = g^{\mathrm{W}}_{u,v}(t,t')$. The antisymmetrized correlation function is defined through the phase-space Poisson bracket $\mathscr{A}^{\mathrm{W}}_{u,v}(t,t') = \frac{1}{2\mathrm{i}}\left\{\Phi_u^{\mathrm{W(I)}}(t),\Phi_v^{\mathrm{W(I)}}(t')\right\}_{\mathrm{P}}$. It is useful to express the symmetrized correlation function in the form given in Eq. (91) for the comparison with the quantum case discussed below. The quantum limit of the Poisson bracket in the phase-space linear response function corresponds to $\left\{\Phi_u^{\mathrm{W(I)}}(t),\Phi_v^{\mathrm{W(I)}}(t')\right\}_{\mathrm{P}} \to \frac{1}{\mathrm{i}\hbar}\left[\hat{\Phi}_u^{\mathrm{(I)}}(t),\hat{\Phi}_v^{\mathrm{(I)}}(t')\right]$.

Since the state of the photon field is aimed not to be measured, up to second-order in the light-molecule interaction, it is then not possible to distinguish between the dynamics induced by a classical electric field having the same statistics as the quantum electric field Eq. (90) and the actual dynamics generated by the quantum photon field Eq. (79). However, since the light degrees of freedom evolve independently of the molecular dynamics, Eq. (90) and (79) do not consider the back-action of the molecular dynamics on the light field [Csehi et al., 2019].

This formalism can be extended to (i) generalize the effect of classical vibrational baths composed of harmonic oscillators or to (ii) include higher orders in the light-matter interaction; thus, a quantum-classical master equation of the type Nakajima-Zwanzig or time-convolution-less could be deduced through this approach. In addition, if interest is in the dynamics of the light state instead of the molecule state, the role of the system could be inverted above (see

Appendix 3). However, these extensions are beyond the scope of this contribution.

4.2.2. Traditional Semiclassical Approach. To fully appreciate the difference of the present approach to the standard semiclassical approach and the conundrum posed by the results in the NaI molecule [Kowalewski et al., 2016a; Csehi et al., 2017], the standard semiclassical approach is reviewed next. The semiclassical Hamiltonian reads

$$\hat{H}_{\rm sc} = \hat{H}_{\rm m} - \hat{\mu}\cdot\mathbf{E}(t) \tag{94}$$

with $\hat{\mu}$ representing the total molecular dipole operator and the classical electric given by $\mathbf{E}(t) = \mathbf{E}_0\cos(\omega_{\rm c}t+\phi)$. The classical field amplitude $\mathbf{E}_0$ comprises the polarization state which it is assumed parallel to the total molecular dipole operator. The molecular dynamics follow the unitary evolution given by the master equation

$$\frac{\rm d}{{\rm d}t}\hat{\rho}_{\rm m}^{\rm (I)} = -\frac{\rm i}{\hbar}\mathbf{E}(t)\cdot\left[-\hat{\mu}^{\rm (I)},\hat{\rho}^{\rm (I)}\right]. \tag{95}$$

By identifying $\langle\hat{\Phi}_u^{\rm (I)}\rangle = \mathbf{E}(t)$ and $\langle\Phi_u^{\rm W(I)}(t)\rangle = \mathbf{E}(t)$ in and Eqs. (77) and (89), respectively, then the standard semiclassical description of the light-matter interaction in Eq. (95) corresponds to the first-order approximations in Eqs. (77) and (89).

As mentioned above, for quantum states such as the Fock state $\langle\hat{\Phi}_u^{\rm (I)}\rangle = \langle\Phi_u^{\rm W(I)}(t)\rangle = 0$, so that there is no reason for even making use Eq. (95) to account for results such those for the NaI molecule [Kowalewski et al., 2016a; Csehi et al., 2017] but Eqs. (79) and (90). However, results claimed in Ref. [Csehi et al., 2017] using the standard semiclassical description in Eq. (95) fits remarkably well the quantum results in Ref. [Kowalewski et al., 2016a]. To resolve this conundrum the concept of effective electric field is introduce next.

4.2.2.1. Effective Electric Field. To define an effective electric field for case with $\langle\hat{\Phi}_u^{\rm (I)}\rangle = \langle\Phi_u^{\rm W(I)}(t)\rangle = 0$ it is convenient to follow the strategy discussed in the seminal contribution in Ref. [Jiang and Brumer, 1991], (see also Ref. [Brumer, 2018]). Assuming unitary dynamics and pure states, the first key point is to perturbatively solve Eq. (95) at the level of the wave function $\hat{\rho}_{\rm m}^{\rm (I)}(t) = |\Psi_{\rm m}^{\rm (I)}(t)\rangle\langle\Psi_{\rm m}^{\rm (I)}(t)|$. Up to first oder in the light-matter

interaction,

$$|\Psi_{\rm m}^{\rm (I)}(t)\rangle = \left[1+\frac{\mathrm{i}}{\hbar}\int_{t_0}^{t}\mathrm{d}t'\hat{\mu}^{\rm (I)}(t')\cdot\mathbf{E}(t')\right]|\Psi_{\rm m}^{\rm (I)}(t_0)\rangle, \tag{96}$$

with $\hat{\mu}^{\rm (I)}(t)=\hat{U}_{\rm m}^{\dagger}(t,t_0)\hat{\mu}\hat{U}_{\rm m}(t,t_0)$, and $\hat{U}_{\rm m}(t)=\mathrm{e}^{\frac{\mathrm{i}}{\hbar}H_{\rm m}(t-t_0)}$. The molecule density matrix correspondingly reads

$$\hat{\rho}_{\rm m}^{\rm (I)}(t) = \left[1+\left(\frac{\mathrm{i}}{\hbar}\right)^2\int_{t_0}^{t}\mathrm{d}t'\hat{\mu}^{\rm (I)}(t')\cdot\mathbf{E}(t')\int_{t_0}^{t}\mathrm{d}t''\hat{\mu}^{\rm (I)\dagger}(t'')\cdot\mathbf{E}^{*}(t'')\right]|\Psi_{\rm m}^{\rm (I)}(t_0)\rangle\langle\Psi_{\rm m}^{\rm (I)}(t_0)|. \tag{97}$$

The second key point is clear from Eq. (90): classical states of light are also represented by phase-space distributions. Therefore, the expression for $\hat{\rho}_{\rm m}^{\rm (I)}(t)$ needs to be averaged over the phase-space distribution of the classical light field. Assuming the polarization state is parallel to the total molecular dipole operator

$$\hat{\rho}_{\rm m}^{\rm (I)}(t) = \left[1+\left(\frac{\mathrm{i}}{\hbar}\right)^2\int_{t_0}^{t}\mathrm{d}t'\int_{t_0}^{t}\mathrm{d}t''\hat{\mu}^{\rm (I)}(t')\hat{\mu}^{\rm (I)\dagger}(t'')\left\langle E(t')E^{*}(t'')\right\rangle\right]|\Psi_{\rm m}^{\rm (I)}(t_0)\rangle\langle\Psi_{\rm m}^{\rm (I)}(t_0)|. \tag{98}$$

Thus, up to second order in the interaction, the dynamics of the molecule density matrix is governed by the two-point correlation function of the light field. Therefore, as discussed below, it may be possible to define an effective electric field $\mathbf{E}_{\rm eff}$ that mimics the quantum dynamics as long as the two-point correlation function of $\mathbf{E}_{\rm eff}$ coincides with the two-point correlation function of the quantum field, even for fields with $\langle\hat{\Phi}_u^{\rm (I)}\rangle = \langle\Phi_u^{\rm W(I)}(t)\rangle = 0$. An analog result was previously derived in the context of light-haversting systems [Brumer, 2018] under sunlight illumination [Calderón and Pachón, 2020].

Even-though this approach may lead to define an effective electric field, its semi-classical origin brings a conceptual drawback. From a fully quantum perspective, the two-point correlation function of the electric field

$$\langle\hat{E}(t')\hat{E}^{\dagger}(t'')\rangle = \mathrm{tr}_{\rm ph}\mathrm{tr}_{\rm m}[\hat{E}(t')\hat{E}^{\dagger}(t'')\hat{\rho}] \tag{99}$$

depends upon the light-matter entangled state $\hat{\rho}$. Therefore, unless $\hat{\rho}=\hat{\rho}_{\rm ph}\otimes\hat{\rho}_{\rm m}$, for every molecule state, it is necessary to define an effective electric field. Below, a molecule-state-dependent effective electric field is presented

for a number of model systems and molecule states.

4.3. Cavity dynamics with different light field states

Below, the impact of light fields on the reduced molecular dynamics in Eq. (90) is analyzed for three system models: (i) the Rabi model, (ii) the Dicke model and (iii) a vibronic dimer model. By introducing the concept of effective electric field $\mathbf{E}_{\rm eff}$, the results from Eq. (95) are also discussed. The results are confronted to the exact quantum solution.

4.3.1. Rabi Model. To introduce the general framework analyzed here in a concrete model system, consider the Rabi model, namely, a two-level system in interaction with a cavity taking into account the counter-rotating terms described by the Hamiltonian

$$\hat{H}_{\rm R} = \tfrac{1}{2}\hbar\omega_0\hat{\sigma}_z + \hbar\omega_{\rm c}\hat{a}^\dagger\hat{a} + \hbar g\hat{\sigma}_x(\hat{a}^\dagger + \hat{a}). \tag{100}$$

Following Eq. (90), the classical description of the light field yields the following master equation for the two-level system tracing over the light degrees of freedom

$$\begin{aligned}\dot{\hat{\rho}}^{\rm I(2)}_{\rm (m)}(t) = &-\frac{\rm i}{\hbar}\big\langle\Phi^{\rm W(I)}(t)\big\rangle\Big[\hat{\sigma}_x^{\rm (I)}(t),\hat{\rho}^{\rm (I)}_{\rm m}(t)\Big]\\ &-\frac{1}{\hbar^2}\int_{t_0}^{t}{\rm d}t'\Big[\mathscr{C}^{\rm W}(t,t')-\big\langle\Phi^{\rm W(I)}(t)\big\rangle\big\langle\Phi^{\rm W(I)}(t')\big\rangle\Big]\times\Big[\hat{\sigma}_x^{\rm (I)}(t),\Big[\hat{\sigma}_x^{\rm (I)}(t'),\hat{\rho}^{\rm (I)}_{\rm m}(t')\Big]\Big]\\ &-\frac{\rm i}{2\hbar}\int_{t_0}^{t}{\rm d}t'\chi^{\rm W}(t,t')\Big[\hat{\sigma}_x^{\rm (I)}(t),\Big[\hat{\sigma}_x^{\rm (I)}(t'),\hat{\rho}^{\rm (I)}_{\rm m}(t')\Big]_+\Big].\end{aligned} \tag{101}$$

Here, the quantum counterpart of the phase-space light field observable $\Phi^{\rm W}(t)$ corresponds to $\hat{\Phi}^{\rm (I)}(t) = \hbar g(\hat{a}^\dagger {\rm e}^{{\rm i}\omega_{\rm c}t} + \hat{a}\,{\rm e}^{-{\rm i}\omega_{\rm c}t})$. For all models discussed here, many-modes-cavity-effects are neglected and focus is only on one mode of frequency $\omega_{\rm c}$. The possible space dependence of the light-matter coupling strength g is omitted [Kavokin et al., 2007]. Besides, the dipole self-energy term [Rokaj et al., 2018; Schäfer et al., 2020] is neglected in all Hamiltonians discussed in this section.

Following an approach similar to the discussion around Eq. (98), the effective electric field is given by

$$E_{\rm eff} = 2\hbar g\sqrt{\langle n_{\rm c}\rangle + n_{\rm a}}\cos\omega_{\rm c}t, \tag{102}$$

where $n_{\rm a}$ is the number of initial excitations in the two-level system $[0,1]$. This can be understood in relation to the field factors associated with absoption and emission processes [Gerry and Knight, 2005; Cohen-Tannoudji et al., 1998]. Note that this effective electric field depends upon a the state of matter and the state of light. Therefore, the semi-classical Hamiltonian

$$\hat{H}_{\rm eff} = \tfrac{1}{2}\hbar\omega_0\sigma_z + (\hat{\sigma}^- + \hat{\sigma}^+)E_{\rm eff}, \tag{103}$$

allows, up to second order, to mimic the quantum dynamics. The results from this approach are compared to the quantum-classical master-equation formalism [Eq. (101)] and to the full quantum results.

In the simulations below, it is considered that the phase-space correlations [Carmichael, 1999, 2009] in Eq. (101) follow their quantum-mechanical counterparts. Figure 18 depicts the ground electronic state population dynamics $\langle g|\hat{\rho}_{\rm m}(t)|g\rangle$ of the two-level system, comparing the exact quantum (red), the quantum-classical master equation (blue), and the standard semiclassical (yellow) dynamics induced by the corresponding effective electric field. Initially, all the population is in the excited electronic state $\langle e|\hat{\rho}_{\rm m}(t=0)|e\rangle = 1$, and different states for the light field with non-classical signatures [Mandel and Wolf, 1995; Gerry and Knight, 2005; Agarwal, 2013] are considered. The numerical integration of Eq. (101) goes beyond the secular approximation [Dodin et al., 2018; Damanet et al., 2019] and incorporates non-Markovian effects as dynamics are non-local in time [Pachón et al., 2013].

Consider first the case of a Fock state $\left|\psi_{\rm c}\right\rangle = \left|n_{\rm c}\right\rangle$ with $n_{\rm c}$ photons in the cavity; thus, $\hat{\rho}_{\rm ph}(t_0) = |n_{\rm c}\rangle\langle n_{\rm c}|$. The Wigner representation of this state has negative regions consistent with a non-classical character [Mandel and Wolf, 1995; Gerry and Knight, 2005; Agarwal, 2013]. For this light field state, the expected value of the light field operator $\left\langle\hat{\Phi}^{(\rm I)}(t)\right\rangle = 0$, the symmetrized correlation function $\mathscr{C}(t,t') = \hbar^2 g^2(2n_{\rm c}+1)\cos\omega_{\rm c}(t-t')$, and the antisymmetrized correlation function $\mathscr{A}(t,t') = -\hbar^2 g^2\sin\omega_{\rm c}(t-t')$. The value of the antisymmetrized correlation function is independent of the cavity

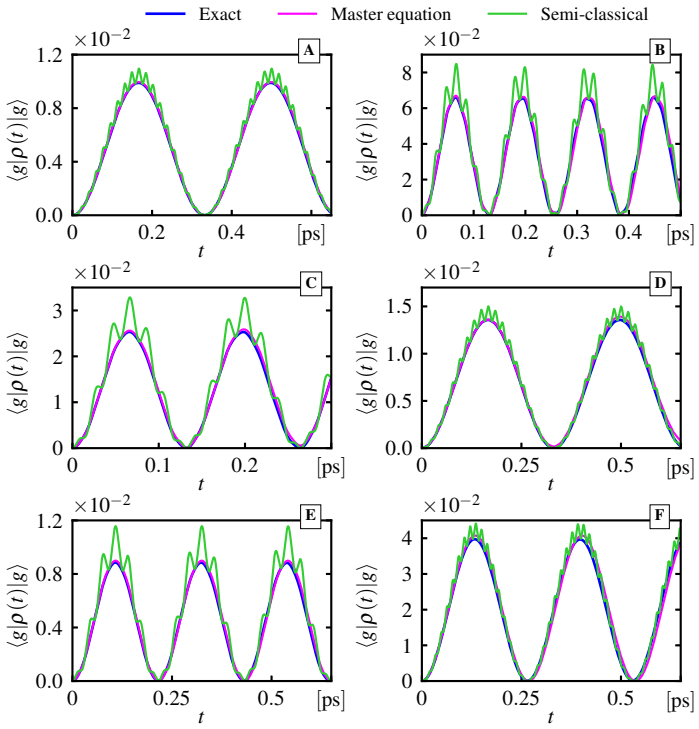

Figure 18. Populations of the ground state for the Rabi model (color coding is shown on top). Initially, the population of the excite state $\langle e|\hat{\rho}_{\rm m}(t=0)|e\rangle = 1$. (A) $\omega_{\rm c} = 0.9\,\omega_0$, $g = 0.005\omega_0$ and $n_{\rm c} = 0$. (B) $\omega_{\rm c} = 0.75\,\omega_0$, $g = 0.01\omega_0$ and $n_{\rm c} = 10$. (C) $\omega_{\rm c} = 0.75\omega_0$, $g = 0.015\omega_0$ and $|\psi_{\rm c}\rangle = \sqrt{0.2}|0\rangle + \sqrt{0.8}|1\rangle$. (D) $\omega_{\rm c} = 0.9\,\omega_0$, $g = 0.0025\omega_0$ and $|\psi_{\rm c}\rangle = \sqrt{0.5}|4\rangle + \sqrt{0.5}|5\rangle$. (E) $\omega_{\rm c} = 0.75\omega_0$, $g = 0.01\omega_0$ and $|\psi_{\rm c}\rangle = |\xi; r = 0.6\rangle$. (F) $\omega_{\rm c} = 0.9\omega_0$, $g = 0.01\omega_0$ and $|\psi_{\rm c}\rangle = |\xi; r = 0.2\rangle$.

state and relies from the commutation relation $[\hat{a}, \hat{a}^{\dagger}] = \hat{1}$ (see Appendix 4).

Fig. 18(A) shows the population of the ground electronic state $\langle g|\hat{\rho}_{\rm m}(t)|g\rangle$ considering the light field in a vacuum state $|\psi_{\rm c}\rangle = |0\rangle$ of frequency $\omega_{\rm c} = 0.9\,\omega_0$, and a coupling strength of $g = 0.01\omega_0$. Compared with the exact quantum results, the quantum-classical master equation dynamics display better results than the standard semiclassical approach. The standard semiclassical dynamics show an oscillatory behavior overestimated compared with the exact quantum results, since no complex part of two-time correlation function is taking into account in the effective electric field. In the Fig. 18(B) the light field is given by a Fock state of ten photons $|\psi_{\rm c}\rangle = |10\rangle$ in resonance with the frequency of the two-level system $\omega_{\rm c} = 0.99\,\omega_0$, and a coupling strength of $g = 0.001\omega_0$. For this case, the standard semiclassical dynamics display a better match with the exact quantum results provided the increase in the photon

number.

Now, consider a Fock state superposition of the form $\left|\psi_{\rm c}\right\rangle = c_n\left|n\right\rangle + c_{n+1}\left|n+1\right\rangle$. For this state $\mathscr{C}(t,t') = \hbar^2 g^2\left(|c_n|^2(2n_{\rm c}+1) + |c_{n+1}|^2(2n_{\rm c}+3)\right)\cos\omega_{\rm c}(t-t')$, and as discussed above, the linear antisymmetrized correlation function $\mathscr{A}(t,t') = -\hbar^2 g^2 \sin\omega_{\rm c}(t-t')$, since it is independent of the light field state. For this state, the expected value of the light field operator is different from zero $\left\langle\hat{\Phi}^{(\rm I)}(t)\right\rangle = 2\hbar g\sqrt{n+1}c_n c_{n+1}\cos\omega t$. It is important to stand out that this light field state has a non-trivial quantum character quantified by a negative value of the Mandel parameter [Mandel and Wolf, 1995; Gerry and Knight, 2005; Agarwal, 2013]. Fig. 18 (C and D cases) depicts the ground state population of the two-level system.

In the Fig. 18(C) the light field state is superposition of the vacuum state and a Fock state of one photon $\left|\psi_{\rm c}\right\rangle = \sqrt{0.2}\left|0\right\rangle + \sqrt{0.8}\left|1\right\rangle$, with a frequency of $\omega_{\rm c} = 0.75\omega_0$, and a coupling strength $g = 0.015\omega_0$. In the Fig. 18(D) the light field state is given by $\left|\psi_{\rm c}\right\rangle = \sqrt{0.5}\left|4\right\rangle + \sqrt{0.5}\left|5\right\rangle$, with a frequency of $\omega_{\rm c} = 0.9\,\omega_0$, and a coupling strength of $g = 0.0025\omega_0$. At first glance, being the Wigner representation of Fock states has negative regions in the phase-space that imply non-classicality would imply that the dynamics generate over the molecular system have to deviate from that one generate for classical sources, but this is not the case as it has been considered so far [Kowalewski et al., 2016a; Csehi et al., 2017, 2019]. Compared with the exact quantum results, the quantum-classical master equation dynamics display better results than the standard semiclassical approach. The standard semiclassical dynamics show an oscillatory behavior overestimated compared with the exact quantum results.

Consider the case of a squeezed vacuum state [Breuer and Petruccione, 2002; Agarwal, 2013] $\left|\psi_{\rm c}\right\rangle = \left|\xi\right\rangle$ (see Appendix 4), with $\varphi = 0$, so $\xi = r$, where r represents the squeezed parameter. For this state the symmetrized correlation function reads $\mathscr{C}(t,t') = \hbar^2 g^2\big((2\sinh^2 r + 1)\cos\omega_{\rm c}(t-t') - 2(\cosh r\sinh r)\cos\omega_{\rm c}(t+t')\big)$, and the expected value of the light field operator $\left\langle\hat{\Phi}^{(\rm I)}(t)\right\rangle = 0$. The non-classicality of the vacuum squeezed state is provided by the negative value of the squeezing parameter [Agarwal, 2013] $S = -\frac{1}{2}(1-{\rm e}^{-2r})$.

Fig. 18 (E and F cases) depicts the ground state population in the two-level system considering two values for the squeeze parameter $r = 0.2$ and $r = 0.6$. For these values of the squeeze parameter the quantum-classical

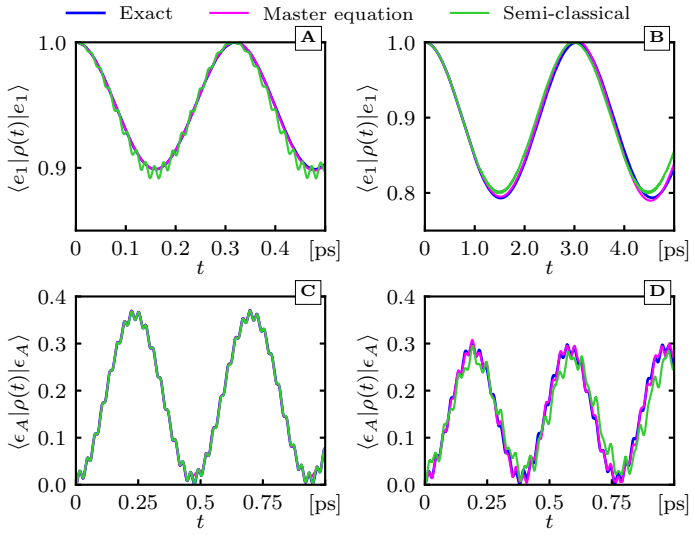

Figure 19. Top panels: Populations of the excited state of one of the TLS in the Dicke model of 4 atoms initially in their excited states (color coding is shown on top). (A) $\omega_c = 0.9\,\omega_0$, $g = 0.005\omega_0$ and $n_c = 10$. (B) $\omega_c = 0.99\,\omega_0$, $g = 0.00075\omega_0$ and $n_c = 10$. Bottom panels: Populations of the acceptor excited state in the vibronic dimer model. Initially, the population of donor the excite state $\langle \varepsilon_D\,|\hat{\rho}_m(t=0)|\,\varepsilon_D\rangle = 1$. (C) $\omega_c = 0.973\,\omega_0$, $g = 0.0005\omega_0$ and $n_c = 0$. (D) $\omega_c = 0.973\,\omega_0$, $g = 0.0035\omega_0$ and $n_c = 0$.

master equation dynamics display better results than the standard semiclassical approach, since standard semiclassical dynamics show an oscillatory behavior overestimated compared with the exact quantum results (see above). However, for high values of the squeeze parameter r, even if it is for a weak light-matter coupling strength, the quantum-classical master equation and the standard semiclassical approach do not model the molecular-only dynamics correctly (not shown). The above mentioned represents an evident deviation from the dynamics produced by classical light sources [Triana et al., 2018], and therefore, a purely quantum signature at the molecular-only dynamics.

4.3.2. Dicke Model. The Dicke model describes an ensemble of N two-level atoms collectively coupled to a single quantized cavity mode [Kirton et al., 2019]. The Dicke model has a ground-state transition to a superradiant phase. The Dicke Hamiltonian reads

$$\hat{H}_D = \tfrac{1}{2}\hbar\omega_0 \sum_{i=1}^{N} \hat{\sigma}_{z(i)} + \hbar\omega_c \hat{a}^\dagger \hat{a} + \hbar g \sum_{i=1}^{N} \hat{\sigma}_{x(i)}(\hat{a}^\dagger + \hat{a}). \tag{104}$$

This Hamiltonian has been widely studied and represents a cornerstone of many-body dynamics in quantum optics. It has recently been studied in the context of atom-only dynamics using the non-secular Redfield master equation approach [Damanet et al., 2019]. Fig. 19 (A and B cases) depicts the population of the excited state of one of the four two-level atoms that initially are in their excited states. In the Fig. 19(A) the quantized cavity mode corresponds to a Fock state of ten photons $\left|\psi_{\rm c}\right\rangle = \left|10\right\rangle$, with a frequency of $\omega_{\rm c} = 0.9\,\omega_0$, and a coupling strength of $g = 0.005\omega_0$. Fig. 19(B) consider a quantized cavity mode in a Fock state of ten photons $\left|\psi_{\rm c}\right\rangle = \left|10\right\rangle$ in resonance with the two-level atom excitation energy $\omega_{\rm c} = 0.99\,\omega_0$, and a coupling strength of $g = 0.00075\omega_0$. For both cases considered, the quantum-classical master equation approach display better results than the standard semiclassical dynamics concerning the exact quantum dynamics.

4.3.3. Vibronic dimer model. Recently, energy transfer dynamics have been a widely discussed topic in natural light-induced excitation and coherent pulsed laser excitation of photosynthetic light-harvesting systems [Brumer and Shapiro, 2012; Pachón and Brumer, 2012; Dodin et al., 2016a,b; Pachón et al., 2017; Reppert and Brumer, 2018; Brumer, 2018; Jung and Brumer, 2020; Calderón and Pachón, 2020]. To account for nonadiabatic effects and vibronic coherence dynamics in photosynthetic complexes [Tiwari et al., 2013, 2017; Bennett et al., 2018; Yeh et al., 2019; Calderón and Pachón, 2020], consider N chromophores, each with electronic energy ε_i, that interact through an inter-chromophore Coulomb coupling J_{ij}. Each chromophore is coupled to a quantized intramolecular vibrational mode of frequency ϖ_i. The molecular aggregate Hamiltonian reads (see Chapter 2)

$$\hat{H}_{\rm vd} = \sum_{i\neq j}^{N}\left(\varepsilon_i\hat{\sigma}_i^{+}\hat{\sigma}_i^{-} + J_{ij}\hat{\sigma}_i^{+}\hat{\sigma}_j^{-} + \hbar\lambda_i\hat{\sigma}_i^{+}\hat{\sigma}_i^{-}\left(\hat{b}_i^{\dagger}+\hat{b}_i\right) + \hbar\varpi_i\hat{b}_i^{\dagger}\hat{b}_i\right) \tag{105}$$

where $\hat{\sigma}_i^{+}$ ($\hat{\sigma}_i^{-}$) creates (annihilates) an electronic excitation in the $i^{\rm th}$ chromophore. Here, $\hat{b}_i^{\dagger}$ ($\hat{b}_i$) is the creation (annihilation) operator of the $i^{\rm th}$ intramolecular vibrational mode, $\lambda_i = \sqrt{S_i}\varpi_i$ represents the coupling between the $i^{\rm th}$ excited electronic state and the $i^{\rm th}$ intramolecular vibrational mode, and S_i is the Huang-Rhys factor. The presence of intramolecular vibrational modes resonant with the excitonic energy difference promote better efficiency in the energy transport under initial coherent excitation conditions [Yeh et al., 2019].

To explore the effect of the cavity on a photosynthetic complex prototype, consider the following donor-acceptor vibronic dimer model [Bennett et al., 2018], with a quantized intramolecular vibrational mode coupled to the acceptor. The vibronic dimer is coupled to a light field single-cavity-mode of frequency $\omega_{\rm c}$. The Hamiltonian reads

$$\begin{aligned}\hat{H}_{\rm vd-c} = &\varepsilon_{\rm D}\hat{\sigma}_{\rm D}^{+}\hat{\sigma}_{\rm D}^{-} + \varepsilon_{\rm A}\hat{\sigma}_{\rm A}^{+}\hat{\sigma}_{\rm A}^{-} + J_{\rm DA}(\hat{\sigma}_{\rm D}^{+}\hat{\sigma}_{\rm A}^{-} + \hat{\sigma}_{\rm A}^{+}\hat{\sigma}_{\rm D}^{-}) \\ &+ \hbar\lambda_{\rm A}\,\hat{\sigma}_{\rm A}^{+}\hat{\sigma}_{\rm A}^{-}\left(\hat{b}_{\rm A}^{\dagger} + \hat{b}_{\rm A}\right) + \hbar\varpi_{\rm A}\hat{b}_{\rm A}^{\dagger}\hat{b}_{\rm A} + \hbar g\hat{\sigma}_{D,x}(\hat{a}+\hat{a}) + \hbar g\hat{\sigma}_{A,x}(\hat{a}+\hat{a}) + \hbar\omega_{\rm c}\hat{a}^{\dagger}\hat{a},\end{aligned} \tag{106}$$

where $\varepsilon_{\rm D}$ is the electronic energy of the donor, $\varepsilon_{\rm A}$ is the electronic energy of the acceptor, and $J_{\rm DA}$ is the donor-acceptor electronic coupling. Fig. 19 (C and D cases) depicts the population of the excited state of the acceptor, considering parameters that correspond to the PEB dimer, the two phycoerythrobilin ($\rm PEB_{50/61\,C}$ and $\rm PEB_{50/61\,D}$) chromophores from the protein-antenna phycoerythrin 545 (PE545) [Doust et al., 2004; Novoderezhkin et al., 2010]. At $t = 0$ all the population is in the excited state of the donor, and for both cases the cavity is found in a vacuum state of frequency $\omega_{\rm c} = 0.973\,\omega_0$, in resonance with half of the donor-acceptor energy difference ω_0.

The results in Fig. 19(C) correspond to a coupling strength $g = 0.0005\omega_0$. In this regime of weak light-matter interaction, the molecular-only dynamics display barely the same results as in absence of the cavity. Therefore, the quantum-classical master equation, the standard semiclassical, and the exact quantum dynamics coincide. Increasing the coupling strength to $g = 0.0035\omega_0$ leads to an increasing of the rate of donor-acceptor energy transfer [see Fig. 19(D)], which shows the nonadiabatic enhancement driven by the coupling to light field [Kowalewski et al., 2016a,b; Gu and Mukamel, 2020; Csehi et al., 2017; Szidarovszky et al., 2018; Csehi et al., 2019]. In this coupling regime, the effect of the single vacuum cavity mode is better captured by the quantum-classical master equation approach than the standard semiclassical dynamics. However, even in a weak light-matter coupling regime, if a vacuum squeezed state has a high value of the squeeze parameter r, neither the quantum-classical master equation nor the standard semiclassical approach does not model the molecular-only dynamics correctly, which implies non-trivial quantum

molecular-only dynamics.

5. Conclusions

The role of intramolecular vibrations resonant with excitonic transitions in light-harvesting systems was analyzed under natural sunlight illumination Calderón and Pachón [2020]. The inclusion of the intramolecular vibrational modes reinforces the exciton coherence by up to one order of magnitude, as was shown for the DBV dimer. However, the comprehensive analysis shows that the populations of single exciton and site states of vibronic dimers are not significantly affected as compared to their corresponding electronic dimers. Therefore, there is no direct evidence of an enhancement in the energy transport mediated by the inclusion of resonant intramolecular vibrational degrees of freedom under natural conditions. Recently, similar conclusions were elucidated on the impact of the vibronic coupling in the electronic and vibrational coherences observed in two-dimensional-electronic-spectroscopies Duan et al. [2019].

Under incoherent light excitation conditions, the initial state of the light-harvesting system is of incoherent nature, namely, an incoherent mixture of eigenstates. For this scenario (see Fig. 16), it was further shown that intramolecular vibrational modes evolve devoid of non-classical correlations. Therefore, the generation of non-classical correlations via the transient formation of vibronic exciton states lacks of theoretical support since the quantum correlations come from the quantum superposition encoded in the initial state. Thus, that picture should be replaced in favor of the natural dynamics of the initial quantum correlations established in the light-harvesting system by the pulsed-laser-preparation of the initial state.

The perspective to contribute to the development of sustainable energy sources will always be an exciting challenge. To try to implement more sophisticated and physical models for energy transfer dynamics in natural and synthetic light-harvesting complexes excited by sunlight, it is necessary to include complete vibrational-electronic degrees of freedom interactions in diverse energy scales. Thus, this work could be extended to include the effect of the phonon bath at an intermediate energy regime, beyond the Redfield approach, respecting the blackbody-radiation-induce dynamics, and focusing on efficiency issues with the help of thermodynamics.

A second-order quantum-classical master equation formalism was developed to analyze the conditions under

which classical light field states can mimic the effects of quantum light sources on molecular systems Calderón and Pachón [2021]. The molecular-only dynamics were simulated, comparing the quantum-classical, quantum-exact, and the standard semiclassical approaches for different systems considered in the field of molecular polaritonics. An effective electric field used in the standard semiclassical light-matter approximation was discussed in the base of the second-order light-field correlation function. At second-order in light-matter interaction, the quantum-classical approach better fits the quantum exact molecular-only dynamics than the standard semiclassical approach. Thus, in principle, it is impossible to distinguish between the dynamics induced by a classical electric field having the same statistics as the quantum electric field.

Therefore, the non-classical character of a light quantum state does not guarantee that the molecular dynamics induced by the light field will be different from that in the excitation from a classical source, as it was shown in the case of Fock states. Previously, also confirmed by other studies in polaritonic chemistryCsehi et al. [2017, 2019]. Thus, the effects of the cavity can be mimic by classical light fields outside of the cavity. However, even in a weak light-matter coupling regime, if a vacuum squeezed state has a high value of the squeeze parameter r, neither the quantum-classical master equation nor the standard semiclassical approach does not model the molecular-only dynamics correctly, which implies non-trivial quantum molecular-only dynamics induced by quantum light.

The quantum-classical open quantum system approach discussed in this thesis could be extended to consider many cavity modes with the subsequent dissipation and decoherence effects that are not taking into account in light-matter interaction wave function approaches. It is also important to highlight that shedding light on these semiclassical methodologies could motivate the searching of experimental setups where the quantum fluctuations of the light field play a critical role and classify interesting light-induced-molecular-effects that could be reproduced without using sophisticated microcavities setups.

Bibliography

Agarwal, G. S. (2013). *Quantum optics*. Cambridge University Press.

Alharbi, F. H. and Kais, S. (2015). Theoretical limits of photovoltaics efficiency and possible improvements by intuitive approaches learned from photosynthesis and quantum coherence. *Renew. Sustainable Energy Rev.*, 43:1073–1089.

Arsenault, E. A., Yoneda, Y., Iwai, M., Niyogi, K. K., and Fleming, G. R. (2020). Vibronic mixing enables ultrafast energy flow in light-harvesting complex ii. *Nat. Commun.*, 11(1):1–8.

Beck, G. M. and Sergi, A. (2013). Quantum dynamics in the partial Wigner picture. *J. Phys. A*, 46(39):395305.

Beck, M. H., Jäckle, A., Worth, G. A., and Meyer, H.-D. (2000). The multiconfiguration time-dependent hartree (MCTDH) method: A highly efficient algorithm for propagating wavepackets. *Phys. Rep.*, 324(1):1–105.

Bennett, D. I., Maly, P., Kreisbeck, C., van Grondelle, R., and Aspuru-Guzik, A. (2018). Mechanistic regimes of vibronic transport in a heterodimer and the design principle of incoherent vibronic transport in phycobiliproteins. *J. Phys. Chem. Lett.*, 9(10):2665–2670.

Blankenship, R. E. (2014). *Molecular mechanisms of photosynthesis*. WILEY.

Brédas, J.-L., Sargent, E. H., and Scholes, G. D. (2017). Photovoltaic concepts inspired by coherence effects in photosynthetic systems. *Nat. Mater.*, 16(1):35–44.

Breuer, H. and Petruccione, F. (2002). *The Theory of Open Quantum Systems*. Oxford University Press.

Breuer, H.-P. (2012). Foundations and measures of quantum non-Markovianity. *J. Phys. B*, 45(15):154001.

Breuer, H.-P., Laine, E.-M., Piilo, J., and Vacchini, B. (2016). Colloquium: Non-Markovian dynamics in open quantum systems. *Rev. Mod. Phys.*, 88(2):021002.

Brixner, T., Stenger, J., Vaswani, H. M., Cho, M., Blankenship, R. E., and Fleming, G. R. (2005). Two-dimensional spectroscopy of electronic couplings in photosynthesis. *Nature*, 434(7033):625–628.

Brumer, P. (2018). Shedding (incoherent) light on quantum effects in light-induced biological processes. *J. Phys. Chem. Lett.*, 9(11):2946–2955.

Brumer, P. and Shapiro, M. (2012). Molecular response in one-photon absorption via natural thermal light vs. pulsed laser excitation. *Proc. Natl. Acad. Sci. U.S.A.*, 109(48):19575–19578.

Brunk, E. and Rothlisberger, U. (2015). Mixed quantum mechanical/molecular mechanical molecular dynamics simulations of biological systems in ground and electronically excited states. *Chem. Rev.*, 115(12):6217–6263.

Caldeira, A. O. and Leggett, A. J. (1983). Quantum tunnelling in a dissipative system. *Ann. Phys.*, 149(2):374–456.

Calderón, L. F. and Pachón, L. A. (2020). Nonadiabatic sunlight harvesting. *Phys. Chem. Chem. Phys.*, 22(22):12678–12687.

Calderón, L. F. and Pachón, L. A. (2021). Quantum to classical chemistry electrodynamics. *In preparation*.

Calhoun, T. R., Ginsberg, N. S., Schlau-Cohen, G. S., Cheng, Y.-C., Ballottari, M., Bassi, R., and Fleming, G. R. (2009). Quantum coherence enabled determination of the energy landscape in light-harvesting complex ii. *J. Phys. Chem. B*, 113(51):16291–16295.

Cao, J., Cogdell, R. J., Coker, D. F., Duan, H.-G., Hauer, J., Kleinekathöfer, U., Jansen, T. L., Mančal, T., Miller, R. D., Ogilvie, J. P., et al. (2020). Quantum biology revisited. *Sci. Adv.*, 6(14):eaaz4888.

Carmichael, H. J. (1999). *Statistical methods in quantum optics 1: master equations and Fokker-Planck equations*. Springer-Verlag.

Carmichael, H. J. (2009). *Statistical methods in quantum optics 2: Non-classical fields*. Springer-Verlag.

Chan, H. C., Gamel, O. E., Fleming, G. R., and Whaley, K. B. (2018). Single-photon absorption by single photosynthetic light-harvesting complexes. *J. Phys. B*, 51(5):054002.

Chen, H.-T., Li, T. E., Sukharev, M., Nitzan, A., and Subotnik, J. E. (2019). Ehrenfest + R dynamics. i. a mixed quantum–classical electrodynamics simulation of spontaneous emission. *J. Chem. Phys.*, 150(4):044102.

Cheng, Y.-C. and Fleming, G. R. (2009). Dynamics of light harvesting in photosynthesis. *Annu. Rev. Phys. Chem.*, 60(1):241–262.

Chenu, A., Brańczyk, A. M., Scholes, G. D., and Sipe, J. E. (2015). Thermal light cannot be represented as a statistical mixture of single pulses. *Phys. Rev. Lett.*, 114(21):213601.

Chenu, A. and Brumer, P. (2016). Transform-limited-pulse representation of excitation with natural incoherent light. *J. Chem. Phys.*, 144(4):044103.

Chenu, A., Christensson, N., Kauffmann, H. F., and Mančal, T. (2013). Enhancement of vibronic and ground-state vibrational coherences in 2D spectra of photosynthetic complexes. *Sci. Rep.*, 3:2029.

Chenu, A., Malỳ, P., and Mančal, T. (2014). Dynamic coherence in excitonic molecular complexes under various excitation conditions. *Chem. Phys.*, 439:100–110.

Chenu, A. and Scholes, G. D. (2015). Coherence in energy transfer and photosynthesis. *Annu. Rev. Phys. Chem.*, 66:69–96.

Chin, A. W., Prior, J., Rosenbach, R., Caycedo-Soler, F., Huelga, S. F., and Plenio, M. B. (2013). The role of non-equilibrium vibrational structures in electronic coherence and recoherence in pigment-protein complexes. *Nat. Phys.*, 9(2):113–118.

Christensson, N., Kauffmann, H. F., Pullerits, T., and Mančal, T. (2012). Origin of long-lived coherences in light-harvesting complexes. *J. Phys. Chem. B*, 116(25):7449–7454.

Cohen-Tannoudji, C., Diu, B., and Laloe, F. (1992). *Quantum Mechanics, 2 Volume Set*. Wiley.

Cohen-Tannoudji, C., Dupont-Roc, J., and Grynberg, G. (1998). *Atom-photon interactions: basic processes and applications*. John Wiley & Sons, Inc.

Collini, E., Wong, C. Y., Wilk, K. E., Curmi, P. M. G., Brumer, P., and Scholes, G. D. (2010). Coherently wired light-harvesting in photosynthetic marine algae at ambient temperature. *Nature*, 463(7281):644–647.

Csehi, A., Halász, G. J., Cederbaum, L. S., and Vibók, A. (2017). Competition between light-induced and intrinsic nonadiabatic phenomena in diatomics. *J. Phys. Chem. Lett.*, 8(7):1624–1630.

Csehi, A., Vibók, Á., Halász, G. J., and Kowalewski, M. (2019). Quantum control with quantum light of molecular nonadiabaticity. *Phys. Rev. A*, 100(5):053421.

Curutchet, C. and Mennucci, B. (2016). Quantum chemical studies of light harvesting. *Chem. Rev.*, 117(2):294–343.

Damanet, F., Daley, A. J., and Keeling, J. (2019). Atom-only descriptions of the driven-dissipative Dicke model. *Phys. Rev. A*, 99(3):033845.

De Vega, I. and Alonso, D. (2017). Dynamics of non-Markovian open quantum systems. *Rev. Mod. Phys.*, 89(1):015001.

Dean, J. C., Mirkovic, T., Toa, Z. S., Oblinsky, D. G., and Scholes, G. D. (2016). Vibronic enhancement of algae light harvesting. *Chem*, 1(6):858–872.

Dijkstra, A. G., Wang, C., Cao, J., and Fleming, G. R. (2015). Coherent exciton dynamics in the presence of underdamped vibrations. *J. Phys. Chem. Lett.*, 6(4):627–632.

Dodin, A., Tscherbul, T., Alicki, R., Vutha, A., and Brumer, P. (2018). Secular versus nonsecular Redfield dynamics and fano coherences in incoherent excitation: An experimental proposal. *Phys. Rev. A*, 97(1):013421.

Dodin, A., Tscherbul, T. V., and Brumer, P. (2016a). Coherent dynamics of V-type systems driven by time-dependent incoherent radiation. *J. Chem. Phys.*, 145(24):244313.

Dodin, A., Tscherbul, T. V., and Brumer, P. (2016b). Quantum dynamics of incoherently driven V-type systems: Analytic solutions beyond the secular approximation. *J. Chem. Phys.*, 144(24):244108.

Doust, A. B., Marai, C. N., Harrop, S. J., Wilk, K. E., Curmi, P. M., and Scholes, G. D. (2004). Developing a structure–function model for the cryptophyte phycoerythrin 545 using ultrahigh resolution crystallography and ultrafast laser spectroscopy. *J. Mol. Biol.*, 344(1):135–153.

Dovzhenko, D., Ryabchuk, S., Rakovich, Y. P., and Nabiev, I. (2018). Light–matter interaction in the strong coupling regime: configurations, conditions, and applications. *Nanoscale*, 10(8):3589–3605.

Du, M., Martínez-Martínez, L. A., Ribeiro, R. F., Hu, Z., Menon, V. M., and Yuen-Zhou, J. (2018). Theory for polariton-assisted remote energy transfer. *Chem. Sci.*, 9(32):6659–6669.

Du, M., Ribeiro, R. F., and Yuen-Zhou, J. (2019). Remote control of chemistry in optical cavities. *Chem*, 5(5):1167–1181.

Duan, H.-G., Thorwart, M., and Miller, R. D. (2019). Does electronic coherence enhance anticorrelated pigment vibrations under realistic conditions? *J. Chem. Phys.*, 151(11):114115.

Ebbesen, T. W. (2016). Hybrid light–matter states in a molecular and material science perspective. *Acc. Chem. Res.*, 49(11):2403–2412.

Engel, G. S., Calhoun, T. R., Read, E. L., Ahn, T.-K., Mančal, T., Cheng, Y.-C., Blankenship, R. E., and Fleming, G. R. (2007). Evidence for wavelike energy transfer through quantum coherence in photosynthetic systems. *Nature*, 446(7137):782–786.

Fassioli, F., Olaya-Castro, A., and Scholes, G. D. (2012). Coherent energy transfer under incoherent light conditions. *J. Phys. Chem. Lett.*, 3(21):3136–3142.

Feist, J., Galego, J., and Garcia-Vidal, F. J. (2018). Polaritonic chemistry with organic molecules. *ACS Photonics*, 5(1):205–216.

Feynman, R. P. and Hibbs, A. R. (1965). *Quantum Mechanics and Path Integrals*. McGraw-Hill Publishing Company.

Flick, J., Rivera, N., and Narang, P. (2018). Strong light-matter coupling in quantum chemistry and quantum photonics. *Nanophotonics*, 7(9):1479–1501.

Flick, J., Ruggenthaler, M., Appel, H., and Rubio, A. (2017). Atoms and molecules in cavities, from weak to strong coupling in quantum-electrodynamics (QED) chemistry. *Proc. Natl. Acad. Sci. U.S.A.*, 114(12):3026–3034.

Förster, T. (1948). Zwischenmolekulare energiewanderung und fluoreszenz. *Ann. Phys.*, 437:55–75.

Förster, T. (1965). Delocalized excitation and excitation transfer. In Sinanoglu, O., editor, *Modern Quantum Chemistry, Part 3*, page 93. Academic Press, Inc., New York.

Fuller, F. D., Pan, J., Gelzinis, A., Butkus, V., Senlik, S. S., Wilcox, D. E., Yocum, C. F., Valkunas, L., Abramavicius, D., and Ogilvie, J. P. (2014). Vibronic coherence in oxygenic photosynthesis. *Nat. Chem.*, 6(8):706–711.

Galego, J., Garcia-Vidal, F. J., and Feist, J. (2015). Cavity-induced modifications of molecular structure in the strong-coupling regime. *Phys. Rev. X*, 5(4):041022.

Gardiner, C. (1991). *Quantum noise: a handbook of Markovian and non-Markovian quantum stochastic methods with applications to quantum optics*. Springer.

Garrison, J. C. and Chiao, R. Y. (2008). *Quantum Optics*. Oxford University Press.

Gerasimenko, V. I. (1982). Dynamical equations of quantum-classical systems. *Theor. Math. Phys.*, 50(1):49–55.

Gerry, C. and Knight, P. L. (2005). *Introductory quantum optics*. Cambridge University Press.

Glauber, R. J. (1963). Coherent and incoherent states of the radiation field. *Phys. Rev.*, 131(6):2766–2788.

Grabert, H., Schramm, P., and Ingold, G.-L. (1988). Quantum Brownian motion: the functional integral approach. *Phys. Rep.*, 168(3):115–207.

Grinev, T. and Brumer, P. (2015). Realistic vs sudden turn-on of natural incoherent light: Coherences and dynamics in molecular excitation and internal conversion. *J. Chem. Phys.*, 143(24):244313.

Grunwald, R., Kelly, A., and Kapral, R. (2009). Quantum dynamics in almost classical environments. In *Energy Transfer Dynamics in Biomaterial Systems*, pages 383–413. Springer.

Grynberg, G., Aspect, A., and Fabre, C. (2010). *Introduction to quantum optics: from the semi-classical approach to quantized light*. Cambridge University Press.

Gu, B. and Mukamel, S. (2020). Manipulating nonadiabatic conical intersection dynamics by optical cavities. *Chem. Sci.*, 11(5):1290–1298.

Hayes, D., Wen, J., Panitchayangkoon, G., Blankenship, R. E., and Engel, G. S. (2011). Robustness of electronic coherence in the Fenna–Matthews–Olson complex to vibronic and structural modifications. *Farad. Discuss.*, 150:459–469.

Herrera, F. and Owrutsky, J. (2020). Molecular polaritons for controlling chemistry with quantum optics. *J. Chem. Phys.*, 152(10):100902.

Herrera, F. and Spano, F. C. (2018). Theory of nanoscale organic cavities: The essential role of vibration-photon dressed states. *ACS Photonics*, 5(1):65–79.

Hertzog, M., Wang, M., Mony, J., and Börjesson, K. (2019). Strong light–matter interactions: a new direction within chemistry. *Chem. Soc. Rev.*, 48(3):937–961.

Higgins, J. S., Lloyd, L. T., Sohail, S. H., Allodi, M. A., Otto, J. P., Saer, R. G., Wood, R. E., Massey, S. C., Ting, P.-C., Blankenship, R. E., et al. (2021). Photosynthesis tunes quantum-mechanical mixing of electronic and vibrational states to steer exciton energy transfer. *Proc. Natl. Acad. Sci. U.S.A.*, 118(11):e2018240118.

Hillery, M., O'Connell, R. F., Scully, M. O., and Wigner, E. P. (1984). Distribution functions in physics: fundamentals. *Phys. Rep.*, 106:121–167.

Hoffmann, N. M., Schäfer, C., Rubio, A., Kelly, A., and Appel, H. (2019a). Capturing vacuum fluctuations and photon correlations in cavity quantum electrodynamics with multitrajectory Ehrenfest dynamics. *Phys. Rev. A*, 99(6):063819.

Hoffmann, N. M., Schäfer, C., Säkkinen, N., Rubio, A., Appel, H., and Kelly, A. (2019b). Benchmarking semiclassical and perturbative methods for real-time simulations of cavity-bound emission and interference. *J. Chem. Phys.*, 151(24):244113.

Huelga, S. F. and Plenio, M. B. (2013). Vibrations, quanta and biology. *Contemp. Phys.*, 54(4):181–207.

Ingold, G.-L. (2002). Path integrals and their application to dissipative quantum systems. In *Coherent Evolution in Noisy Environments*, pages 1–53. Springer.

Ishizaki, A., Calhoun, T. R., Schlau-Cohen, G. S., and Fleming, G. R. (2010). Quantum coherence and its interplay with protein environments in photosynthetic electronic energy transfer. *Phys. Chem. Chem. Phys.*, 12(27):7319–7337.

Ishizaki, A. and Fleming, G. R. (2009). Unified treatment of quantum coherent and incoherent hopping dynamics in electronic energy transfer: Reduced hierarchy equation approach. *J. Chem. Phys.*, 130(23):234111.

Ishizaki, A. and Tanimura, Y. (2005). Quantum dynamics of system strongly coupled to low-temperature colored noise bath: reduced hierarchy equations approach. *J. Phys. Soc. Jpn.*, 74(12):3131–3134.

J. E. Moyal (1949). Quantum mechanics as a statistical theory. *Proc. Camb. Phil. Soc.*, 45:99–124.

Jang, S. (2011). Theory of multichromophoric coherent resonance energy transfer: A polaronic quantum master equation approach. *J. Chem. Phys.*, 135(3):034105.

Jang, S. J. and Mennucci, B. (2018). Delocalized excitons in natural light-harvesting complexes. *Rev. Mod. Phys.*, 90:035003.

Jiang, X. and Brumer, P. (1991). Creation and dynamics of molecular states prepared with coherent vs partially coherent pulsed light. *J. Chem. Phys.*, 94(9):5833–5843.

Johansson, J. R., Nation, P. D., and Nori, F. (2012). QuTiP: An open-source Python framework for the dynamics of open quantum systems. *Comp. Phys. Comm.*, 183:1760–1772.

Jonas, D. M. (2003). Two-dimensional femtosecond spectroscopy. *Annu. Rev. Phys. Chem.*, 54(1):425–463.

Jung, K. A. and Brumer, P. (2020). Energy transfer under natural incoherent light: Effects of asymmetry on efficiency. *J. Chem. Phys.*, 153(11):114102.

Kapral, R. (2015). Quantum dynamics in open quantum-classical systems. *J. Phys. Condens. Matter*, 27(7):073201.

Kapral, R. and Ciccotti, G. (1999). Mixed quantum-classical dynamics. *J. Chem. Phys.*, 110(18):8919–8929.

Kavokin, A., Baumberg, J. J., Malpuech, G., and Laussy, F. P. (2007). *Microcavities*. Oxford University Press.

Kirton, P., Roses, M. M., Keeling, J., and Dalla Torre, E. G. (2019). Introduction to the Dicke model: From equilibrium to nonequilibrium, and vice versa. *Adv. Quantum Technol.*, 2:1800043.

Kockum, A. F., Miranowicz, A., De Liberato, S., Savasta, S., and Nori, F. (2019). Ultrastrong coupling between light and matter. *Nat. Rev. Phys.*, 1(1):19–40.

Kolli, A., O'Reilly, E. J., Scholes, G. D., and Olaya-Castro, A. (2012). The fundamental role of quantized vibrations in coherent light harvesting by cryptophyte algae. *J. Chem. Phys.*, 137(17):174109.

Kowalewski, M., Bennett, K., and Mukamel, S. (2016a). Cavity femtochemistry: Manipulating nonadiabatic dynamics at avoided crossings. *J. Phys. Chem. Lett.*, 7(11):2050–2054.

Kowalewski, M., Bennett, K., and Mukamel, S. (2016b). Non-adiabatic dynamics of molecules in optical cavities. *J. Chem. Phys.*, 144(5):054309.

Kubo, R., Toda, M., and Hashitsume, N. (1985). *Statistical physics II: nonequilibrium statistical mechanics*. Springer-Verlag.

Levi, F., Mostarda, S., Rao, F., and Mintert, F. (2015). Quantum mechanics of excitation transport in photosynthetic complexes: a key issues review. *Rep. Prog. Phys.*, 78(8):082001.

Li, T. E., Chen, H.-T., Nitzan, A., and Subotnik, J. E. (2020). Quasiclassical modeling of cavity quantum electrodynamics. *Phys. Rev. A*, 101(3):033831.

Malý, P., Somsen, O. J., Novoderezhkin, V. I., Mančal, T., and Van Grondelle, R. (2016). The role of resonant vibrations in electronic energy transfer. *ChemPhysChem*, 17(9):1356–1368.

Mančal, T. (2020). A decade with quantum coherence: How our past became classical and the future turned quantum. *Chemical Physics*, 532:110663.

Mančal, T. and Valkunas, L. (2010). Exciton dynamics in photosynthetic complexes: excitation by coherent and incoherent light. *New J. Phys.*, 12(6):065044.

Mandel, L. (1979). Sub-poissonian photon statistics in resonance fluorescence. *Opt. Lett.*, 4(7):205–207.

Mandel, L. and Wolf, E. (1995). *Optical coherence and quantum optics*. Cambridge University Press.

Martínez-Martínez, L. A., Du, M., Ribeiro, R. F., Kéna-Cohen, S., and Yuen-Zhou, J. (2018). Polariton-assisted singlet fission in acene aggregates. *J. Phys. Chem. Lett.*, 9(8):1951–1957.

Martínez-Martínez, L. A., Eizner, E., Kéna-Cohen, S., and Yuen-Zhou, J. (2019). Triplet harvesting in the polaritonic regime: A variational polaron approach. *J. Chem. Phys.*, 151(5):054106.

May, V. and Kühn, O. (2011). *Charge and Energy Transfer Dynamics in Molecular Systems*. John Wiley & Sons, Ltd.

Mirkovic, T., Ostroumov, E. E., Anna, J. M., van Grondelle, R., Scholes, G. D., et al. (2017). Light absorption and energy transfer in the antenna complexes of photosynthetic organisms. *Chem. Rev.*, 117(2):249–293.

Mukamel, S. (1995). *Principles of Nonlinear Spectroscopy*. Oxford University Press.

Nakajima, S. (1958). On quantum theory of transport phenomena: steady diffusion. *Prog. Theor. Phys.*, 20(6):948–959.

Nitzan, A. (2006). *Chemical Dynamics in Condensed Phases*. Oxford University Press.

Novelli, F., Nazir, A., Richards, G. H., Roozbeh, A., Wilk, K. E., Curmi, P. M., and Davis, J. A. (2015). Vibronic resonances facilitate excited-state coherence in light-harvesting proteins at room temperature. *J. Phys. Chem. Lett.*, 6(22):4573–4580.

Novoderezhkin, V. I., Doust, A. B., Curutchet, C., Scholes, G. D., and Van Grondelle, R. (2010). Excitation dynamics in phycoerythrin 545: modeling of steady-state spectra and transient absorption with modified redfield theory. *Biophys. J.*, 99(2):344–352.

Novoderezhkin, V. I. and van Grondelle, R. (2017). Modeling of excitation dynamics in photosynthetic light-harvesting complexes: exact versus perturbative approaches. *J. Phys. B*, 50(12):124003.

O'Reilly, E. J. and Olaya-Castro, A. (2014). Non-classicality of the molecular vibrations assisting exciton energy transfer at room temperature. *Nat. Commun.*, 5(3012).

Pachón, L. A., Botero, J. D., and Brumer, P. W. (2017). Open system perspective on incoherent excitation of light harvesting systems. *J. Phys. B*, 50:184003.

Pachón, L. A. and Brumer, P. (2011). Physical basis for long-lived electronic coherence in photosynthetic light-harvesting systems. *J. Phys. Chem. Lett.*, 2(21):2728–2732.

Pachón, L. A. and Brumer, P. (2012). Computational methodologies and physical insights into electronic energy transfer in photosynthetic light-harvesting complexes. *Phys. Chem. Chem. Phys.*, 14(29):10094–10108.

Pachón, L. A. and Brumer, P. (2013). Incoherent excitation of thermally equilibrated open quantum systems. *Phys. Rev. A*, 87(2):022106.

Pachón, L. A. and Brumer, P. (2014). Direct experimental determination of spectral densities of molecular complexes. *J. Chem. Phys.*, 141(17):174102.

Pachón, L. A., Yu, L., and Brumer, P. (2013). Coherent one-photon phase control in closed and open quantum systems: A general master equation approach. *Faraday Discuss.*, 163:485–495.

Panitchayangkoon, G., Hayes, D., Fransted, K. A., Caram, J. R., Harel, E., Wen, J., Blankenship, R. E., and Engel, G. S. (2010). Long-lived quantum coherence in photosynthetic complexes at physiological temperature. *Proc. Natl. Acad. Sci. U.S.A.*, 107(29):12766–12770.

Redfield, A. G. (1957). On the theory of relaxation processes. *IBM J. Res. Dev.*, 1(1):19–31.

Reppert, M. and Brumer, P. (2018). Quantumness in light harvesting is determined by vibrational dynamics. *J. Chem. Phys.*, 149(23):234102.

Ribeiro, R. F., Martínez-Martínez, L. A., Du, M., Campos-Gonzalez-Angulo, J., and Yuen-Zhou, J. (2018). Polariton chemistry: controlling molecular dynamics with optical cavities. *Chem. Sci.*, 9(30):6325–6339.

Rivas, A. and Huelga, S. F. (2012). *Open Quantum Systems: An Introduction*. Springer-Verlag.

Rivas, A., Huelga, S. F., and Plenio, M. B. (2014). Quantum non-Markovianity: characterization, quantification and detection. *Rep. Prog. Phys.*, 77(9):094001.

Rokaj, V., Welakuh, D. M., Ruggenthaler, M., and Rubio, A. (2018). Light–matter interaction in the long-wavelength limit: no ground-state without dipole self-energy. *J. Phys. B*, 51(3):034005.

Romero, E., Augulis, R., Novoderezhkin, V. I., Ferretti, M., Thieme, J., Zigmantas, D., and Van Grondelle, R. (2014). Quantum coherence in photosynthesis for efficient solar energy conversion. *Nat. Phys.*, 10(9):676.

Romero, E., Novoderezhkin, V. I., and van Grondelle, R. (2017). Quantum design of photosynthesis for bio-inspired solar-energy conversion. *Nature*, 543(7645):355–365.

Ruggenthaler, M., Tancogne-Dejean, N., Flick, J., Appel, H., and Rubio, A. (2018). From a quantum-electrodynamical light–matter description to novel spectroscopies. *Nat. Rev. Chem.*, 2(3):1–16.

Sadeq, Z. S. and Brumer, P. (2014). Transient quantum coherent response to a partially coherent radiation field. *J. Chem. Phys.*, 140(7):074104.

Sáez-Blázquez, R., Feist, J., Fernández-Domínguez, A., and García-Vidal, F. (2018). Organic polaritons enable local vibrations to drive long-range energy transfer. *Phys. Rev. B*, 97(24):241407.

Sáez-Blázquez, R., Feist, J., Romero, E., Fernández-Domínguez, A. I., and García-Vidal, F. J. (2019). Cavity-modified exciton dynamics in photosynthetic units. *J. Phys. Chem. Lett.*, 10(15):4252–4258.

Sarovar, M., Ishizaki, A., Fleming, G. R., and Whaley, K. B. (2010). Quantum entanglement in photosynthetic light-harvesting complexes. *Nat. Phys.*, 6(6):462–467.

Schäfer, C., Ruggenthaler, M., Rokaj, V., and Rubio, A. (2020). Relevance of the quadratic diamagnetic and self-polarization terms in cavity quantum electrodynamics. *ACS Photonics*, 7(4):975–990.

Schlosshauer, M. (2007). *Decoherence and the Quantum-To-Classical Transition*. Springer-Verlag.

Scholak, T. and Brumer, P. (2017). An approach to "Quantumness" in coherent control. *Adv. Chem. Phys*, 62:39–135.

Scholes, G. D., Fleming, G. R., Chen, L. X., Aspuru-Guzik, A., Buchleitner, A., Coker, D. F., Engel, G. S., van Grondelle, R., Ishizaki, A., Jonas, D. M., and et al. (2017). Using coherence to enhance function in chemical and biophysical systems. *Nature*, 543(7647):647–656.

Scholes, G. D. and Rumbles, G. (2006). Excitons in nanoscale systems. *Nat. Mater.*, 5(9):683–696.

Scully, M. O. and Zubairy, M. S. (1997). *Quantum Optics*. Cambridge University Press.

Shapiro, M. and Brumer, P. (2003). *Principles of the quantum control of molecular processes*. John Wiley & Sons, Ltd.

Sudarshan, E. (1963). Equivalence of semiclassical and quantum mechanical descriptions of statistical light beams. *Phys. Rev. Lett.*, 10(7):277–279.

Szidarovszky, T., Halász, G. J., Császár, A. G., Cederbaum, L. S., and Vibók, Á. (2018). Conical intersections induced by quantum light: Field-dressed spectra from the weak to the ultrastrong coupling regimes. *J. Phys. Chem. Lett.*, 9(21):6215–6223.

Tanimura, Y. and Kubo, R. (1989). Time evolution of a quantum system in contact with a nearly Gaussian-Markoffian noise bath. *J. Phys. Soc. Jpn.*, 58(1):101–114.

Tiwari, V., Peters, W. K., and Jonas, D. M. (2013). Electronic resonance with anticorrelated pigment vibrations drives photosynthetic energy transfer outside the adiabatic framework. *Proc. Natl. Acad. Sci. USA*, 110(4):1203–1208.

Tiwari, V., Peters, W. K., and Jonas, D. M. (2017). Electronic energy transfer through non-adiabatic vibrational-electronic resonance. i. theory for a dimer. *J. Chem. Phys.*, 147(15):154308.

Toutounji, M. and Kapral, R. (2001). Subsystem dynamics in mixed quantum–classical systems. *Chem. Phys.*, 268(1-3):79–89.

Triana, J. F., Pelaez Ruiz, D., and Sanz-Vicario, J. L. (2018). Entangled photonic-nuclear molecular dynamics of LiF in quantum optical cavities. *J. Phys. Chem. A*, 122:2266–2278.

Tscherbul, T. V. and Brumer, P. (2014). Long-lived quasistationary coherences in a V-type system driven by incoherent light. *Phys. Rev. Lett.*, 113(11):113601.

Ullersma, P. (1966). An exactly solvable model for Brownian motion: I. Derivation of the Langevin equation. *Physica*, 32:27–55.

Valkunas, L., Abramavicius, D., and Mancăl, T. (2013). *Molecular Excitation Dynamics and Relaxation*. WILEY-VCH.

Van Amerongen, H., Van Grondelle, R., and Valkunas, L. (2000). *Photosynthetic excitons*. World Scientific.

Wang, C., Ren, J., and Cao, J. (2015). Nonequilibrium energy transfer at nanoscale: A unified theory from weak to strong coupling. *Sci. Rep.*, 5:11787.

Wang, L., Allodi, M. A., and Engel, G. S. (2019). Quantum coherences reveal excited-state dynamics in biophysical systems. *Nat. Rev. Chem.*, 3(8):477–490.

Weinberg, S. (2015). *Lectures on Quantum Mechanics*. Cambridge University Press.

Weiss, U. (2012). *Quantum Dissipative Systems*. World Scientific.

Weyl, H. (1927). Quantenmechanik und gruppentheorie. *Z. Phys.*, 46(1-2):1–46.

Wigner, E. P. (1932). On the quantum correction for thermodynamic equilibrium. *Phys. Rev.*, 40:749–759.

Wu, L.-A., Kurizki, G., and Brumer, P. (2009). Master equation and control of an open quantum system with leakage. *Phys. Rev. Lett.*, 102(8):080405.

Xiong, H.-N., Lo, P.-Y., Zhang, W.-M., Feng, D. H., and Nori, F. (2015). Non-Markovian complexity in the quantum-to-classical transition. *Sci. Rep.*, 5:13353.

Yeh, S.-H., Hoehn, R. D., Allodi, M. A., Engel, G. S., and Kais, S. (2019). Elucidation of near-resonance vibronic coherence lifetimes by nonadiabatic electronic-vibrational state character mixing. *Proc. Natl. Acad. Sci. U.S.A.*, 116(37):18263–18268.

Zhong, X., Chervy, T., Wang, S., George, J., Thomas, A., Hutchison, J. A., Devaux, E., Genet, C., and Ebbesen, T. W. (2016). Non-radiative energy transfer mediated by hybrid light-matter states. *Angew. Chem.*, 128(21):6310–6314.

Zhong, X., Chervy, T., Zhang, L., Thomas, A., George, J., Genet, C., Hutchison, J. A., and Ebbesen, T. W. (2017). Energy transfer between spatially separated entangled molecules. *Angew. Chem. Int. Ed.*, 56(31):9034–9038.

Zwanzig, R. (1960). Ensemble method in the theory of irreversibility. *J. Chem. Phys.*, 33(5):1338–1341.

Appendices

Appendix A Comparison between the Redfield master equation and the hierarchical equations of motion method

Figure 20 shows the vibronic dynamics of the PEB dimer solved with the Redfield master equation (RME)[4] and the hierarchical equations of motion (HEOM) method [Ishizaki and Tanimura, 2005; Johansson et al., 2012] for several values of the reorganization energy $\Lambda^{(\mathrm{e})}$ of the phonon bath coupled to the electronic degrees of freedom (e), and characterized by the spectral density

$$\omega^2 J_j^{\mathrm{PB}}(\omega) = \frac{2\Omega_j^{(\mathrm{e})}\Lambda_j^{(\mathrm{e})}\omega}{\hbar(\omega^2+\Omega_j^{(\mathrm{e})2})}. \tag{107}$$

The subspace of vibronic single exciton states can be described by the effective Hamiltonian [O'Reilly and Olaya-Castro, 2014]

$$\hat{H} = \frac{\Delta\varepsilon}{2}\sigma_z + V\sigma_x - \frac{g}{\sqrt{2}}(\hat{b}_{\mathrm{ac}}^{\dagger}+\hat{b}_{\mathrm{ac}})\sigma_z + \omega_{\mathrm{ac}}\hat{b}_{\mathrm{ac}}^{\dagger}\hat{b}_{\mathrm{ac}}, \tag{108}$$

being $\Delta\varepsilon$ the site energy difference, V the electronic coupling and g the vibronic coupling. Here, $\sigma_z = \sigma_2^+\sigma_2^- - \sigma_1^+\sigma_1^-$ and $\sigma_x = \sigma_1^+\sigma_2^- + \sigma_2^+\sigma_1^-$, where $\sigma_{i=1,2}^+$ ($\sigma_{i=1,2}^-$) creates (annihilates) an electronic excitation at the site $i = 1,2$. The creation (annihilation) operator $\hat{b}_{\mathrm{ac}}^{\dagger}$ ($\hat{b}_{\mathrm{ac}}$) of the anticorrelated vibrational mode of frequency $\omega_{\mathrm{ac}} = \omega_1 = \omega_2$ reads $\hat{b}_{\mathrm{ac}}^{\dagger} = (\hat{b}_1^{\dagger} - \hat{b}_2^{\dagger})/\sqrt{2}$ $\left(\hat{b}_{\mathrm{ac}} = (\hat{b}_1 - \hat{b}_2)/\sqrt{2}\right)$, where $\hat{b}_{i=1,2}^{\dagger}$ ($\hat{b}_{i=1,2}$) creates (annihilates) an intramolecular vibrational excitation at the site $i = 1,2$.

Figure 20 shows the population dynamics of the reduced lowest energy single exciton state $\langle e|\hat{\rho}_t|e\rangle$ and coherence dynamics $\langle e|\hat{\rho}_t|e'\rangle$ between the reduced single exciton states $|e\rangle$ and $|e'\rangle$, assuming as initial electronic state, the state prepared by the incoherent blackbody radiation bath only after 2.0 [ps], and a equilibrium thermal state

---

[4] See section 1.3.4.

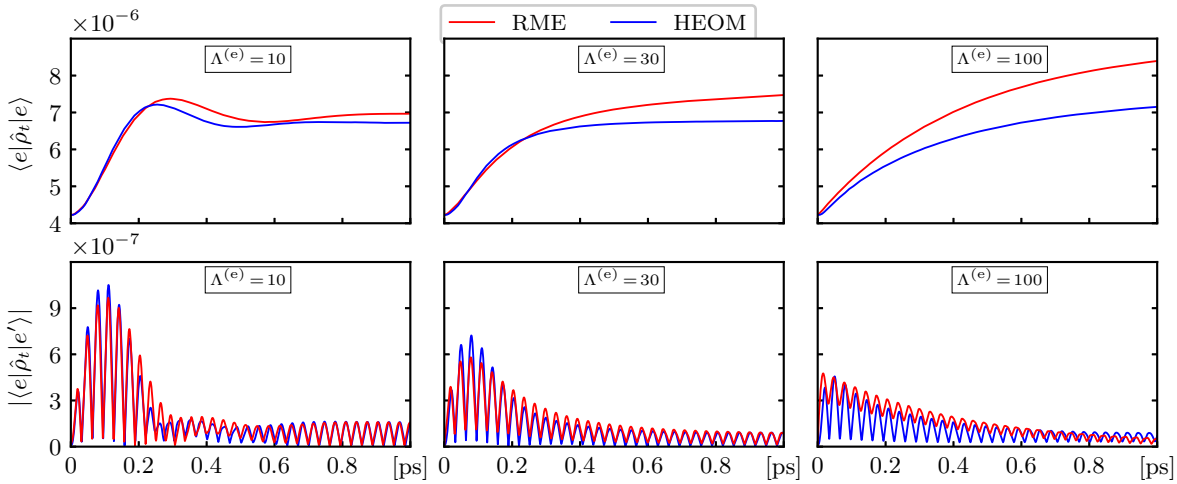

Figure 20. Comparison between the Redfield master equation (RME) and the hierarchical equations of motion (HEOM) method for several values of reorganization energy $\Lambda^{(e)}$ $[\mathrm{cm}^{-1}]$ of the PEB dimer. Top panels: Population dynamics of the reduced lowest energy single exciton state $|e\rangle$. Bottom panels: Coherence dynamics (absolute value) between the reduced single exciton states $|e\rangle$ and $|e'\rangle$.

($T = 300$ K) for the anticorrelated vibrational mode. The values adopted for the simulations are $\Delta\varepsilon = 1042\ \mathrm{cm}^{-1}$, $V = 92\ \mathrm{cm}^{-1}$, $g = 267.1\ \mathrm{cm}^{-1}$, $\omega_{\mathrm{ac}} = 1058\ \mathrm{cm}^{-1}$ and $T_{\mathrm{PB}}^{(e)} = 300\,\mathrm{K}$.

Appendix B Coherent states

A harmonic oscillator of frequency ω described through the Hamiltonian

$$\hat{H} = \hbar\omega\left(\hat{n} + \frac{1}{2}\right), \tag{109}$$

where $\hat{n} = \hat{a}^\dagger\hat{a}$ represents the number operator, $\hat{a}^\dagger$ ($\hat{a}$) the creation (annihilation) operator, that satisfies the commutation relation $\left[\hat{a}, \hat{a}^\dagger\right] = 1$. The eigenstates $\left|n\right\rangle$ of the number operator $\hat{n}$ satisfy the equation

$$\hat{n}\left|n\right\rangle = n\left|n\right\rangle; \quad n = 0, 1, 2, 3, \ldots, \infty. \tag{110}$$

The states $\left|n\right\rangle$ are called Fock states or number states [Mandel and Wolf, 1995; Gerry and Knight, 2005; Grynberg et al., 2010; Agarwal, 2013], and related to the creation operator by means of

$$\left|n\right\rangle = \frac{(\hat{a}^\dagger)^n}{\sqrt{n!}}\left|0\right\rangle, \tag{111}$$

with the vacuum state $\left|0\right\rangle$ given by $\hat{a}\left|0\right\rangle = 0$. The collection of states $\left|n\right\rangle$ represent a complete orthonormal basis

$$\left\langle n|n'\right\rangle = \delta_{nn'}, \quad \sum_{n=0}^{\infty} |n\rangle\langle n| = 1. \tag{112}$$

A coherent state $\left|\alpha\right\rangle$ is defined as an eigenstate of the annihilation operator $\hat{a}$ [Mandel and Wolf, 1995; Gerry and Knight, 2005; Grynberg et al., 2010; Agarwal, 2013], that satisfies

$$\hat{a}\left|\alpha\right\rangle = \alpha\left|\alpha\right\rangle, \tag{113}$$

where α is a complex number. The coherent states represent the most "classical" quantum states of the harmonic oscillator, since can represent states with well-defined amplitude and phase, such as the electromagnetic field states associated with laser sources [Mandel and Wolf, 1995; Gerry and Knight, 2005; Grynberg et al., 2010; Agarwal, 2013].

The solution of Eq. (113) for $\left|\alpha\right\rangle$ can be described in terms of Fock states $|n\rangle$

$$\left|\alpha\right\rangle = \mathrm{e}^{-\frac{1}{2}|\alpha|^2} \sum_{n=0}^{\infty} \frac{\alpha^n}{\sqrt{n!}} \left|n\right\rangle. \tag{114}$$

The mean boson number for the coherent state $\langle\alpha|\hat{n}|\alpha\rangle = \langle\hat{n}\rangle = |\alpha|^2$. The probabily to find n bosons in the coherent state $\left|\alpha\right\rangle$ follows the Poisson distribution

$$p(n) = \langle n|\alpha\rangle \langle\alpha|n\rangle = \mathrm{e}^{-|\alpha|^2} \frac{(|\alpha|^2)^n}{n!} = \frac{\mathrm{e}^{-\langle n\rangle} \langle n\rangle^n}{n!}. \tag{115}$$

The variance of this distribution is equal to its mean value

$$\left\langle\hat{n}^2\right\rangle - \langle\hat{n}\rangle^2 = \langle\hat{n}\rangle. \tag{116}$$

The collection of coherent states is a complete set that satisfies

$$\frac{1}{\pi} \int |\alpha\rangle\langle\alpha| \, \mathrm{d}^2\alpha = 1, \quad \alpha = x + \mathrm{i}y, \quad \mathrm{d}^2\alpha = \mathrm{d}x\mathrm{d}y, \quad -\infty \leq x, y \leq \infty. \tag{117}$$

However, coherent states are not orthogonal

$$\langle\alpha|\beta\rangle = \exp\left(\alpha^*\beta - \frac{1}{2}|\alpha|^2 - \frac{1}{2}|\beta|^2\right). \tag{118}$$

Appendix C Light-field dynamics

At first order in the interaction Hamiltonian, the evolution equation for the light field is given by

$$\mathscr{Q}\frac{\mathrm{d}\hat{\rho}^{\mathrm{W(I)}}(t)}{\mathrm{d}t} = -\mathrm{i}\mathscr{Q}\mathscr{L}^{\mathrm{W(I)}}_{\text{ph-m}}(t)\hat{\rho}^{\mathrm{W(I)}}_{\mathrm{ph}}(t_0)\hat{\rho}^{\mathrm{(I)}}_{\mathrm{m}}(t). \tag{119}$$

Taking the partial trace over the molecular degrees of freedom $\rho^{\mathrm{W}}_{\mathrm{ph}} = \mathrm{Tr}_{\mathrm{m}}\,\hat{\rho}^{\mathrm{W}}$ and making use of the orthogonal complement $\mathscr{Q} = \hat{1} - \mathscr{P}$, thus

$$\begin{aligned}\frac{\partial \rho^{\mathrm{W(I)}}_{\mathrm{ph}}(t)}{\partial t} = \frac{1}{2}\sum_u \mathrm{Tr}_{\mathrm{m}}\left[\hat{K}^{\mathrm{(I)}}_u(t), \hat{\rho}^{\mathrm{(I)}}_{\mathrm{m}}(t)\right]_+ \\ \times\left\{\Phi^{\mathrm{W(I)}}_u(t), \rho^{\mathrm{W(I)}}_{\mathrm{ph}}(t_0)\right\}_{\mathrm{P}}.\end{aligned} \tag{120}$$

In the Schrödinger picture the above equation reads

$$\frac{\partial \rho^{\mathrm{W}}_{\mathrm{ph}}(t)}{\partial t} = \left\{H^{\mathrm{W}}_{\mathrm{ph}} + \sum_u \mathrm{Tr}_{\mathrm{m}}\left(\hat{K}_u\hat{\rho}_{\mathrm{m}}(t)\right)\Phi^{\mathrm{W}}_u, \rho^{\mathrm{W}}_{\mathrm{ph}}(t)\right\}_{\mathrm{P}}. \tag{121}$$

The last equation can be compared with the full quantum case

$$\frac{\mathrm{d}\hat{\rho}_{\mathrm{ph}}(t)}{\mathrm{d}t} = -\frac{\mathrm{i}}{\hbar}\left[\hat{H}_{\mathrm{ph}} + \sum_u \mathrm{Tr}_{\mathrm{m}}\left(\hat{K}_u\hat{\rho}_{\mathrm{m}}(t)\right)\hat{\Phi}_u, \hat{\rho}_{\mathrm{ph}}(t)\right]. \tag{122}$$

Appendix D Light field correlation functions

The ladder operators acting on the Fock states are given by:

$$\hat{a}\big|n\big\rangle = \sqrt{n}\big|n-1\big\rangle, \tag{123}$$

$$\hat{a}^{\dagger}\big|n\big\rangle = \sqrt{n+1}\big|n+1\big\rangle. \tag{124}$$

The light field operator that couples to the molecular system reads

$$\hat{\Phi}^{(\mathrm{I})}(t) = \hbar g\left(\hat{a}^{\dagger}\mathrm{e}^{\mathrm{i}\omega t} + \hat{a}\,\mathrm{e}^{-\mathrm{i}\omega t}\right). \tag{125}$$

Symmetic and antisymmetric correlation functions

To calculate the symmetric and antisymmetric parts of two-time correlation function, first compute the operators

$$\begin{aligned}\hat{\Phi}^{(\mathrm{I})}(t)\hat{\Phi}^{(\mathrm{I})}(t') &= \hbar^2 g^2\left(\hat{a}^{\dagger}\mathrm{e}^{\mathrm{i}\omega t} + \hat{a}\,\mathrm{e}^{-\mathrm{i}\omega t}\right)\left(\hat{a}^{\dagger}\mathrm{e}^{\mathrm{i}\omega t'} + \hat{a}\,\mathrm{e}^{-\mathrm{i}\omega t'}\right)\\ &= \hbar^2 g^2\big(\hat{a}^{\dagger}\hat{a}^{\dagger}\mathrm{e}^{\mathrm{i}\omega(t+t')} + \hat{a}^{\dagger}\hat{a}\,\mathrm{e}^{\mathrm{i}\omega(t-t')}\\ &\qquad + \hat{a}\hat{a}^{\dagger}\mathrm{e}^{-\mathrm{i}\omega(t-t')} + \hat{a}\hat{a}\,\mathrm{e}^{-\mathrm{i}\omega(t+t')}\big),\end{aligned}$$

$$\begin{aligned}\hat{\Phi}^{(\mathrm{I})}(t')\hat{\Phi}^{(\mathrm{I})}(t) &= \hbar^2 g^2\left(\hat{a}^{\dagger}\mathrm{e}^{\mathrm{i}\omega t'} + \hat{a}\,\mathrm{e}^{-\mathrm{i}\omega t'}\right)\left(\hat{a}^{\dagger}\mathrm{e}^{\mathrm{i}\omega t} + \hat{a}\,\mathrm{e}^{-\mathrm{i}\omega t}\right)\\ &= \hbar^2 g^2\big(\hat{a}^{\dagger}\hat{a}^{\dagger}\mathrm{e}^{\mathrm{i}\omega(t+t')} + \hat{a}^{\dagger}\hat{a}\,\mathrm{e}^{-\mathrm{i}\omega(t-t')}\\ &\qquad + \hat{a}\hat{a}^{\dagger}\mathrm{e}^{\mathrm{i}\omega(t-t')} + \hat{a}\hat{a}\,\mathrm{e}^{-\mathrm{i}\omega(t+t')}\big).\end{aligned}$$

By using the commutator relation $[\hat{a},\hat{a}^\dagger]=\hat{1}$,

$$\hat{\Phi}^{(\mathrm{I})}(t)\hat{\Phi}^{(\mathrm{I})}(t')+\hat{\Phi}^{(\mathrm{I})}(t')\hat{\Phi}^{(\mathrm{I})}(t)=\hbar^2 g^2\Big(2\hat{a}^\dagger\hat{a}^\dagger \mathrm{e}^{\mathrm{i}\omega(t+t')}$$
$$+2\hat{a}\hat{a}\,\mathrm{e}^{-\mathrm{i}\omega(t+t')}+(2\hat{a}^\dagger\hat{a}+1)\big(\mathrm{e}^{-\mathrm{i}\omega(t-t')}+\mathrm{e}^{\mathrm{i}\omega(t-t')}\big)\Big),$$
$$\hat{\Phi}^{(\mathrm{I})}(t)\hat{\Phi}^{(\mathrm{I})}(t')-\hat{\Phi}^{(\mathrm{I})}(t')\hat{\Phi}^{(\mathrm{I})}(t)=-2\mathrm{i}\hbar^2 g^2\sin\omega(t-t').$$

Observables are related to the real or imaginary parts of two-time correlation function. For the analysis of one mode of the radiation, the antisymmetric part of two-time correlation function is independent of the state of the light field considered.

Fock state superposition

Consider a state of the light field given by a superposition of Fock states of the form

$$\big|\psi_{\mathrm{c}}\big\rangle=c_n\big|n\big\rangle+c_{n+1}\big|n+1\big\rangle, \tag{126}$$

where $|c_n|^2+|c_{n+1}|^2=1$.

The action of the operator $\hat{\Phi}^{(\mathrm{I})}(t)$ on the state $\big|\psi_{\mathrm{c}}\big\rangle$ reads

$$\hat{\Phi}^{(\mathrm{I})}(t)\big|\psi_{\mathrm{c}}\big\rangle=\hbar g\left(\hat{a}^\dagger\mathrm{e}^{\mathrm{i}\omega t}+\hat{a}\,\mathrm{e}^{-\mathrm{i}\omega t}\right)\left(c_n\big|n\big\rangle+c_{n+1}\big|n+1\big\rangle\right)$$
$$=\hbar g[(c_n\sqrt{n+1}\big|n+1\big\rangle+c_{n+1}\sqrt{n+2}\big|n+2\big\rangle)\mathrm{e}^{\mathrm{i}\omega t}$$
$$+(c_n\sqrt{n}\big|n-1\big\rangle+c_{n+1}\sqrt{n+1}\big|n\big\rangle)\mathrm{e}^{-\mathrm{i}\omega t}]$$

The average value of the light field operator for the state defined in the Eq. (126) reads

$$\langle\psi_{\mathrm{c}}|\hat{\Phi}^{(\mathrm{I})}(t)|\psi_{\mathrm{c}}\rangle=\hbar g\sqrt{n+1}\left(c_n^* c_{n+1}\mathrm{e}^{-\mathrm{i}\omega t}+c_{n+1}^* c_n\mathrm{e}^{\mathrm{i}\omega t}\right). \tag{127}$$

Provided that the coefficients c_n and c_{n+1} are real

$$\langle\psi_{\rm c}|\hat{\Phi}^{(\rm I)}(t)|\psi_{\rm c}\rangle = 2\hbar g\sqrt{n+1}c_n c_{n+1}\cos\omega t. \tag{128}$$

The symmetric correlation function reads

$$\begin{aligned}\mathscr{C}_{u,v}(t,t') &= \langle\psi_{\rm c}|\tfrac{1}{2}\big(\hat{\Phi}^{(\rm I)}(t)\hat{\Phi}^{(\rm I)}(t')+\hat{\Phi}^{(\rm I)}(t')\hat{\Phi}^{(\rm I)}(t)\big)|\psi_{\rm c}\rangle \\ &= \hbar^2 g^2\big(|c_n|^2(2n+1)+|c_{n+1}|^2(2n+3)\big)\cos\omega(t-t').\end{aligned} \tag{129}$$

The antisymmetric correlation function is given by

$$\begin{aligned}\mathscr{A}_{u,v}(t,t') &= \langle\psi_{\rm c}|-\tfrac{\rm i}{2}\big(\hat{\Phi}^{(\rm I)}(t)\hat{\Phi}^{(\rm I)}(t')-\hat{\Phi}^{(\rm I)}(t')\hat{\Phi}^{(\rm I)}(t)\big)|\psi_{\rm c}\rangle \\ &= -\hbar^2 g^2\sin\omega(t-t').\end{aligned} \tag{130}$$

Vacuum squeezed state

Defining the unitary operator

$$S(\xi) = \exp\left(\frac{1}{2}\xi\hat{a}^{\dagger 2}+\xi^*\hat{a}^2\right), \tag{131}$$

with $\xi = re^{{\rm i}\varphi}$, and where the squeeze parameter $0\le r<\infty$, and $0\le\varphi\le 2\pi$. The vacuum squeezed state is defined by

$$\big|\xi\big\rangle = S(\xi)\big|0\big\rangle. \tag{132}$$

This state could be decomposed in term of Fock states as

$$\big|\xi\big\rangle = \frac{1}{\sqrt{\cosh r}}\sum_{n=0}^{\infty}\frac{\sqrt{(2n)!}}{2^n n!}e^{{\rm i}n\varphi}(\tanh r)^n\big|2n\big\rangle. \tag{133}$$

$$\langle\xi|\hat{a}^\dagger\hat{a}|\xi\rangle = \sinh^2 r. \tag{134}$$

$$\langle \xi | \hat{a}^2 | \xi \rangle = \langle \xi | \hat{a}^{\dagger 2} | \xi \rangle^* = -\cosh r \sinh r e^{i\varphi}. \tag{135}$$